MICRO JOINING OF ADVANCED ALUMINUM GRAPHITE COMPOSITES

A Thesis

by

MANASA VELAMATI

Submitted to the Office of Graduate Studies of
Texas A&M University
in partial fulfillment of the requirements for the degree of

MASTER OF SCIENCE

May 2011

Major Subject: Mechanical Engineering

MICRO JOINING OF ADVANCED ALUMINUM GRAPHITE COMPOSITES

A Thesis

by

MANASA VELAMATI

Submitted to the Office of Graduate Studies of
Texas A&M University
in partial fulfillment of the requirements for the degree of

MASTER OF SCIENCE

Approved by:

Co-Chairs of Committee,	Wayne N. P. Hung
	Angie Hill Price
Committee Member	Chii-Der Suh
Head of Department,	Dennis O'Neal

May 2011

Major Subject: Mechanical Engineering

ABSTRACT

Micro Joining of Advanced Aluminum Graphite Composites.

(May 2011)

Manasa Velamati, B.E., Birla Institute of Technology and Science

Co-Chairs of Advisory Committee: Dr. Wayne N.P. Hung
Dr. Angie Price

Advanced aluminum graphite composites have unique thermal properties due to opposing coefficients of thermal expansion of aluminum and graphite. The thermal and mechanical properties of such composites are anisotropic due to directional properties of graphite fibers and their designed orientation. A joint with different fiber orientations would theoretically produce an isotropic material for thermal management.

This paper presents results for welding and brazing of the composite using different joining techniques. Laser welding of Al-Gr composite showed that a power density above 30kW/mm^2 gives a weld with microstructure defects. Also, the laser beam melts the matrix and delaminates the graphite fibers. The molten aluminum reacts with graphite to form aluminum carbide (Al_4C_3).

The joint strength is compromised when laser welding at optimal conditions add to minimize the carbide formation. Also, porosity and redistribution of graphite fibers are seen during laser welding. These defects prompt us to consider a low temperature joining. Brazing is considered since the low melting temperature of a filler material suppresses the formation of Al_4C_3 while minimizing pores and

microstructural defects in the joint. Microstructural study and shear test are performed to analyze the joints.

Shear strengths of brazed joints are determined to be 20-21MPa, which is comparable to the composite shear strength (46.5MPa in x-y plane and 19MPa in z plane). The fracture surface is found to be mostly on the composite rather than in brazed material or along the interface. Also, the microstructural study showed no Al_4C_3 formation and minimal porosity in the brazed region. These results show a successful joining of the composite using laser brazing and resistance brazing methods.

DEDICATION

I would like to dedicate my study to my family who made me the person I am today. They always supported my decisions and made my dream as their first priority in life. They have been very loving and provided me with the encouragement and support I always needed.

I also want to dedicate this to my friends who were always there by my side and cheered me up with their pleasant talks and unending support.

ACKNOWLEDGEMENTS

I would like to express my deep thankfulness to my committee chair, Dr. Wayne NP Hung, for his unending dedication to his students. He always made time for my project and guided me to the next step. He helped in building new ideas and developed my desire to explore further. He has great knowledge and experience on composites and manufacturing processes. I learned a lot under his guidance and I was honored to have had the opportunity to work with him. Dr. Hung was a great committee chair in this study. I would also like to thank my committee member, Dr. Angie Hill Price for helping me with her expertise in welding. She was always willing to direct and guide me throughout this study and provided me with books that helped for my research. She also let me use her materials lab for grinding and polishing for the microstructure analysis. I would like to express my gratitude to Dr. Suh Chii Der, for serving as my committee member. He showed interest in my work and was always there to extend his help for my experimental study.

Further, I thank Dr. Jyhwen Wang who allowed me to use his Universal Testing Machine for mechanical testing of my specimens. I would like to thank Mr. Frank Cervantez and Mr. John 'Butch' Macek at the Engineering Technology and Industrial Distribution Department, who were always helpful in providing me with all the equipment and accessories I needed for this study. I also sincerely thank Adam Farmer for his guidance in making fixtures and for his constant help in the machining lab. I profusely thank Sreekar Parimi, my friend, who always accompanied me to the lab when I had to work alone.

LIST OF ACRONYMS

Al-Gr	Aluminum Graphite
CFH	Cubic Foot per Hour
CTE	Coefficient of Thermal Expansion
DOE	Design of Experiments
EDS	Energy Dispersive X-ray Spectroscopy
HAZ	Heat Affected Zone
MMC	Metal Matrix Composite
Nd:YAG	Neodymium-doped Yttrium Aluminum Garnet laser
OM	Optical Microscopy
RSW	Resistance Spot Welding
SEM	Scanning Electron Microscopy
UTM	Universal Testing Machine
YAG	Yttrium Aluminum Garnet laser

TABLE OF CONTENTS

Page

LIST OF FIGURES

Page

Page

Page

Page

LIST OF TABLES

Page

Page

1. INTRODUCTION

Composites are the advanced materials developed for various applications. An enormous amount of research has been carried out to understand their manufacturing routes and improve their metallurgical behavior. Composites inherit properties of both metal matrix and reinforcements resulting in a material which performs better than any monolithic material in satisfying the requirements of a specific application. They have applications ranging from aerospace and automobile to medical industries.

There are various types of metal matrix composites (MMCs) based on the type of matrix, reinforcement and volume percentage of the contents. Matrices are based on polymers, metals or ceramics. The choice of matrix depends on required properties, end application of composite and manufacturing method. Properties of a composite depend on its microstructure which in turn depends on the manufacturing method and thermal and mechanical treatments performed on the composite.

The composite material considered here is an aluminum graphite composite which has unique thermal properties. Graphite due to its negative thermal expansion resulted in a new class of composites with their thermal expansion on the order of 1-$10x10^{-6}$ /°C that matches closely with other engineering materials.

This thesis follows the style of *Machining Science and Technology.*

Their light weight, low coefficient of thermal expansion (CTE), high thermal conductivity, high mechanical strength and high machinability can create cooling solutions for electronics in semiconductor industry. These composites can effectively remove heat without any thermal stress. Hence heat sinks, base plates, housings and thermal spreaders reinforced with graphite fillers are used in these markets. Al-Gr composites are manufactured by casting rather than extrusion as casting is the more economically feasible method for large production. Due to the directional alignment of the fibers in the composite, the properties of the composite are different in different planes. As a result, thermal and mechanical properties in the x-y basal plane are different than in the z direction.

When measured in different directions, there is 50-60% difference in thermal conductivity, 350-600% difference in thermal expansion and a 40% difference in tensile strength. Table 1 shows the properties of some Al-Gr composites and compares them to the properties of aluminum and graphite.

Table 1 Comparison of aluminum, graphite and aluminum- graphite composites

	Aluminum A356	**Graphite**	**Al MetGraf * 4-230**	**Al MetGraf * 7-200**
Thermal conductivity (W/m°K)	155	1100	225 (x-y), 120 (z)	190 (x-y), 125 (z)
Thermal expansion (10^{-6}/°K)	23	-1.6	4 (x-y), 24 (z)	7 (x-y), 24 (z)
Tensile strength (MPa)	152	3723	103 (x-y)	93 (x-y), 38 (z)
Density (g/cm^3)	2.66	2.20	2.40	2.46

*MetGraf is the trademark product of MMCC (http://www.metalmatrixcomposites.com)

This anisotropic property of the composite will limit its application to one and two dimensions. To make it applicable to 3 dimensional designs, it has to be made isotropic. This enables the designers to be more creative in their designing using 3 dimensional concepts. An economically feasible way to achieve this without changing existing manufacturing methods is by joining the composite in different fiber directions. This research work investigates the best joining method for Al-Gr composite that uses current manufacturing methods and is also economical.

1.1 OBJECTIVES AND SCOPE

The main objectives of the research are to determine the joinability of the Al-Gr composite and to develop suitable joining processes for Al-Gr composite. A proper method has to be selected which results in a strong joint without compromising the microstructure quality of the joint zone.

The scope of the project lays in the following:

A413 aluminum alloy with 38% volume fraction of carbon fibers is considered for this study. Joining the composite by welding and brazing methods is studied. Laser and electrical sources are employed in our work. Quality of the weld is evaluated by studying the microstructure and mechanical shear test at optimal process conditions.

2. LITERATURE REVIEW

A composite in engineering sense is any material that has been physically assembled to form one single mass without physical blending to form a theoretically homogenous material with unique properties. Usually, it is made of two separate components, a matrix and reinforcement. A soft phase of material is the matrix which holds the reinforcements.

Composites are classified based on the following criteria:

- matrix
- reinforcement
- shape and orientation
- processing methods employed

Matrices are classified broadly as polymer based, metal based and ceramic based composites. The composite of our interest is metal matrix composite, so it is discussed in detail below.

2.1 METAL MATRIX COMPOSITE

A metal matrix composite is a composite material with at least one metal part, other parts can be ceramic or polymer. To have improved mechanical and thermal properties, MMCs are used instead of pure metals or alloys. MMCs are classified based on type of reinforcement components. Figure 1 shows these classifications.

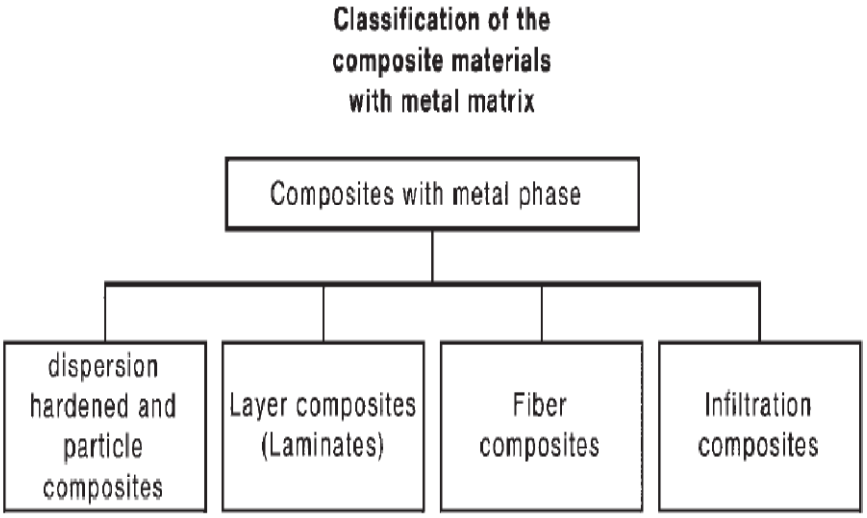

Figure 1 Classification of composites with metal matrix (Kainer, 2006)

Figure 2 shows the schematic representation of three shapes of metal matrix composites. They vary based on the particle/fiber reinforcements used.

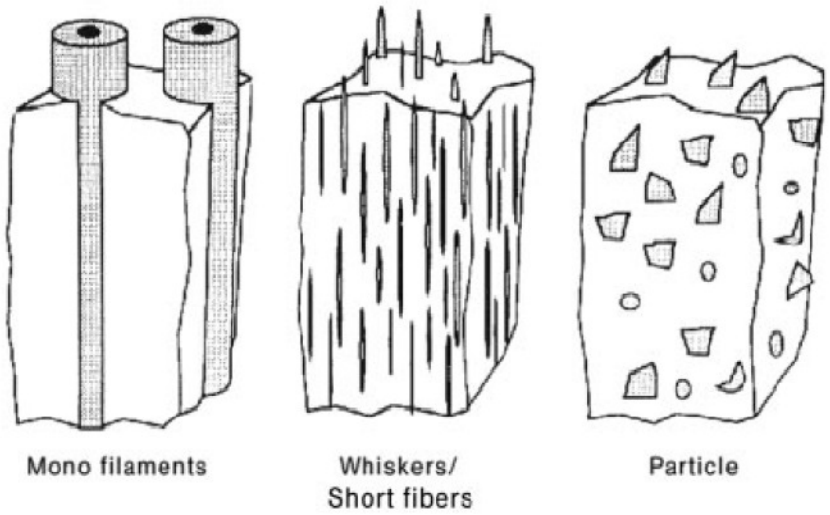

Figure 2 Different shapes of MMCs (Kainer, 2006)

The right combination of matrix-reinforcement and the processing methods should be used to meet the demands of the composite applications.

Following are the properties which will influence their usage:

- low density
- mechanical and chemical compatibility
- thermal stability
- high Young's modulus and tensile strength

These are met with a non-metal inorganic component. For metal reinforcement, ceramic or carbon is used in fiber or particle form. Various manufacturing techniques can be used for making MMCs. Different properties can be obtained by altering the manufacturing method, processing, finishing, and the reinforcement components. The properties of MMCs are based on their microstructure and internal interfaces, which in turn are affected by their manufacturing method. Microstructure covers the structure of matrix and reinforcement. The chemical composition, grain size, texture, precipitation behavior and lattice defects are important in a matrix. Reinforcement is characterized by its volume percentage, kind, size, distribution and orientation (Kainer, 2006).

Thermal expansion coefficients can be reduced by reinforcing light metals with ceramic fibers. Interactions between the matrix and the reinforcement determine the interface adhesion and the overall composite properties. These properties will determine the thermal stability and failure of MMCs.

Fibers act as reinforcement in the composite structure. They also influence the properties of the composite. In absence of air or oxidizing environments, carbon fibers show exceptionally good high temperature properties, hence carbon fiber

reinforcements will improve the thermal properties of the material thereby retaining their properties even above 2000°C (Kainer, 2006).

Carbon fibers have the following properties which make them more feasible and highly useful:

- low density
- low coefficient of thermal expansion
- good thermal and electrical conductivity
- high strength
- high Young's modulus (Kainer, 2006)

Carbon fibers/aluminum composites have better properties over aluminum alloys. Carbon fibers also add dimensional stability as they have a negative coefficient of thermal expansion. In addition, aluminum graphite composites are cost effective.

2.2 ALUMINUM GRAPHITE COMPOSITES

The composite used is Al-Gr METGRAF -7200 provided by MMCC. They are in the form of as-cast plates of $4\times6\times0.5$ in^3. Graphite fibers, with axes distributed preferably in the base x-y plane (4×6 in^2), are perpendicular to the z direction.

The microstructure of the composite can be seen in the Figure 3 and Figure 4.

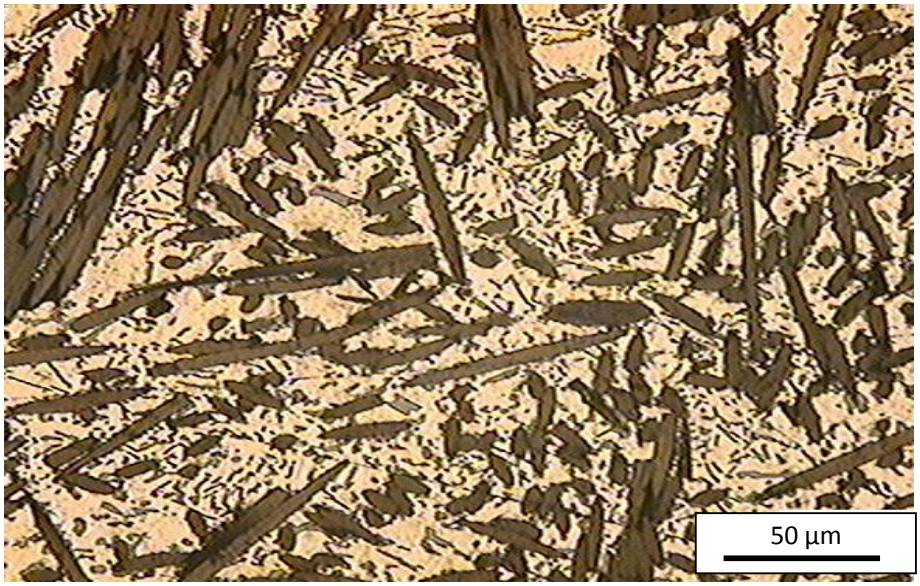

Figure 3 Microstructure of the Al-Gr composite in basal plane

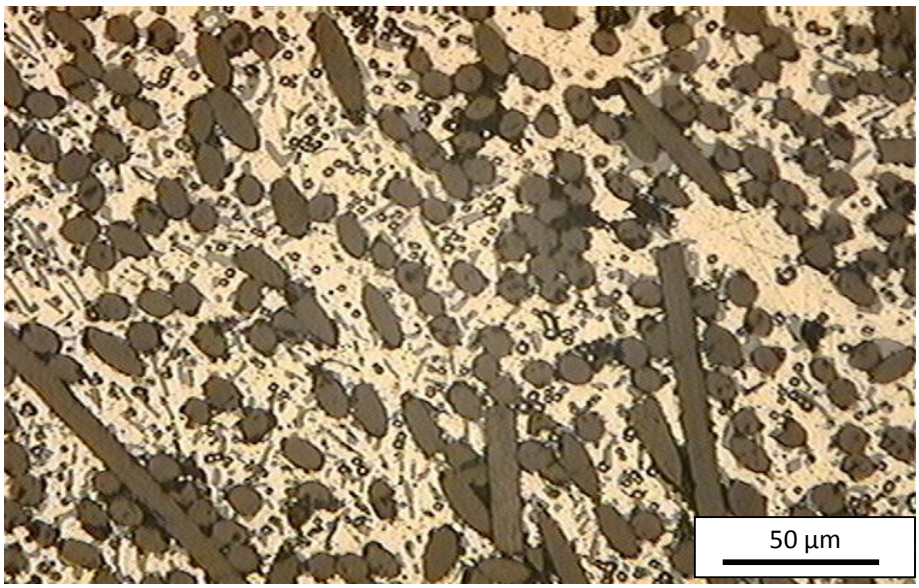

Figure 4 Microstructure of the Al-Gr composite in normal plane

As seen in Figure 3 and Figure 4, graphite fibers are aligned differently in the x-y basal plane than in the normal z-direction. This alignment varies the thermal and

mechanical properties in different directions. The chemical composition of the A413 is listed in Table 2.

Table 2 Composition of A413 (MMCC- http://www.metalmatrixcomposites.com)

Si	**Fe**	**Cu**	**Mg**	**Mn**	**Ni**	**Zn**	**Sn**	**Others**	**Al**
11.0-13.0	2.0	1.0	0.10	0.35	0.50	0.50	0.15	0.25	remaining

The thermo-physical and mechanical properties of the parent MMC is listed in Table 3.

Table 3 Properties of Al-Gr composite (MMCC-http://www.metalmatrixcomposites.com)

TC (W/m°K)	In Plane (x-y)	185-200
	Thickness (z)	125
Cp (J/g-°K)		0.879
CTE (Avg. 20°C to 150°C ppm/C)	In Plane (x-y)	7
	Thickness (z)	24
Tensile Strength (MPa)	In Plane (x-y)	93
	Thickness (z)	37.9
Compressive Strength (MPa)		202.7
Yield Strength (MPa)		109.6
Young's Modulus (MPa)		88942
Flexure Strength (MPa)		158
Electrical Resistivity (µ.ohm.cm)		6.89
Hardness (Rockwell E)		60-80
Density (g/cc)		2.46
Machinability		Excellent

Carbon fibers have high tensile strength and thermal conductivity. Also, as graphite has a negative co-efficient of thermal expansion (CTE), an increase in fiber content will result in a reduction in CTE. The matrix alloy is a pure version of alloy 413, which is essentially an eutectic alloy with some addition of magnesium.

2.3 APPLICATIONS

Short fiber reinforced aluminum alloy is found to replace the conventional metals successfully with improved high temperature properties. Al-Gr composites are used in commercial and defense markets due to their light weight, high thermal conductivity, controlled expansion and thermal management. They also have high applications in telecommunications, automotive, power semiconductor, opto-electronics, military and aerospace heavy transportation, space systems and satellites, medical and industrial lighting. Applications in these areas include microwave, radio frequency (RF), insulated gate bipolar transistor (IGBT), micro-electronic, packaging, laser diode, high brightness LED (HB-LED) and advanced radar. Ultra precision and thermally stable machinery are also designed with these composites (Cornie, et.al; 2003). Figure 5 shows some of the products made with Al-Gr composites for defense markets.

Figure 5 Thermal management products
(MMCC-http://www.metalmatrixcomposites.com)

All the applications requiring high specific stiffness, low CTE, and no out gassing are best suited for these composites. All components are custom engineered, and suitability is determined depending on part geometry and other application requirements. These materials can also replace steel, beryllium, aluminum, and others where weight and thermo/mechanical performance are major drivers (MMCC, 2004).

2.4 SELECTED JOINING METHODS

Most of the published work was on Al-SiC composites. Very limited published information was found on joining of Al-Si composites with Gr fibers. Though MMCs have extraordinary properties, they need special techniques for joining due to their microstructural damage in processing. Lot of creative ways to join composites were found and studied. Controlled heat source from an exothermic reaction of reactive foil can be used to melt a solder layer (Powers, 2004). Inertia friction welding was also performed on SiC reinforced aluminum. It is a solid state welding process

where heat was generated from friction between the parts to be welded. Inertia friction welding of 8009 aluminum alloy with 11% SiC particles was done at 5000 rpm and an initial kinetic energy of 22.9kJ at two different levels of axial force, 111.6kN and 156.2kN respectively, for a weld time of 2 seconds. Welds with tensile strength of weldments exceeding 90% of the parent composite were achieved. Also no evidence of SiC reacting with the matrix was found, and the average micro hardness of the weld zones was comparable to the base material (Lienert, et.al; 1996). Interfacial reactions between carbon fiber and aluminum had been studied as they lead to matrix embrittlement, fiber degradation and brittle phase formation at the interface. For this study, woven carbon fibers were coated with aluminum by PVD under vacuum. These were then heat treated starting at 300°C and going up to 700°C and above to study the effect. Most of the matrix/reinforcement systems were thermodynamically unstable; therefore, any joining process involving high heat input will disturb the existing metastable micro-environment. Prolonged exposure of Al-based/C composites at reasonably high temperatures will promote reactions between aluminum and carbon resulting in the formation of Al carbide phases which will reduce the corrosion resistance and toughness of the material. Many gases such as H_2, CO, CO_2 were released during the heat treatments of the carbon composites (Mercier, et.al; 1993). These gases reacted with aluminum in the matrix to form aluminum carbides and oxides other than the carbide formed by the direct reaction between aluminum and carbon.

The effect of surface tension on microjoining was studied using different models, as it majorly influences the wetting and spreading of brazers. For mm-size beam weld pools, the vapor recoil force acts on the central portion of the weld zone and

displaces the material out. Depression can lead to complete penetration depending on heat flux and material thickness. The effect of beam intensity distribution on melt ejection depends on interplay between reduced dynamic pressure caused by lower velocities and lower restraining pressure caused by decreased radius of curvature (Knorovsky, et.al; 2005). The effect of laser and resistance as thermal sources on welding and brazing is discussed below.

2.4.1 LASER WELDING

Laser welding is a modern welding technique used to join multiple pieces of metal using laser source. Also laser welding is a type of fusion welding which can provide both spot welds and seam welds. This is a high energy beam process and has high welding performance with deep weld penetration and less heat input. In this process, the focal spot is targeted on the workpiece which needs to be welded. Due to its high power density (power delivered by laser per unit area), this highly concentrated light energy will convert into thermal energy and start to melt the surface. This progresses through the material by surface conductance, and thus welding is achieved (Duley, 1998).

Major welding problems of MMCs like poor weld penetration and porosity remained unsolved when CO_2 lasers are used (Yue, et.al; 1998). Nd:YAG lasers are used to overcome these problems as metals show a higher absorbability to YAG laser than CO_2 lasers. Most of the commercially available YAG lasers can produce output wave in a continuous form, and when the laser is operated in pulse mode, different forms of high power waves like sine wave and square wave can be generated (Yue, et.al; 1998). Laser welding of 2124 aluminum alloy reinforced with 17% SiC particles is

performed. Figure 6 below shows the effect of laser waveform and the mean power on the porosity in the welds. It is observed that the best wave form to operate is sin wave mode at high peak power as it is porosity free with a reasonable depth of penetration.

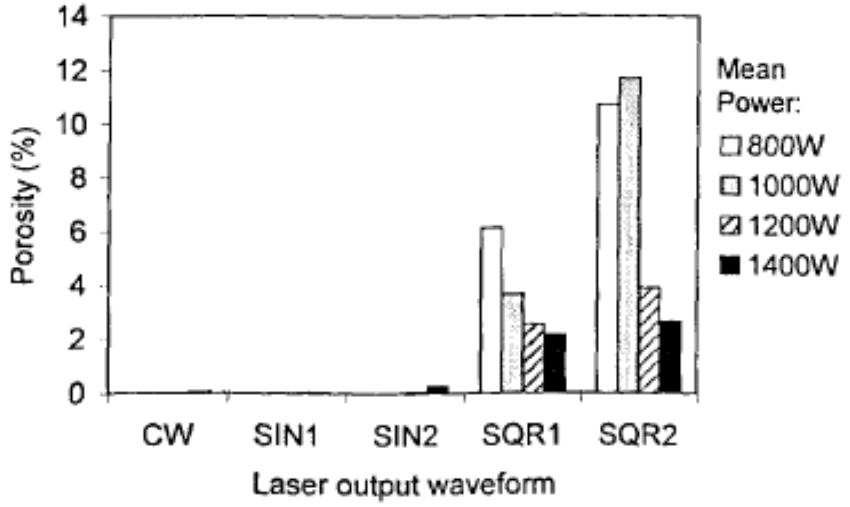

Figure 6 Effects of waveform and mean power on the porosity of the weld (Yue, et.al; 1998)

Figure 7 shows the depth of zone for different mean powers and laser waveforms. It is observed that at same mean power, the square wave produced a deeper weld than the sine wave, and depth increased with the increase in mean power. Results show that the square waveform produces greatest depth penetration of the three different waveforms studied; this is due to the inherent rapid cooling rate of the square wave process.

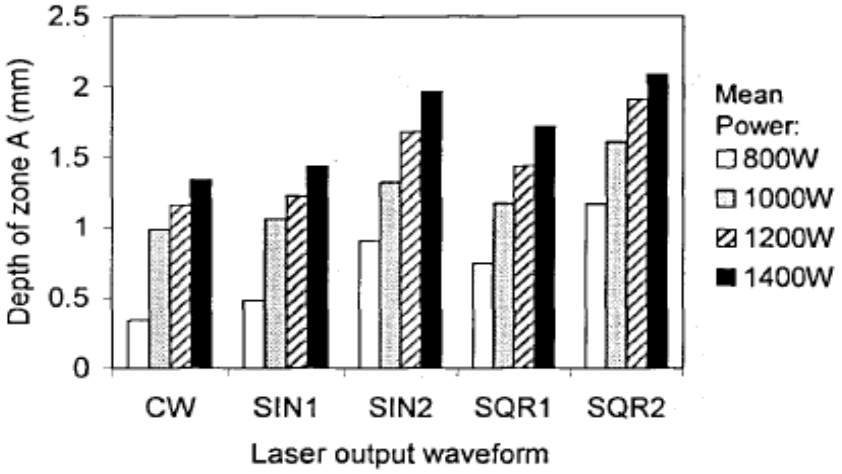

Figure 7 Effects of waveform and mean power on the depth of the weld (Yue, et.al; 1998)

Laser welding of aluminum composites reinforced with SiC particles forms aluminum carbide Al_4C_3 needles at 700-1400 °C that degrade the mechanical properties of the weld (Hung, et.al; 1995). At even higher temperatures, other reaction products, such as Al_4SiC_4 can be formed. When 6061 Al with 20% Vol. SiC is laser welded using 1.06µm YAG laser, it is observed that the increase in the output power increased the interfacial reaction between the SiC and the Al matrix (Liu et.al, 2002). Al_4C_3 can be suppressed by slower heat rate in tungsten inert gas welding; a weldment of Al-SiC composites can have tensile strength approaching 90% of the parent MMC (Mitul, 2005).

Table 4 shows the amount of Al_4C_3 formed with the increase in output power

Table 4 Laser welding parameters for 6061 Al/SiC composite (Liu, et.al; 2002)

Relationship between content of reactant in weld and laser welding parameters

Laser output power (W)	Strength of welded joint (MPa)	Al_4C_3 (wt%)	Si (wt%)
250	187	<1	<1
300	105	<3	<3
350	101	<3	<3
400	74	5	8
450	61	7	13
500	57	7	13

Also a pre-welding treatment with nickel using a brush plating technique is adopted to avoid the carbide formation (Yue, et.al; 1998). Here, laser weld is accomplished using a multiwave YAG laser which operates at a maximum average output power of 2kW. Welds without Al_4C_3 are observed when the samples are coated with nickel. It is observed that the size and volume fraction of Al_4C_3 are inversely proportional to the welding speed (Chen, et.al; 1999). Laser welding of 6061 Al with 25% Vol. SiC is done with CO_2 9kW continuous wave. Table 5 shows the process conditions used for this method. This is because a higher welding speed leads to a higher cooling rate as well as a short interaction time between SiC particles and the aluminum alloy melt, and hence less and finer Al_4C_3 phases are formed. Weld surface quality is better when the feeding direction of shielding gas is the same as the welding direction. This is because the shielding gas opposite to the welding direction pushes the hot plasma plume away from the center, increasing the welding pool temperature and giving more time for the weld to solidify.

Table 5 Process conditions for laser welding of 6061 Al /SiC (Chen, et.al; 1999)

Laser beam diameter (mm)	Laser beam power (kW)	Welding speed (mm/sec)	Shielding gas flow (l/min)	Direction of shielding gas
1.0	2.5	9.0	4.0	Same as welding direction
	3.0	15.0		
	3.5	20.0		
	4.0	20.0		
	4.5	20.0		
	3.0	15.0		Opposite to welding direction

In other words, the shifted plasma leads to more dissolution time of SiC particles into the melt and a lower weld cooling rate during laser beam welding. As a result we have a rougher weld surface and coarser Al_4C_3 formation.

A new method is used to prevent the formation of Al_4C_3 (Chen, et.al; 2000). In this laser beam welding is used to join 6061 aluminum reinforced with 25 vol. % SiC particles with titanium as alloying element. Figure 8 shows the welding process. For this study, a 5kW continuous wave CO_2 laser is used under protection of argon atmosphere. The microstructure of the weld is characterized as functions of alloying content and processing parameters. It is observed that the Al_4C_3 content is suppressed, and a composite reinforced by TiC and Ti_5Si_3 phases is produced in-situ in the laser beam welding joint on this MMC by weld alloying with titanium.

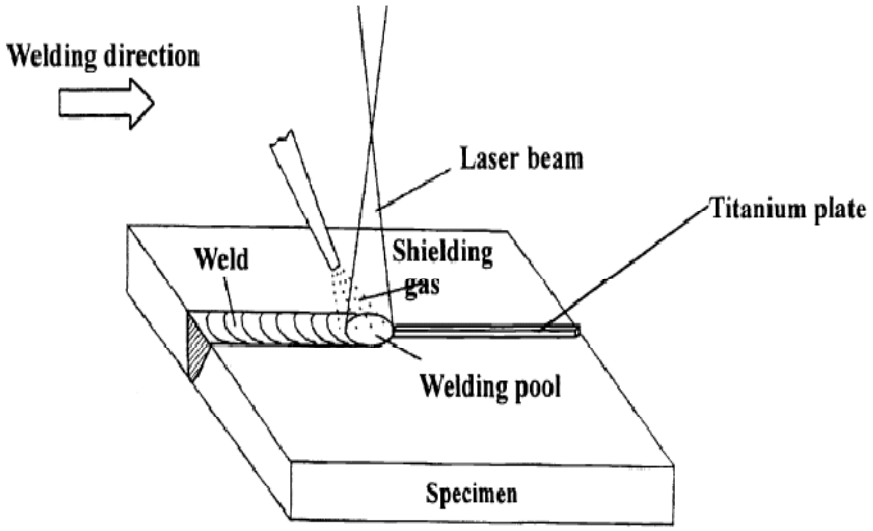

Figure 8 Laser welding setup for 6061 Al with SiC (Chen, et.al; 2000)

2.4.2 BRAZING

Brazing is a metal joining process where a filler metal or alloy is heated to melting temperature and distributed between the close fitting parts by capillary action. Filler then interacts with the base metal and solidifies instantly to form a sealed joint. High frequency induction brazing is used for joining Al-Gr (He, et.al; 2006). A PID is set to control the heat rate. Because of thermal lag, indirect heating is done using a graphite trough. The graphite fibers are 4µm in diameter and comprised of 50 vol %. Three filler materials are utilized: aluminum copper (Al 28Cu 6Si, T_m = 525-535°C), aluminum silicon (Al 10Si 4Cu, T_m = 521-585°C), and aluminum zinc silicon (Al 10Zn 10Si 4Cu, T_m=516-560°C). The filler elements Si, Cu and Zn diffused into the base metal to form Al_4C_3, SiC and $CuAl_2$. Table 6 lists the fillers and their physical/mechanical properties.

Table 6 Composition and properties of fillers used in brazing of Al-C composite (He, et.al; 2006)

Filler	Composition (%)	Melting point: Solidus-liquidus (°C)	Shear Strength (MPa)	Fracture Position
1	Al-6Si-28Cu	525- 535	63.04	Filler + base
2	Al-10Si-4Cu	521-585	75.18	Filler + base
3	Al-10Si-4Cu-10Zn	516-560	35.60	Filler

The aluminum silicon filler produced the best braze with shear strength as high as 75MPa. Fracture is seen at both filler and base materials. Low shear strength is contributed by the development of brittle intermetallic compounds of aluminum carbide and silicon carbide during brazing. This could be due to the high percentage of Si content in the filler materials.

The joining performance of SiC particulate reinforced aluminum metal matrix is investigated by means of vacuum brazing process (Zhang, et.al; 1999). A composite is made using the powder metallurgy method with pure aluminum and silicon powder (particles of 5, 10 and 20μm). The filler material used is Al-Si-Mg alloy. The tests are carried out in a commercial vacuum furnace. Magnesium particles are placed in the furnace during brazing as they deoxidize the oxides. The vacuum levels at the brazing temperatures are 1.2×10^{-3} Pa and 5×10^{-3} Pa. Table 7 is the conditions used for this process.

Table 7 Conditions for vacuum brazing of SiC particles reinforced Al (Zhang, et.al; 1999)

Temperature (°C)	Brazing holding time (min)	Heating rate (°C/h)
580	15	400
590	10	400
600	5	400

The influence of SiC reinforcement, size and volume percentage and brazing parameters on the joint quality is observed. Figure 9 show the influence of SiC amount and brazing temperature on the joint strength.

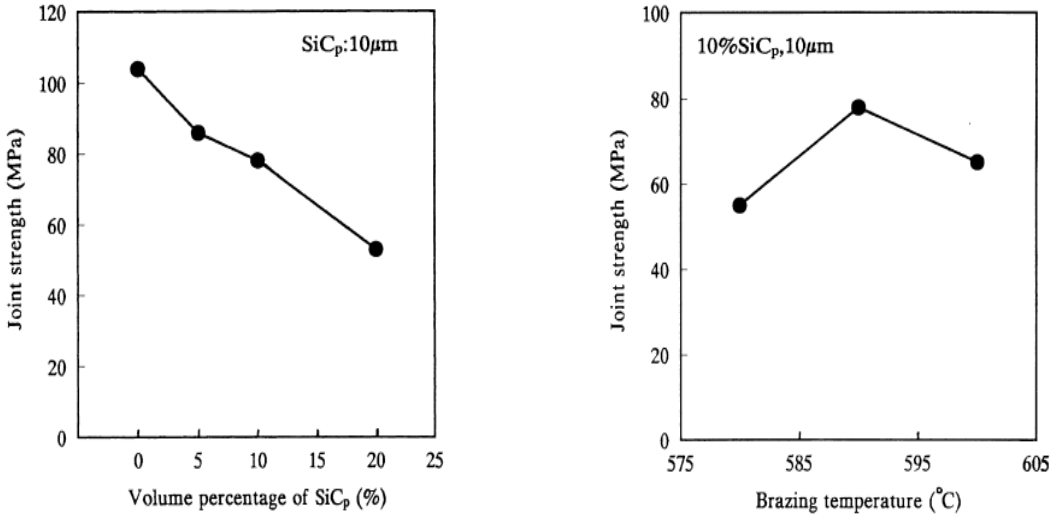

Figure 9 Influence of SiC vol% and temperature on the joint strength of SiC/Al composite (Zhang, et.al; 1999)

As the percentage of SiC increases, more of the SiC exists in the brazed joints resulting in more SiC/Al and SiC/SiC weak bonding interfaces in the joint region; this shows reduced joint strength as indicated in the graph above. The brazing temperature influences the flowability and activity of the liquid filler. This also

affects the metallurgical processes of composite in brazed regions which changes the properties of the joint region (Zhang, et.al; 1999).

Brazeability of aluminum matrix composites is evaluated using BAlSi4 filler material. It is conducted for 6061 and 7005 aluminum alloys reinforced with 10-20% alumina particles. Wettability of the molten braze is found using the sessile drop method. A brazing gap of less than 0.1 mm is maintained in the process. A brazing furnace is used for heating the samples. Specimens are heated at 30°C/min from room temperature to brazing temperature, held at this temperature for 10 min and cooled in the furnace. It is observed that the wettability and spreading increase with the brazing temperature and decrease when the reinforcement proportion is increased (Urena, et.al; 1997). The effect of brazing gap on the properties of the joint was observed (Saida, et.al; 2006). Ni based alloy was brazed with Ag-Pd filler. The tensile strength of the braze joint produced increased with a decreasing brazing gap and reached 70% of the base metal strength at a brazing gap of 0.1mm. Wide gap brazed joints failed at the brazing layer during tensile testing due to the coarsening of the eutectic structure owing to slower cooling rate in the braze layer. The heating method also influences the joint quality. The heating method determines the efficient transfer of heat throughout the joint and doing so within the heat capacity of individual base metals used. Geometry of size and the temperatures needed also play a crucial role in determining the heating method. The rate of heating, thermal gradients, and cooling rates vary primarily based on the heating method chosen (Schwartz, 2003).

2.4.3 RESISTANCE SPOT WELDING

Resistance spot welding is a process in which contacting metal surfaces are joined by the Joule effect. Here the workpieces are held together under the pressure exerted by the electrodes. Resistance microwelding for thin wires is studied. In this the weldability and mechanism of crossed fine nickel wires are observed by controlled trials, and mechanical testing and metallurgical testing were performed (Fukumoto, et.al; 2004).

A study is made to understand the relationship between the input and output variables. Here the effect of change of heat input on the electrode displacement is found for different sheet metals (Jou, 2003). As there is a range of acceptable nugget size for a particular material composition and thickness, there will be an acceptable range for electrode displacement, which is shown in the Figure 10.

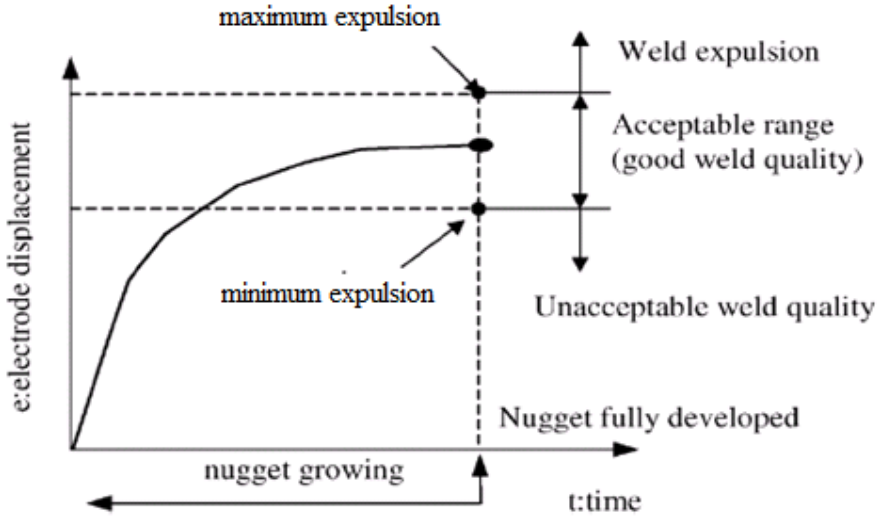

Figure 10 Acceptable range of electrode displacement for spot welding of sheet metals (Jou, 2003)

As the material and joint expansion displaces the electrode, measuring the displacement will determine the weld. Experiments are conducted for different heat inputs, and the electrode displacements are found.

As shown in the Figure 11, the electrode displacement started expanding when the power is given. The drop as observed in the Figure 11 at the second welding time cycle is due to the roughness on the surface which gets flattened from the electrode force. Figure 12 shows the maximum loading for different heat inputs.

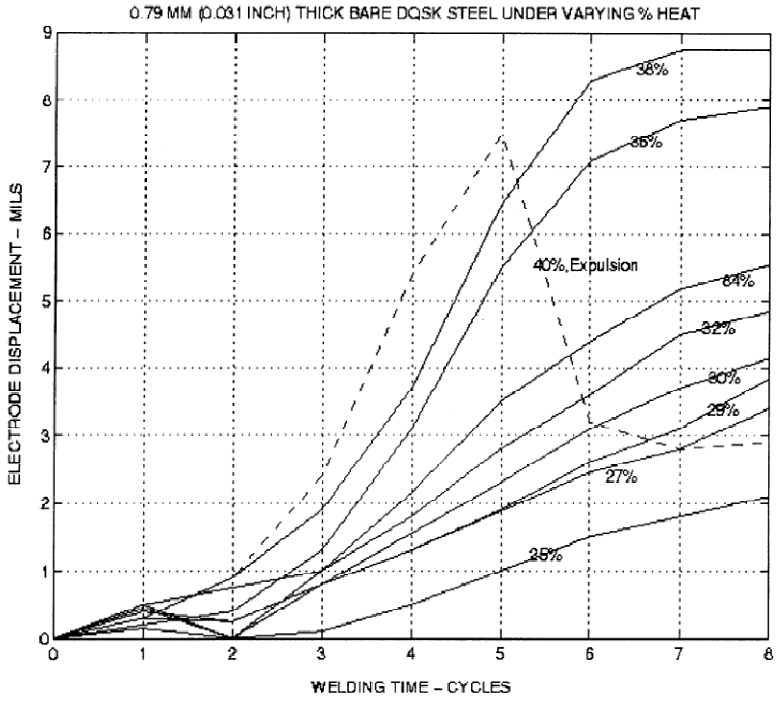

Figure 11 Electrode displacement for different percentage of heat input for spot welding (Jou, 2003)

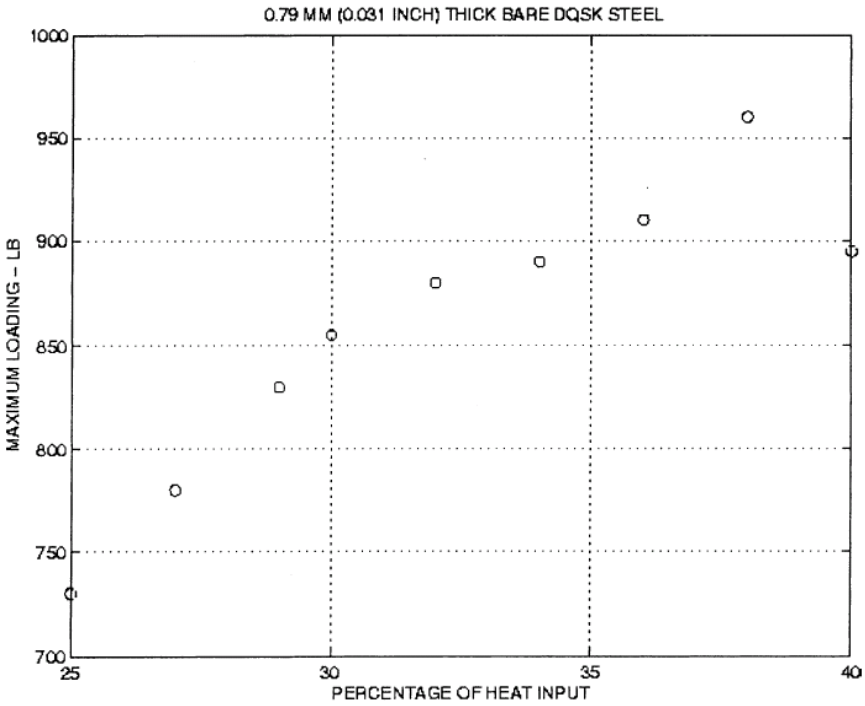

Figure 12 Maximum loading for welds with different heat inputs for spot welding of sheet metals (Jou, 2003)

This will determine the heat inputs to make good welds. It is observed that higher heat inputs can be exposed to higher loadings.

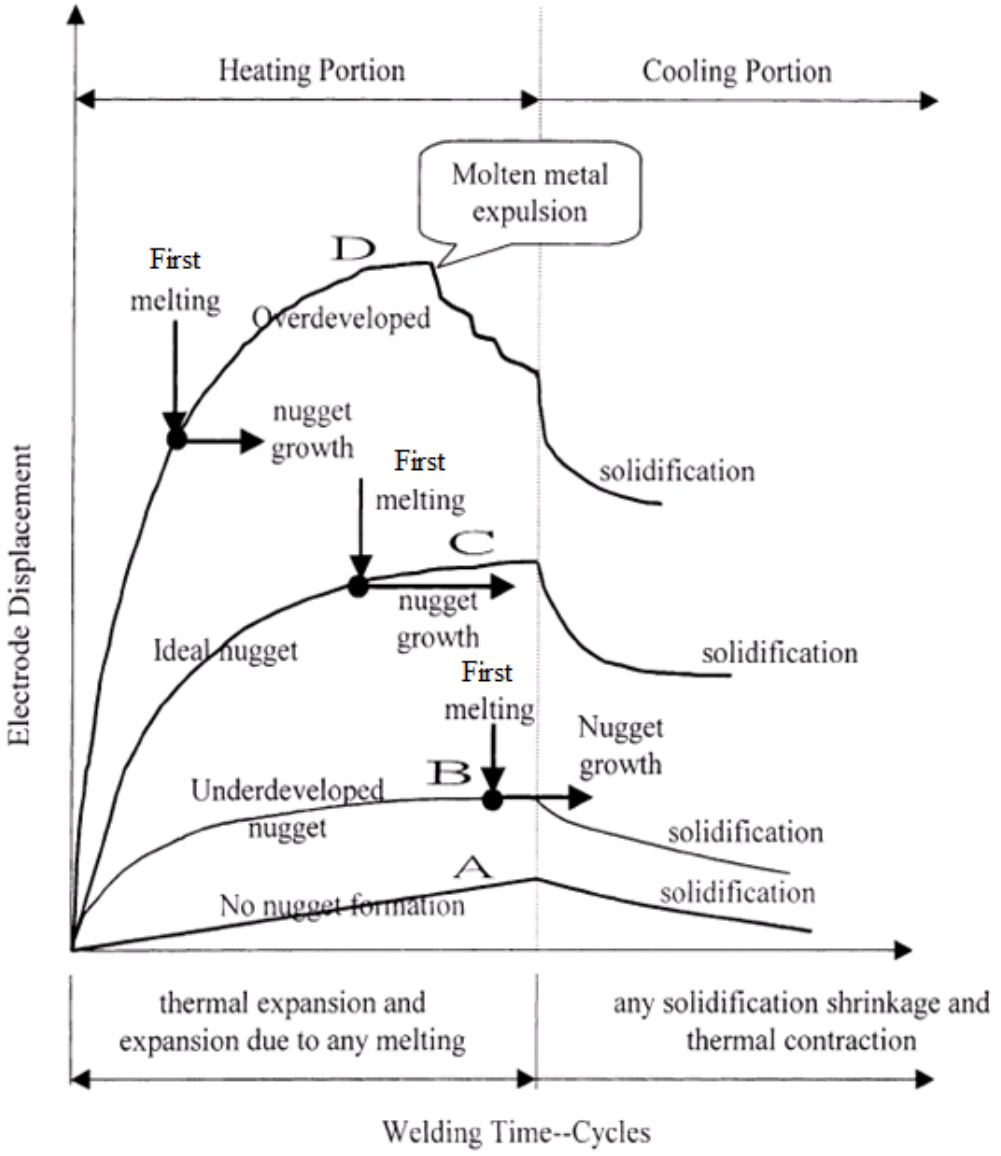

Figure 13 Electrode displacement curves for varying levels of heat input for spot welding (Jou, 2003)

Figure 13 shows the electrode displacement curves for varying levels of applied current. Initially due to the increase in heat and thermal expansion happens due to melting which expands the electrode displacement. Once the current flow is stopped, joints will contract due to the cooling and conduction. This reduces the electrode

displacement. If the applied heat input is too high, melted metal will expel out from the joint. This will create shrinkages and an inconsistent effect on electrode displacement. So, high input has to be avoided to get good welds (Jou, 2003).

2.5 TECHNICAL CHALLENGES IN JOINING OF ALUMINUM COMPOSITES

As discussed earlier, though composites offer many advantages over metals, their implementation depends on how reliably the materials can be fabricated and joined to themselves and to other structural materials. Due to the microstructural heterogeneity and chemical reactions between the components, thermal distortions will occur which will cause microstructural damage and deteriorate the quality of the joints.

General issues with the welding of these composites are as follows:

- degrading interface reactions
- cracks
- improper wetting

2.5.1 EFFECT ON MICROSTRUCTURE

The microstructure of the weld reflects the quality of a joint. A proper blend of matrix and reinforcement can be seen in the microstructure. The following defects are observed in the microstructure of Al-SiC composite joints.

- carbide
- voids
- reinforcement redistribution

Aluminum 6061 reinforced with 25% volume SiC particles is laser welded using 9kW continuous wave CO_2 laser in argon shielding atmosphere using a bead on

plate joint (Chen, et.al; 1999). As the composite has both matrix and reinforcement, the interaction between them and also with the filler material can be known by comparing the microstructure of the weld with the base metal. In most of the work done on SiC composites, formation of carbide is seen in the microstructure of the joint as shown in the Figure 14 below. In this study, interpenetrating graphite/aluminum composites are produced by gas infiltration of aluminum alloys with varying silicon content into graphite preforms. Severe aluminum carbide formation is seen when composites are exposed to ambient conditions. At 750°C and 18 % weight silicon content, reduced Al_4C_3 formation is observed. Further analysis on the formation of Al_4C_3 is shown in thermodynamic analysis (He, et.al; 2006).

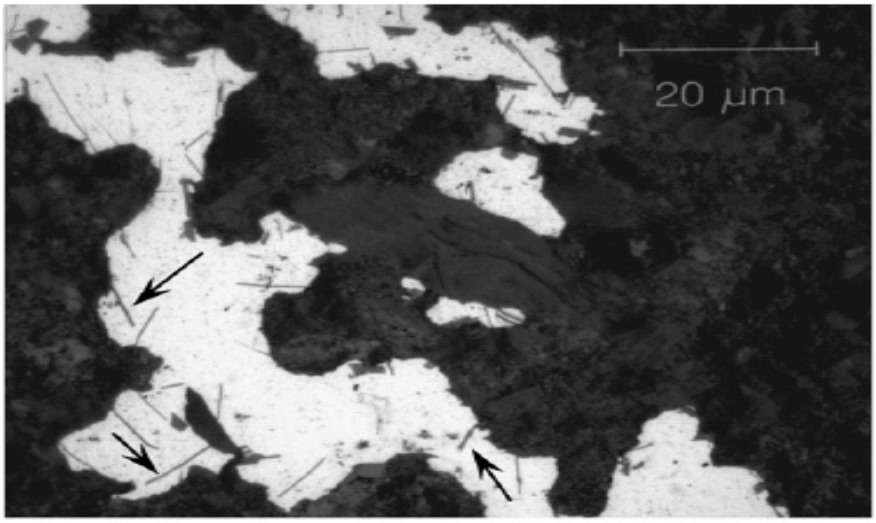

Figure 14 Aluminum carbide formation due to the exposure to ambient conditions (Etter, et.al; 2007)

The size and volume fraction of aluminum carbide are proportional to the laser power density. This results in a higher welding-pool temperature and increased dissolution of SiC particles in the welding pool. Also, the size and volume fraction of the carbide are inversely proportional to the welding speed. Higher welding speed leads to higher

cooling rate and a short interaction time between the matrix and reinforcement. This carbide formation will reduce the corrosion resistance and toughness of the composite. At higher temperatures it can also form Al_4SiC_4. To reduce these formations, various new methods have been employed like plating the composite with nickel coating using titanium alloy. Laser welding of 2124 aluminum alloy reinforced with 17% SiC particles is performed (Yue, et.al; 1998). Bead on plate and square butt welds are made using Nd-YAG laser, with maximum output power of 2kW. Due to the high power density and high temperature concentration, there were pores/voids in the microstructure. Also, the reinforcement (fibers) will redistribute in the weld area and matrix due to high welding speed and high pressure of the shielding gas (Yue, et.al; 1998).

2.5.2 CRACKS

Cracking occurs due to the presence of tensile stress and susceptible microstructure in the weld metal or heat-affected zone. Different types of weld cracking like weld solidification cracking, HAZ liquation cracking, ductility-dip cracking and strain age cracking occur based on the temperature range used for welding. Hot cracking is due to the presence of liquid films along grain boundaries or in the structure. Warm cracking occurs in solid state at temperatures between the solidus and half the melting temperature of the material either during fabrication or during post-weld treatment. If the shrinkage strain exceeds the inherent ductility of the solidifying weld metal, cracking will occur. Variety of methods have been used to calculate cracking. The temperature at which cracking occurs is called Brittle Temperature Range (BTR) (Lippold, 2005). It is the drop in ductility between the liquidus and

solidus temperature, where the width (temperature) and the depth (ductility) of the BTR determines the probability for cracking. Though BTR can determine cracking, the experimental method is proven to be difficult. The transverse varestraint test also measures crack susceptibility. This method gives a range of temperatures over which cracking occurs. Influence of welding variables like travel speed and heat input can be eliminated by using temperature rather than crack length to measure cracking. Ductility dip cracking and strain age cracking occur at elevated temperatures. Tests are made to measure the degradation in ductility as a function of temperature and time and in post weld heat treatment temperature range. These tests can also standardize the weldability techniques after improving them to quantify cracking (Lippold, 2005).

2.5.3 WETTING

One of the major problems with joining carbon composites is the selection of the filler material. Rocher (1989) used the sessile drop method to measure the contact angle of pure aluminum with carbon, around 160°. Since the angle is large, it indicates that the wettability is poor and the surface is highly hydrophilic (Rocher, et.al; 1989). A filler material which has a better wetting with carbon composites has to be selected for a good joint.

2.6 JOINT ASSESSMENT

To determine the weld quality, the microstructure of the weld is compared to the base metal. The strength of the joint is determined by mechanical testing such as tensile, shearing or bending of the joints.

2.6.1 MICROSTRUCTURE

The microstructure of the weld is characterized using optical microscopy and scanning electron microscopy. Welding conditions and the process methods determine the microstructure of the composite joint. Examination of microstructural changes (as discussed in 2.5.1) helps to explain the results from mechanical testing.

2.6.2 MECHANICAL TESTING

Fracture analysis of the joint is done to determine the strength of the joints. Mechanical testing is performed on carbon reinforced aluminum matrix brazed joints (He, et.al; 2006). For this Al-C composite with 4µm carbon fibers are used. High frequency induction equipment is used for brazing. Al-Si-Cu-Zn material is filled between the joints. Phases found at the interface of the fracture surface are Al_4C_3, SiC when Al-C composites are brazed. Usage of zinc in the filler material reduces the shear strength by about 50% as it made the material more brittle. The shear fracture surface of brazed joints using Al-6Si-28Cu filler can be viewed in the Figure 15.

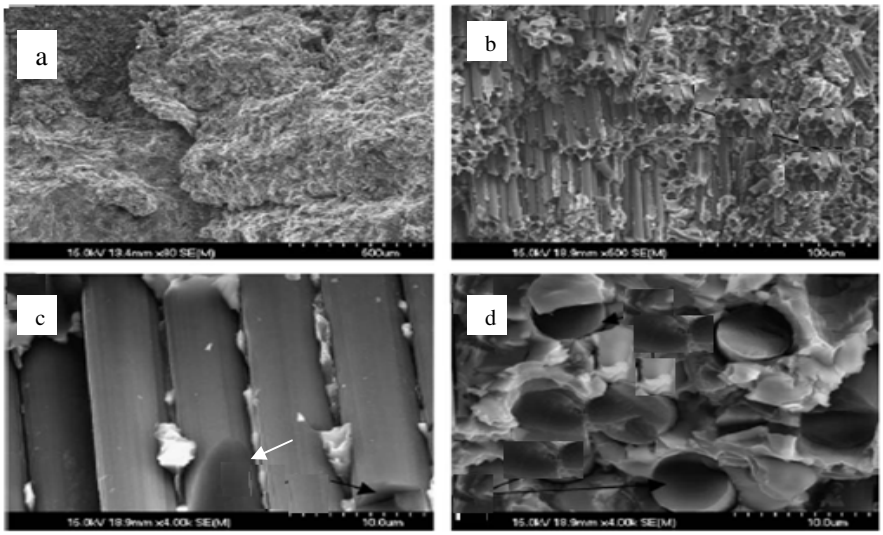

Figure 15 Shear fracture surfaces of the brazed joint (He, et.al; 2006)

The fracture took place in the base metal and seam (as shown in Figure 15a). Fracture mainly happened in the carbon fiber enriched zone. Also the fractured surface of the carbon fiber is very glossy (as shown in Figure 15c). This indicates that though the carbon fiber is brittle, it strengthened the composite and there is no plastic deformation when fracture occurred. Figure 15d shows that the aluminum near the fracture surface had some plastic deformation but the base Al deep inside had no deformation (He, et.al; 2006).

2.7 THERMODYNAMIC ANALYSIS

As previously discussed, interfacial reaction between aluminum matrix and graphite is a major limiting factor in making of sound welds of carbon composites. These reactions between matrix and the fibers can lead to matrix embrittlement, fiber degradation and formation of brittle interfacial phases. These reactions degrade the mechanical properties of the welds and make it more vulnerable to corrosion.

Gibbs free energy is the energy associated with a chemical reaction that can be used to do work. It is defined by the equation,

$$G = H - TS \quad (1)$$

where, H = Enthalpy of the system

T = Temperature (°K)

S = Entropy of the system

For a chemical reaction given as,

$$A + B \leftrightarrow C + D \quad (2)$$

$$\triangle G = G_{products} - G_{reactants} = H_{products} - H_{reactants} - T(S_{products} - S_{reactants}) = \triangle H - T\triangle S \quad (3)$$

where,

C, D are the products

A, B are the reactants

If $G < 0$, the reaction will be spontaneous

Several researchers have suggested that the Al_3C and Al_4C_3 carbides produced by various chemical reactions existed in the Al-C system, but further investigations have supported the existence of aluminum carbide only. It is observed that the formation of aluminum carbide is based on two factors – cooling rate and temperature. It is found that a minimum temperature of $11000\,^{\circ}K$ and a cooling rate of $120000\,^{\circ}Ks^{-1}$ are necessary for the formation of aluminum carbide. Knowledge of these values can help us to control or reduce the aluminum carbide content formed during the welding process (Gopinathan, et.al; 1993). It is concluded that a critical temperature of 727°C would be required for formation of Al_4C_3 plates (Ellis, 1996). This explains no carbide formation at low laser power and the significant transformation of graphite into Al_4C_3 in aluminum matrix at high laser power.

Aluminum carbide crystals are highly sensitive to water due to their hydrophilic nature. This increases their crack growth rates and makes them brittle. Also aluminum carbide decomposes to methane when it comes in contact with moisture. Fibers with high degree of graphitization are smooth, and this prevents the nucleation of carbides (Etter, et.al; 2007).

$$Al_4C_3 + 12H_2O \rightarrow 4Al(OH)_3 + 3CH_4 \qquad (4)$$

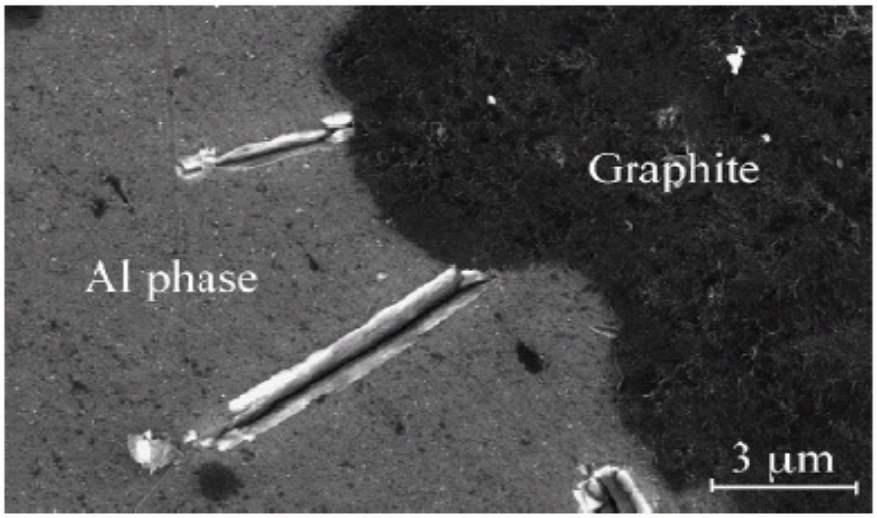

Figure 16 Degradation of carbide in presence of moisture (Etter, et.al; 2007)

Figure 16 shows the degradation of carbide in the presence of moisture. Reaction products are deposited at the Al/Al_4C_3 phase boundary. Also cracks are observed in the aluminum carbide. This is due to the difference in CTE between the Al and C phases and due to thermal stresses generated during the cooling process. Cracks in Al_4C_3 can be seen in Figure 17.

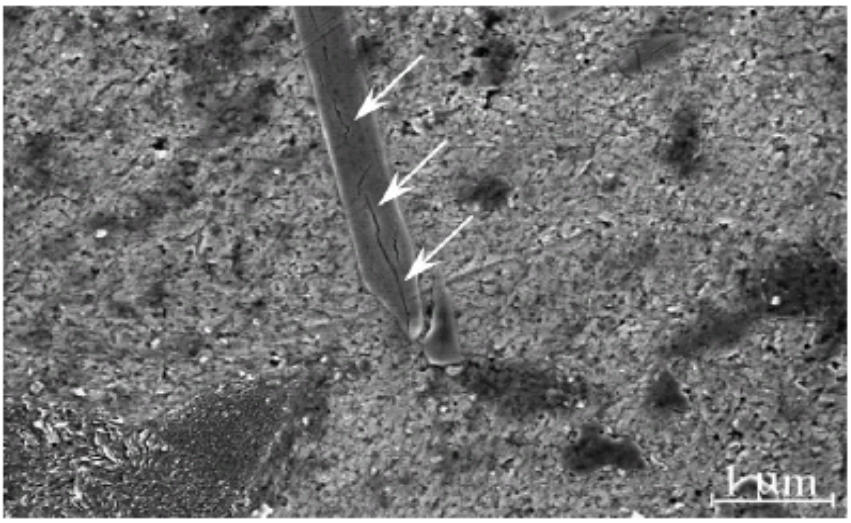

Figure 17 Cracks in aluminum carbide fiber (Etter, et.al; 2007)

The reaction between aluminum and carbon can be seen in the following equations:

$$6Al + 3CO \rightarrow Al_4C_3 + Al_2O_3 \quad (5)$$

$$8Al + 3CO_2 \rightarrow Al_4C_3 + 2Al_2O_3 \quad (6)$$

$$4Al + 3C \rightarrow Al_4C_3 \quad (7)$$

Other researchers reported additional chemical reactions that form silicon carbide when joining aluminum graphite:

$$Al_4C_3 + 3Si \leftrightarrow 4Al + 3SiC \quad (8)$$

$$C + Si \leftrightarrow SiC \quad (9)$$

He (2006) calculated the changes of Gibbs free energy ΔG for these reactions as functions of temperature. If $\Delta G < 0$ then these reactions would happen in the direction from left to right (He, et.al; 2006).

For reaction (7), $\Delta G < 0$ when $(-265{,}000 + 95.06T) < 0$, or $T < 2515°C$

For reaction (8), $\Delta G < 0$ when $(45{,}850 - 72.08T) < 0$, or $T > 363°C$

For reaction (9), $\Delta G < 0$ when $(-73{,}050 + 7.66T) < 0$, or $T < 9263°C$

Different methods are employed to suppress the formation of carbide like coating the reinforcing component with an inert layer. This layer acts as a diffusion barrier and prevents the reaction of aluminum with carbon. Also addition of an appropriate alloying element like silicon can reduce the solubility of carbon atoms in aluminum.

$$G(Jmol^{-1}) = 113900 - 12.06TlnT + 8.92 \times 10^{-3}T^2 + 7.53 \times 10^{-4}T^{-1} + 21.5T + 3RTlna_{[Si]} \quad (10)$$

where, G = Gibbs free energy ($Jmol^{-1}$)

T = Absolute temperature (°K)

R = Gas constant ($J°K^{-1}mol^{-1}$)

a = Activity of silicon in liquid Al

Equation (10) shows the free energy for the formation of aluminum carbide. From this equation we can see that the Gibbs energy goes negative only when the temperature exceeds 1000°K. Also the increase in Si content will reduce the rate at which the reaction (equation 8) proceeds. Hence addition of Si will reduce the Al_4C_3 formation.

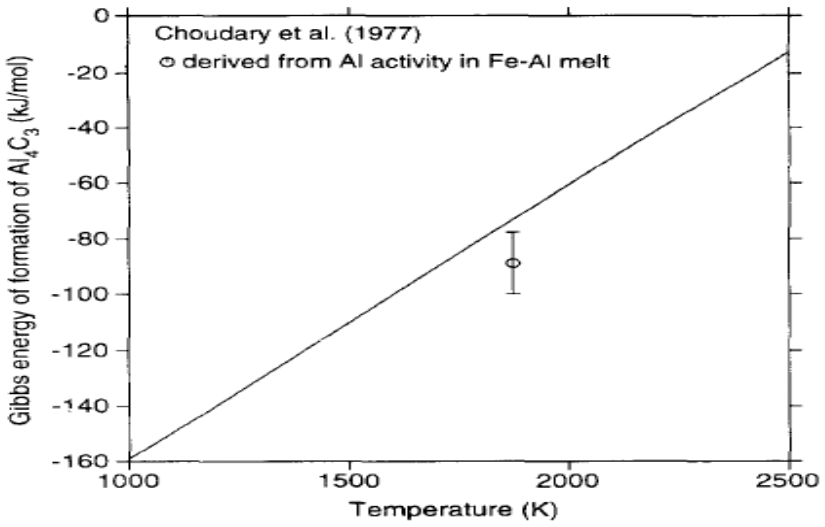

Figure 18 Gibbs energy of formation of Al_4C_3 (Qiu and Metselaar 1994)

Figure 18 shows the Gibbs energy of formation of Al_4C_3 according to the chemical reaction (7). The calculated value of Gibbs free energy at 1873°K is -72.919 $kJmol^{-1}$. Gibbs energy for room temperature is given by for equation (11),

$$\Delta G°_T = \Delta H°_{298} + \int_{298}^{T} \Delta C°_p dT - T\Delta S°_{298} - T\int_{298}^{T} \frac{\Delta C°p}{T} dT \quad (11)$$

Substituting and integrating gives,

$$\Delta G°_T = 33.352lnT - 192.37T - \frac{1.3180\times10^6}{T} - 3.4934\times10^{-2}T^2 - 1.5126\times10^5 \quad (12)$$

As this equation is applicable only between 298 and 932 °K to evaluate the free energy of reaction above this temperature range, free energy for melting aluminum has to be considered. For melting 4 moles of aluminum, free energy is given by,

$$\Delta G°_{4Al_{Liq}\leftrightarrow 4Al_{Sol}} = 34.48TlnT - 177.91T - 0.02477T^2 - 32392 \quad (13)$$

From this the final equation for Gibbs free energy is given by,

$$\Delta G°_T = 67.832lnT - 370.28T - \frac{1.318000}{T} - 5.9704\times10^{-2}T^2 - 183650 \quad (14)$$

Equation (14) is formed by adding equations (12) and (13). Equation (14) is used in this study as it is reliable upto 1273 °K (Aguilar, 2010).

3. EXPERIMENTATION

Several different processes were applied to join the composite. The method of joining influences the strength of the joint, properties and the microstructure of the composite. Also the steps followed for preparing the samples will influence the joint ability. Based on the kind of matrix and the fiber used, suitable filler material has to be selected. For this, melting temperature of matrix and the fiber plays an important role. Since this research concerns a good quality joining of the composite, optimizing the process parameters and following a methodological strategy was needed.

3.1 EQUIPMENT

The following equipment was used for the experiments:

1. IPG laser source (200W max, 1.075µm wavelength) integrated to Haas VF1 computer controlled milling system (Appendix B- Figure B1)
2. Miller Resistance Spot welder (Appendix B- Figure B2)
3. Universal Testing Machine – United Calibration Corp. SFM 30
4. Handimet Grinder Buehler Ltd
5. Buehler Micro polisher
6. Optical Microscope – Olympus STM6
7. Sandblaster Model PBH1000
8. Struers Ultrasonic Cleaning Machine – Metason 200
9. Buehler Isomet low speed saw
10. JEOL JSM-6400 Scanning Electron Microscope
11. Raytek ST- Model Infrared Torch

12. Caswell brush plating equipment

13. Hot plate-WAAGE Electric Inc, Model No: INF 120P, 120V, 1300W

3.2 SAMPLE PREPARATION

The composite was provided by Metal Matrix Cast Composites under the trade name MetGraf 7-200. It was a cast plate of 100x150x12.5 mm^3 (4x6x0.5 in^3). A series of steps were followed to prepare the samples for microjoining.

3.2.1 MACHINING

The plates were sawed using a band saw and then milled to smaller specimens for joining them. The milling cutters used for machining were standard carbide tools. Samples were machined in different fiber orientations and in different shapes, as shown in Figures 19, 20 and 21 based on the experiments performed. Dimensions and views of the models are shown in the Appendix A (drawings 4, 5, 6, 7).

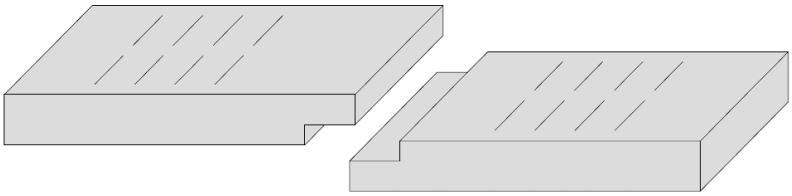

Figure 19 Machined composite samples for resistance brazing

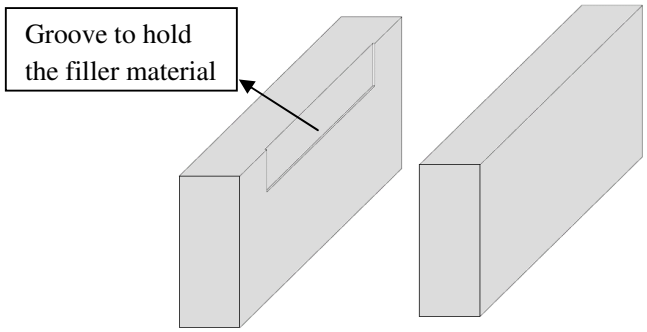

Figure 20 Machined composite samples for laser brazing

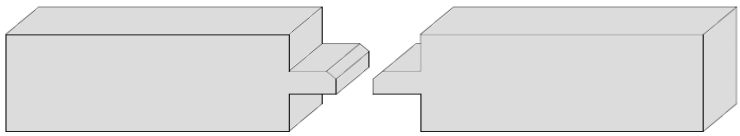

Figure 21 Machined composite sample for laser welding

3.2.2 CLEANING

Once the specimens were machined with the required dimensions, they were cleaned and made ready for experimentation.

The following steps were used before the experiment:

1. The surface to be joined was sandblasted as shown in the Figure 22 for 1 minute covering the area to be welded at a pressure of 482 kPa. Aluminum oxide microabrasives of 120 grit grade were used by placing the nozzle at a distance of 10-15 mm.

Figure 22 Sandblasting composite sample

2. To remove the sand, dry air was blown at 482 kPa

3.2.3 PLATING

Tin and zinc were coated on the composite surface to modify the surface properties. A few samples were electroplated and joined to understand the effect of plating on the joint efficiency. For this purpose, the brush plating method was selected. Plug N' Plate Tin solution has the composition shown in Table 8.

Table 8 Composition of Plug N' Plate tin solution (Caswell-www.caswellplating.com)

Chemical name	**Wt.%**
Sulfuric acid	30
Stannous Sulfate	6
Water & other non hazardous materials	64

Plug N' Plate Zinc composition is shown in Table 9.

Table 9 Composition of Plug N' Plate zinc solution (Caswell-www.caswellplating.com)

Chemical name	**Wt.%**
Zinc chloride	30 – 50
Proprietary non hazardous ingredients	50 – 70

Brush plating was done by following the steps:

1. Plug in the adapter.
2. Clip the negative polarity to the composite to be plated. Composite will act as a cathode.
3. Soak the wand with bandage into the electrolyte solution. Soaked wand acts as an anode and has positive polarity.
4. Brush the wand over the cleaned part which needs to be plated.

Parameters in Table 10 were followed to do the tests.

Table 10 Variable parameters of coated samples

Test number	**Coating type**	**Plating time (min)**
1	Zn	5
2	Zn	10
3	Zn	15
4	Sn	5
5	Sn	10
6	Sn	15

Once the tests were done, microstructure analysis was done to measure the thickness of the coating. Based on that, 10 min coating was selected for further testing.

3.3 EXPERIMENTAL DESIGN AND PROCEDURE

The primary intention of this study was to determine the weldability of Al-Gr composite. For this, it was required to find the optimum conditions for joining. Also the chemical composition and the microstructure of the joint interface and the near interface region play an important role in determining the strength of the joint and its mechanical properties. Typically in graphite composites, the interface reactions between the matrix and the reinforcement at high temperature conditions will deteriorate the properties of the composite. To have the mechanical properties close to the parent composite, the processing parameters should provide the right environment for an adequate bonding between the filler and the base composite used. It thus was vital to find the optimized conditions for joining the MMC. A design of experiments tool was used to analyze the process parameters and determine the process conditions. Two level factorial designs were used. These levels are designated with symbols ‘1’ for ‘high’ and ‘0‘for ‘low’, respectively.

Design of Experiments follows the following steps:

1. To identify all the possible process variables.

2. Preliminary factorial tests to rule out the non-significant variables.

3. Final factorial tests with significant variables.

4. Optimize these variables for best processing conditions.

3.3.1 WELDING

Design of Experiments - Several input parameters for laser welding of carbon composites were considered for this study. It was observed that welding power, welding speed, and the depth of focus have major influence on the joint quality. They were selected for preliminary factorial tests. All these variables were independent of each other. The number of input parameters was limited based on the MMC blocks available, amount of time required for laser welding and preparation for metallographic analysis. All the possible process parameters were: laser power, laser speed, shielding gas pressure, preheats temperature, joint design and depth of focus.

Once the input variables were determined, output variables were also selected which can determine the strength and the quality of the weld. Microstructure analysis was considered as it will determine the effect of heat on the weld. By studying the literature data and conducting preliminary tests some independent variables were selected. By varying these variables and keeping the others constant, final experimental work was conducted. Figure 23 below shows the input parameters that were varied and the output parameters selected to know the weldability of the joint.

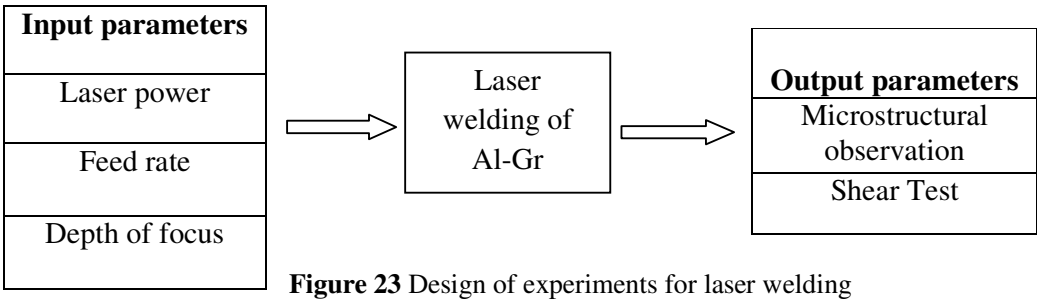

Figure 23 Design of experiments for laser welding

Values of input parameters varied at 2 levels are shown in Table 11:

Table 11 Input parameter values for laser welding

Input parameters	**Low level**	**High level**
Feed rate (mm/min)	50.8	102
Laser Power (W)	120	160
Depth of focus (mm)	1.27 below	1.27 above

Values of the constant parameters are shown below in Table 12:

Table 12 Constant parameters for laser welding

Constant parameters	**Value/Description**
Welding position	Flat
Shielding gas (type, pressure, flow rate)	Argon, 413.6 kPa, 5625 cm^3/min
Preheat temperature	175°C

Factorial experimentation is shown in Table 13:

Table 13 Factorial experimentation for laser welding

Test run	**Laser Power**	**Feed rate**	**Depth of focus**
1	1	1	1
2	1	1	0
3	1	0	1
4	0	1	1
5	1	0	0
6	0	1	0
7	1	0	0
8	0	0	0

Experiment procedure- Before conducting the experiment on the CNC laser, the nozzle gap was found.

Following steps were taken to measure the optimal nozzle gap:

- A NC program was coded which moves the nozzle by 2.54 mm high with a dwell time of 1sec for every point until it moves to 25.4 mm.
- From these points, the smallest hole formed was considered and for that height a similar program with increments of 0.254 mm was run for 10 times.
- Again, the smallest hole formed through this program was considered and third program with increments of 0.0254 mm was run.
- After 3 runs like this, the smallest hole was found and that height would be the required nozzle gap.

The gap measured through this experiment was 2.65 mm.

The following criteria were considered for designing the fixture for laser welding:

- Samples have to be held with no space in between them.
- We should be able to preheat the fixture and place it on the machine for welding. For holding it, side screws were fixed.
- Fixture should be able to hold pieces of different lengths and thicknesses.

A fixture for laser welding is shown in Figure 24, and Figure 25 shows the fixture holding the composite samples for laser welding; its dimensions are documented in appendix A – Drawing 1.

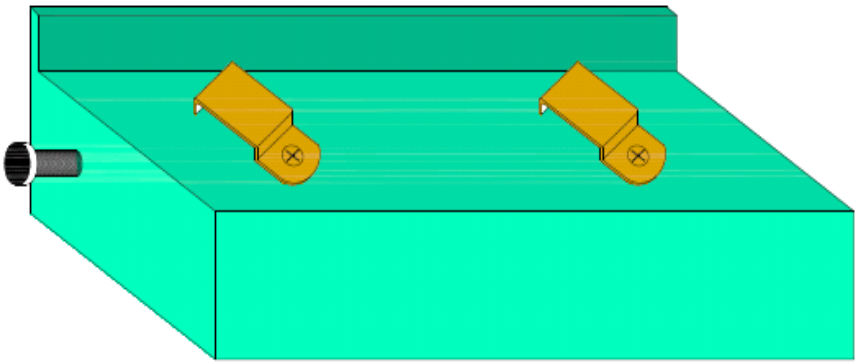

Figure 24 Fixture for laser welding

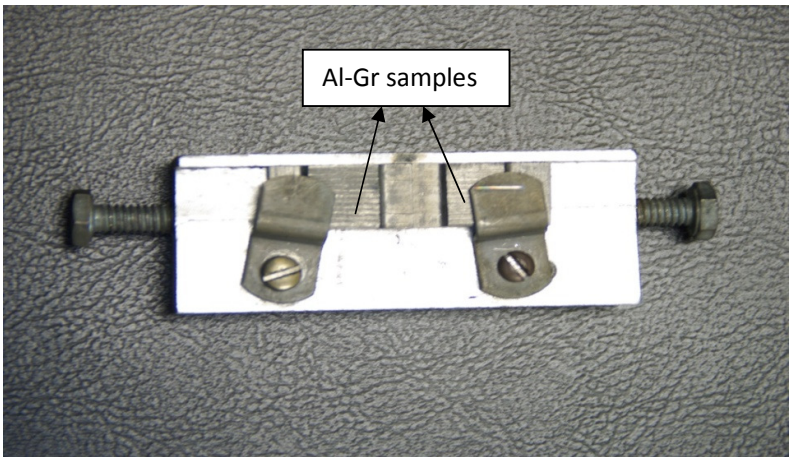

Figure 25 Set up for laser welding

Pieces were clamped tightly together, and the laser heated the joint surface to melt and weld them.

The steps followed for laser welding were:

1. Samples were sandblasted and cleaned ultrasonically.
2. Once the samples were ready, they were placed in position on the fixture and held tightly.
3. These samples were placed on the hot plate for pre heating. An infrared thermometer was used to measure the temperature.

4. Once the samples reached to a temperature higher than the preheat value of 175°C, they were placed in position under the nozzle which was set to the program to be carried.
5. The CNC program shown in appendix C- Program 1 was run in the presence of argon gas at a pressure of 413kPa. The laser parameters, like power and weld speed, were varied in this experiment following the Design of Experiments tool.
6. Off-focus welding was achieved by moving the nozzle relative to the position of the focal plane.

Once all the conditions as per the DOE were tested, all the welds were further set for microstructure analysis.

3.3.2 BRAZING

Laser brazing and resistance spot brazing were employed in this work.

3.3.2.1 Filler material and Flux

Filler material - The melting temperature of A413 matrix, approximately the eutectic temperature of Al-Si alloy was 577°C. So welding must be done at a higher temperature, while brazing and soldering can be performed at lower temperature. Filler material with a melting point less than A413 matrix was selected. Composition of the filler material used for brazing is shown in Table 14, and its physical properties are shown in the Table 15.

Table 14 Composition of Al822 brazing filler
(Lucas Milhaupt-www.lucasmilhaupt.com)

Element	Aluminum	Zinc	Cadmium	Lead	Other elements
Composition	22% ± 1.0%	Remainder	0.01% Max	0.1% Max	0.15% Max

Table 15 Physical properties of Al822 brazing filler
(Lucas Milhaupt-www.lucasmilhaupt.com)

Property	Color	Melting point (°C)	Flow point (°C)	Brazing range (°C)	Density (Lbs/in^3)
Value	Grayish white	426	482	485 -537	0.231

The properties of a brazed joint were dependent upon numerous factors like base properties, joint design and metallurgical interaction between the base metal and the filler metal. Joint clearances of 0.076 - 0.127mm (0.003 - 0.005in) per side were optimum for achieving highest joint strength.

Flux - Handy Flo 751 is a non-corrosive flux system designed for use with aluminum brazing filler metals for joining them in an open air brazing process. It is applied on the surface to be brazed before joining. This flux consists of an exclusive combination of fluoride compounds. It melts and becomes active by 540°C.

3.3.2.2 Resistance Brazing

Design of experiments- Similar to laser welding, the design of experiments tool was used to determine the significant variables for obtaining a good quality joint. The possible parameters were: braze current, brazing time, preheat, electrode force, brazing gap, joint design and coating type. Coating was considered here to improve the adherence between the filler and the base composite. Few preliminary tests were

conducted to know the possible range of values for the variables. Number of cycles was also selected as a parameter as it gave time for preheating the composite in the first time and then melting the filler to braze in the second cycle. Since the number of cycles and braze time were depending on each other and the time input for the machine was limited from 1-9 sec, Table 16 values were taken for conducting the preliminary tests.

Table 16 Input parameter values for resistance brazing

Current (A)	**Cycle time (s)**	**# cycles**
2.5	8	2
3	6	2
3.5	4	2
3.5	9	1
4	3.5	2
4	7	1

Constant parameters for this process are listed in Table 17.

Table 17 Constant parameters for resistance brazing

Constant Parameter	**Value/Description**
Clamping pressure (kPa)	172
Filler Material	22%Al- 77.74%Zn
Holding time (sec)	2
Joint Design	Lap joint

Based on these tests, values for the final tests were determined. The output variables were then selected which can evaluate the strength and quality of the joint. Out of all the possible input variables, two variables were selected due to the limited number of MMC blocks. All the input and output variables for this process are listed in the Figure 26

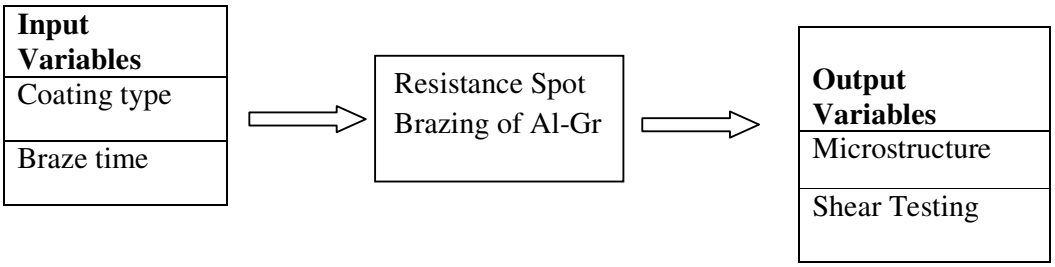

Figure 26 Design of experiments for resistance brazing

Table 18 values were the final parameters considered. Also the tests were repeated twice to know the consistency in the results.

Table 18 Final parameters for resistance brazing

Parameter	**Value/information**
Coating type	No, Zinc, Tin
Braze time (sec)	6, 8
Clamping pressure (psi)	30
Current (A)	3
Coating time (min)	10

Experiment Procedure - Preliminary tests were carried out, and a fixture has been fabricated on mill to hold the samples in position between the electrodes. Design was made considering the following criteria:

- Samples should be held in position firmly for a lap joint.
- Space should be given for holding samples between the electrodes where the joint has to be made.
- Clamp should be able to hold pieces of different thicknesses.
- Concentration of the heat should be on the composite-filler-composite.
- Flow of current should be prevented into the fixture.

Based on these, the following fixture was made and painted to insulate and prevent the flow of current into the fixture.

Fixture can be seen in Figure 27, and its dimensions are shown in Appendix A – Drawing 2.

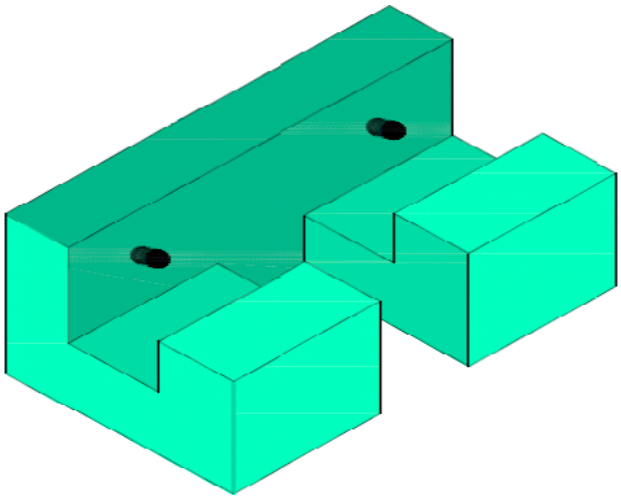

Figure 27 Fixture for resistance spot brazing

The steps followed for resistance brazing were:

1. Sandblast and ultrasonically clean the composite samples.
2. Press the filler material to the required thickness and clean it ultrasonically
3. Apply flux on the composite surfaces to be joined.
4. Filler is placed between the pieces and held firmly in position using the fixture.
5. Required parameters were set on the spot welder and the brazing was done for all the tests.

Spot brazing was done as shown in the Figure 28.

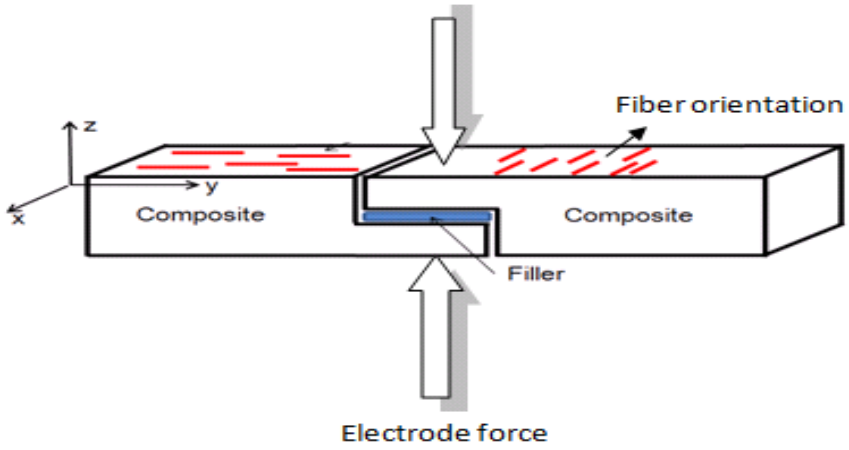

Figure 28 Resistance spot brazing

3.3.2.3 Laser Brazing

Designs of Experiments - Similar to laser welding, preliminary tests were done on the composite to know the heat required to melt the composite. High and low feed rates were considered to know the influence of feed rate, and different powers from low (60) to high (140) were considered. Laser spot size was measured to be 5.024×

10^{-3} mm^2. A very high power range was not considered as it can melt the composite. Feed rates and the laser power values are tabulated in Table 19. An experiment was run on the Al-Gr composite with the laser integrated VF1 to measure the efficiency of the machine. The microstructure of the composite for these tests was evaluated to measure the weld area. The area of the weld was measured by drawing a grid of 0.4mm × 0.4mm on the picture of the melted area and counting the grids. Also the total resistance of 2 Al-Gr and 2 Cu pieces used in resistance brazing of Al-Gr composite was measured using an RMS multimeter 430 and found to be 0.7 Ω. Based on these, calculations were done and further analysis was made (refer to 4.3). The design of experiments tool was used. Parameters considered for laser brazing were: laser power, feed rate, filler thickness, gas flow rate, joint design, number of passes, clamping pressure, and the filler material. Of these possible parameters based on their influence on the brazing, a few were selected as significant, and factorial experiments were conducted, varying these variables.

Table 19 Preliminary test variables for laser brazing

Trial	**Power (Watt)**	**Power density (kW/mm^2)**	**Feedrate (mm/min)**	**Feedrate (mm/sec)**
1	60	12	25.4	0.42
2	80	16	25.4	0.42
3	100	20	25.4	0.42
4	120	24	25.4	0.42
5	140	28	25.4	0.42
6	140	28	254	4.23
7	120	24	254	4.23
8	100	20	254	4.23
9	80	16	254	4.23
10	60	12	254	4.23

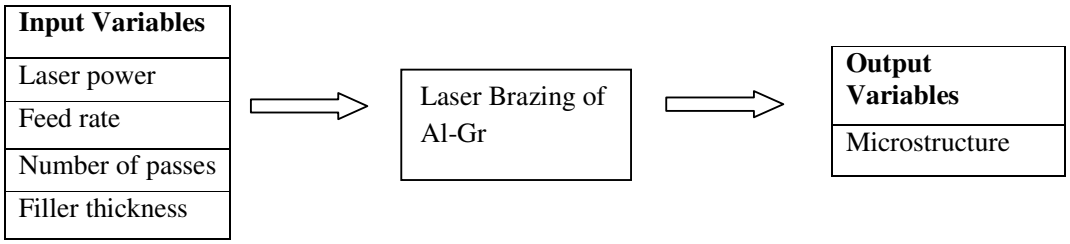

Figure 29 Design of experiments for laser brazing

Figure 29 shows the design of experiments for laser brazing and Table 20 shows the tabulated values of these input variables.

Table 20 Input variables and values for laser brazing

Parameter	Low Level	High level
Power (W)	80	90
Feed Rate (mm/min)	25.4	50.8
Number of passes	2	5
Filler thickness (mm)	1	0.5

A vertical slot, 2mm ×2mm ×0.1mm, was made on the samples as shown in Figure 30. Its dimensions are shown in appendix A – Drawing 6.

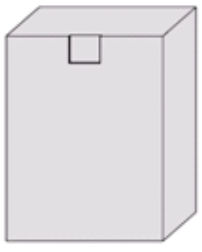

Figure 30 Machined sample for laser brazing

Also care has to be taken that the volume of the filler was greater than the volume of the slot made in the composite sample for holding it.

Parameters left constant are shown in Table 21 with the values considered.

Table 21 Constant parameters and values for laser brazing

Constant Parameter	**Value**
Argon gas pressure (kPa)	413
Filler type	22%Al- 77.74%Zn
Argon gas Flow rate (cm^3/min)	5625
Compressed air pressure (kPa)	400

Experiment Procedure - Preliminary tests were carried to understand the influence of process variables. Flux and filler material used for resistance brazing were also used for this process. A fixture was fabricated to hold the pieces and to apply the pneumatic pressure using the compressed air. Figure 31 shows the fixture made for this process. Dimensions of the fixture are shown in detail in appendix A – Drawing 3.

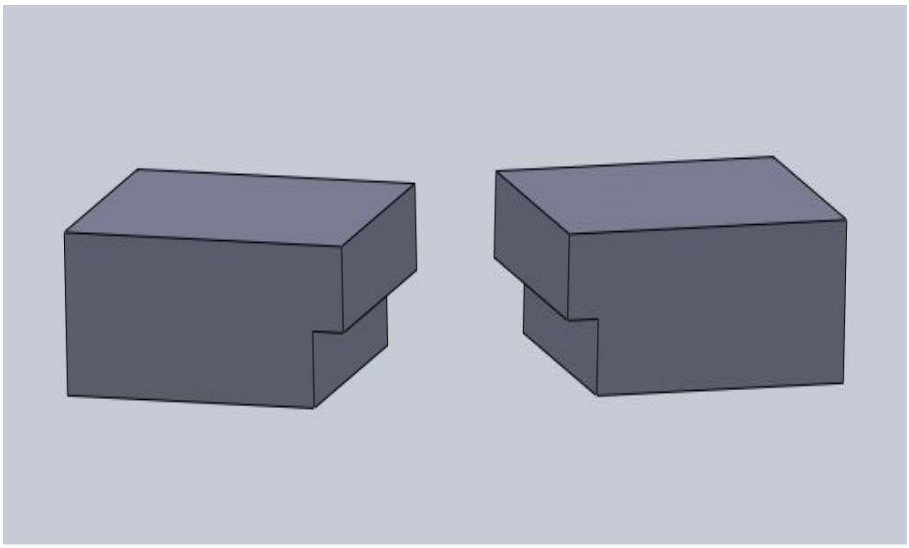

Figure 31 Fixture components made for laser brazing

The set up for laser brazing is shown in Figure 32.

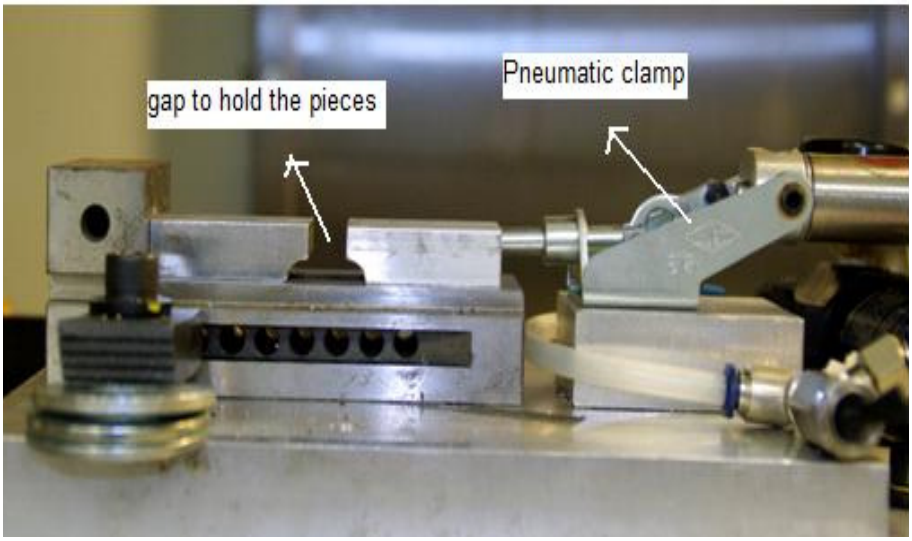

Figure 32 Set up for laser brazing

The steps followed for laser brazing were:

1. Samples were sand blasted and cleaned ultrasonically.
2. Filler material was pressed and flux was applied on the surfaces in contact with the filler material.

3. Filler was placed between the samples and held in position on the fixture using the pneumatic clamp.
4. All the parameters were controlled based on the design of experiments.
5. Argon gas was allowed to flow on the surface and care was taken to avoid the laser rays.
6. All the samples were brazed using laser and all the tests were performed.

Clamping pressure was applied to hold the pieces firmly in position. The height of the fixture was made less than the height of the samples held to avoid the laser nozzle crashing onto the fixture. Based on the height at which the clamp probe was held, a fixture was made such that the maximum probe force was applied on the fixture. Once the pieces were held firmly, the laser was used for brazing the samples with the process parameters mentioned, and a CNC program shown in appendix C- Program 2 was run on the brazing area.

3.4 METALLOGRAPHIC SAMPLE PREPARATION

The following steps were performed to study the microstructure of the joints.

- Mounting
- Grinding
- Polishing
- Etching

Mounting: Samples were cold mounted using Epofix embedding resin and a Epofix hardener.

The steps followed were:

1. Degreased the specimen before it was placed in the mold.
2. Mixed 15 parts by volume of resin with 2 parts by volume of hardener (25 parts by weight of resin with 3 parts by weight of hardener) in a paper cup and stirred carefully for at least 2 minutes.
3. Poured the mixture carefully over the specimen in the mould; so that no air bubbles were caught, and let the mixture harden.

This mold was left undisturbed for 24 hrs to solidify.

Grinding: Figure 33 shows the grinding of molded samples. Manual grinding was done on a Handimet grinder. Pressure sensitive abrasive papers with 4 different grit sizes were used. We used Grits 240, 320, 400 and 600 respectively to obtain a smooth surface.

Figure 33 Grinding the molded samples

Polishing: Figure 34 shows polishing of the composite samples. A buehler micro polisher was used for this process. Alumina powder was mixed in water and poured on the polishing wheel. The sample was placed on the wheel and alumina particles were allowed to rub the surface by rotating the wheel. Alumina particles of 1µm, 0.3µm and 0.05µm were used for this process. By the end of this process, a 0.05µm finish was achieved on the sample surface.

Figure 34 Polishing the molded composite samples

Etching: 3 drops of HNO_3 and 3 drops of HF were mixed in 25ml of water at room temperature and samples were etched in this solution for 12sec. Then the microstructure of the joints was examined using both the optical microscope and the scanning electron microscope.

Shear test: The strength of the joint and the joint quality was determined by shear testing using the UTM. For this analysis, lap joints were made for all three (no coat, tin and zinc), and they were held in the UTM using and "S" shaped joint. The "S" shaped joint was made of steel which was tougher than aluminum. This prevents the deformation of steel joint before maximum force was exerted on the joint. This joint helped the welded joint to align itself to the jaws holding the pieces.

The gauge length was measured and the load cell and the extensometer were connected to the machine. Load cell capacity of 133446 N (30,000 lbs) and a preload of 44 N (10 lbs) were used for the test. Shear testing of the joints was done by applying load to pull the pieces as shown in the Figure 35.

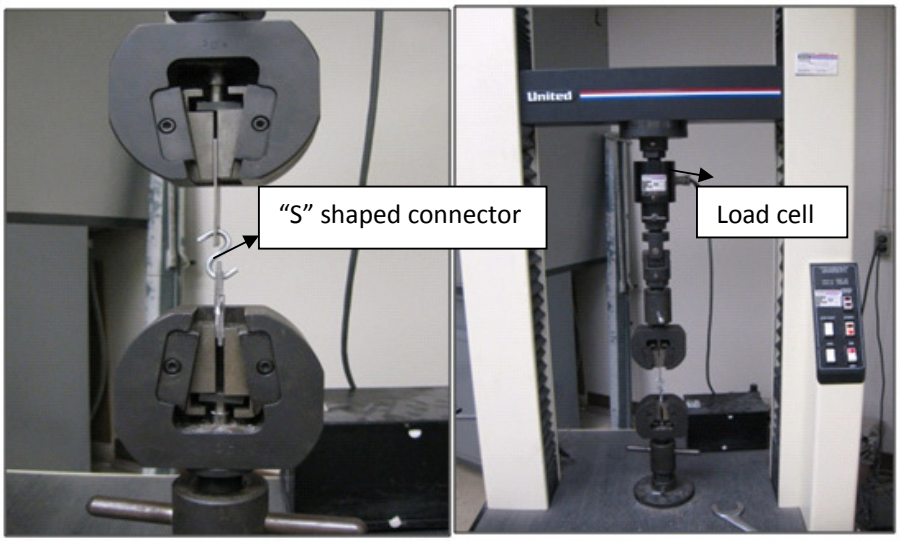

Figure 35 Joints held on the UTM for mechanical testing

4. RESULTS AND DISCUSSION

Once the preliminary tests and the final tests were done, further analysis has been done to evaluate the microstructure and joint strength.

4.1 LASER WELDING

There are 3 zones in the weld which are shown in Figure 36

1. Melting Zone
2. Heat affected Zone (HAZ)
3. Parent composite

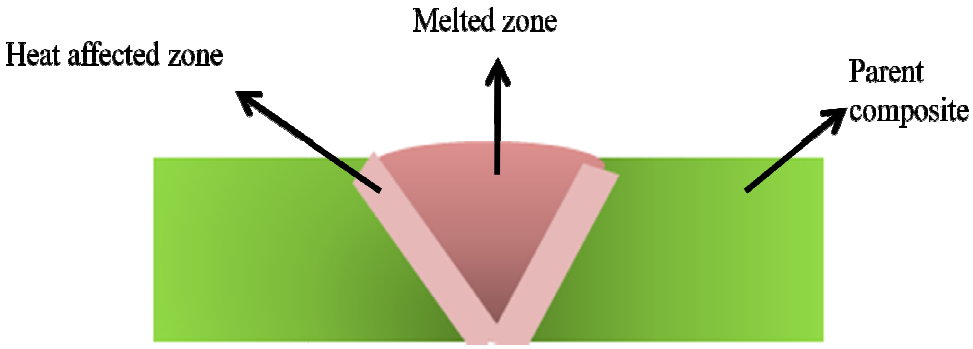

Figure 36 Zones in laser welding

All the three zones are shown in the microstructure in Figure 37.

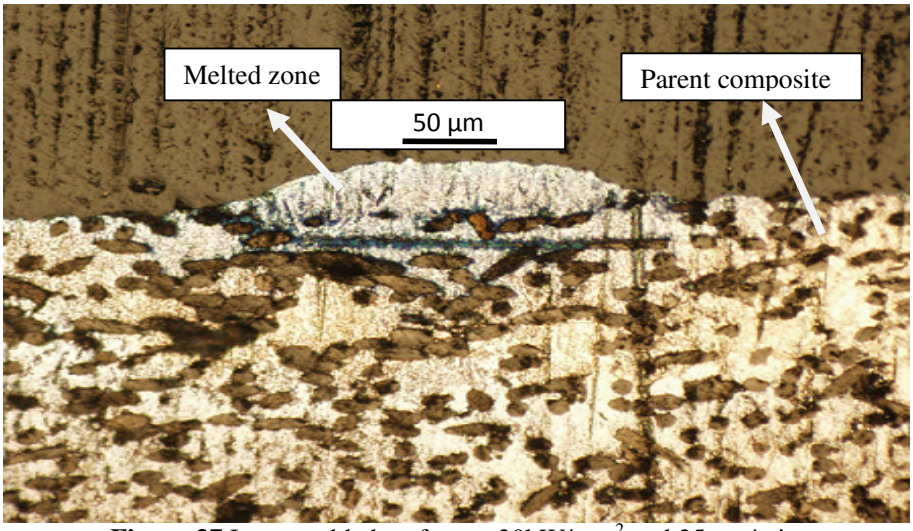

Figure 37 Laser welded surface at 20kW/mm^2 and 25mm/min

The laser beam melted the composite, but it delaminated the fibers in the surrounding heat affected zone (HAZ).

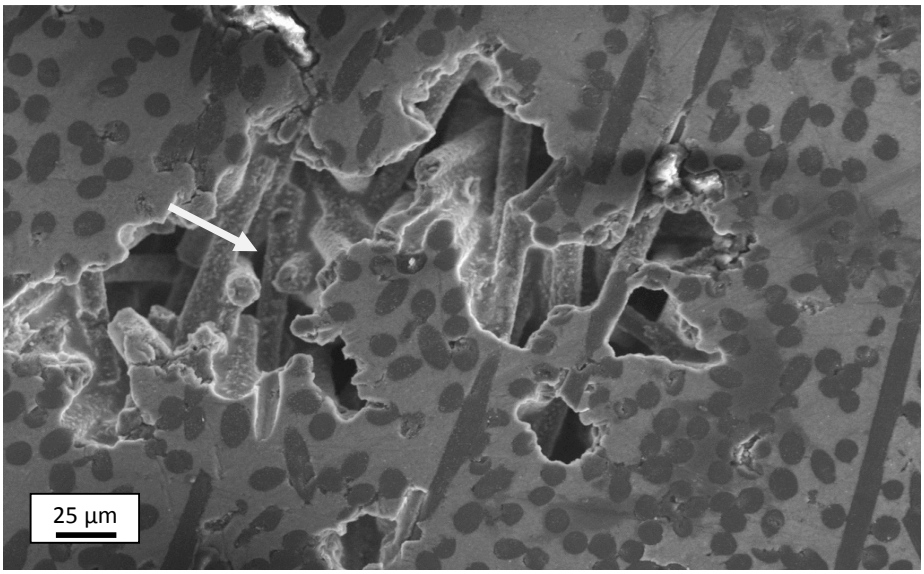

Figure 38 Delaminated fibers (at arrow) from the matrix after laser welding (0.05in below, 350F preheat, 50mm/min, 32kW/mm^2)

Figure 38 shows the delamination of fibers, which is due to the difference in thermal coefficients of fiber and the matrix. These will result in the differential contractions

and cause residual stresses. These residual stresses will delaminate the fibers from the matrix in the heat affected zone. This will degrade the properties of the composite joint and result in a cracked surface once subjected to loading.

Voids and pores are found in the weld and parent composite region. These are due to the solidification defects, low wettability of carbon fiber to matrix and the high viscosity of molten composite which will block the gas bubble from escaping resulting in pores and voids. Figure 39 shows pores. Porosity and cracking also increase with the intensity of the laser.

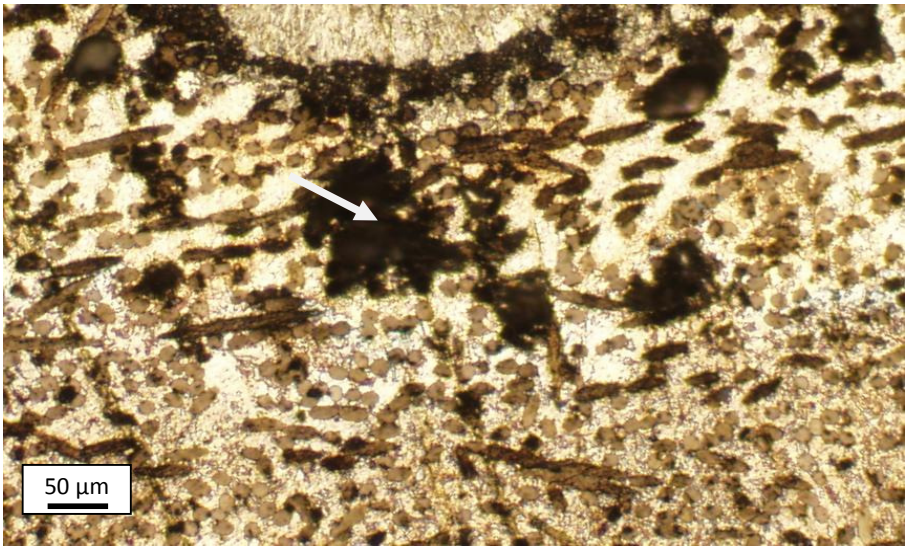

Figure 39 Porosity (at arrow) in the composite due to laser welding (28kW/mm^2, 25mm/min)

Also, melted aluminum matrix reacts with the carbon from fiber to form aluminum carbide as shown in Figure 40.

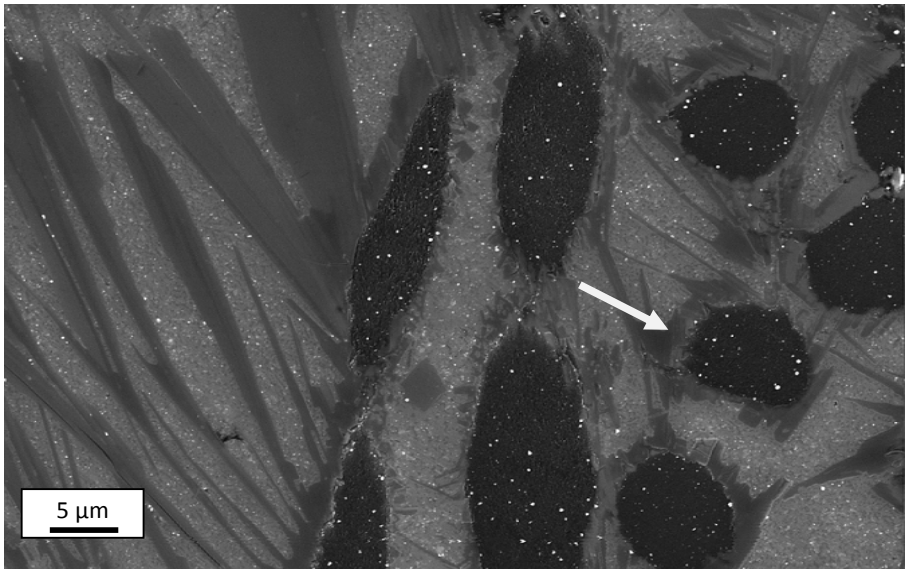

Figure 40 Transformation of carbon to carbide (at arrow) near the interface (0.05in below, 175 °C preheat, 32kW/mm^2, 100mm/min)

It clearly shows the transformation of carbon into carbides in the heat affected zone. This is due to high temperatures and slow cooling rates in the process. During laser welding, the temperature of the composite is more than 1000°K. This will melt the aluminum matrix and leads to the reaction with carbon to form aluminum carbide. Also $\Delta G<0$ for 1000°K temperature when substituted in equation (14). This makes this reaction spontaneous to form Al_4C_3. Reaction kinetics are increased due to the low cooling rates. Formation of aluminum carbide degrades the mechanical properties of the composite and increases the corrosion rate. Also aluminum carbide formation makes the weld more brittle making the joint weak.

To weld A413-Gr successfully, the temperature of the weld must be much higher than its melting temperature of 577°C to overcome significant conduction heat loss from the highly thermal conductive graphite fibers. The risk of laser welding this composite and forming brittle Al_4C_3, SiC, porosity, and redistribution of graphite

fibers prompts us to consider a lower temperature joining. Results for brazing at a temperature lower than 577°C are presented next.

4.2 RESISTANCE SPOT BRAZING

To eliminate the formation of aluminum carbide, a process which joins the composite at relatively low temperatures has to be employed. For this, the brazing process is considered.

4.2.1 MICROSTRUCTURE ANALYSIS

General microstructure of the joint shows a properly formed spot. Electrode force acts as an additional advantage to compel the filler material to stay in between the samples and squeeze them together. Figure 41 shows the zones formed during spot brazing

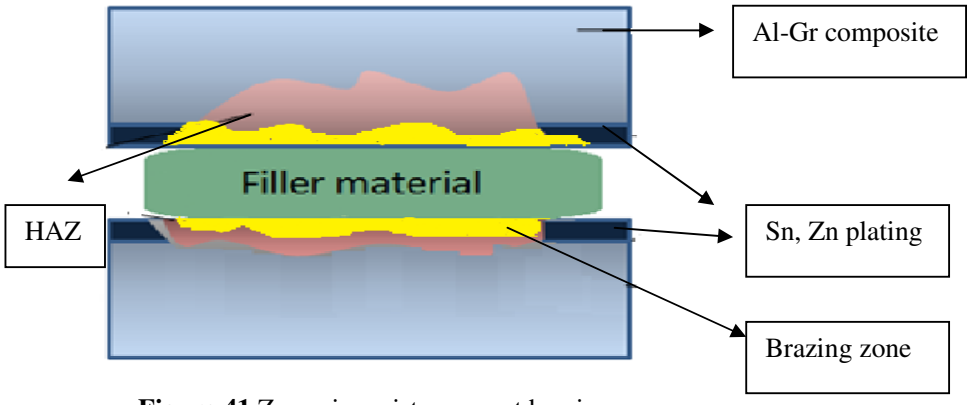

Figure 41 Zones in resistance spot brazing

The microstructure of the resistance brazed joint is shown in the Figure 42.

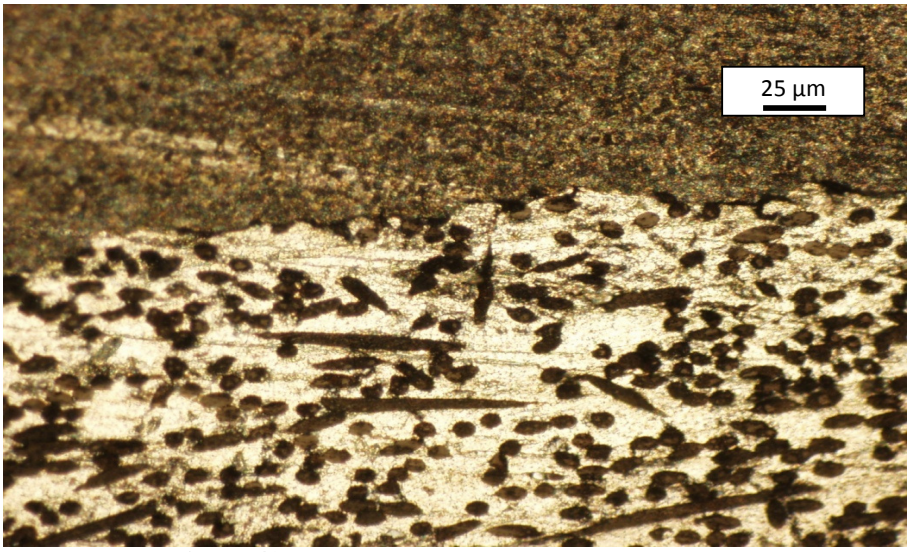

Figure 42 Microstructure of resistance brazed joint
(RSW- AlGr, Al822, 3A, 6sec, 2 cycles)

Also melting the filler material and heating the composite in the same time results in a lesser temperature difference between the two materials resulting in better coalescence at the joint surface. At optimal viscosity and pressure, the molten and fluidic filler material flows and infiltrates a hair-line crack in a sample that is accidently fractured due to excessive impact force of the clamping electrodes. This can be observed in Figure 43. A closer view of Figure 43 shows a mix of filler material with graphite fibers and matrix. This proves that the clamping pressure and heat input to the filler and the composite at the same time results in a mixing of them at the melted zone resulting in a good quality joint.

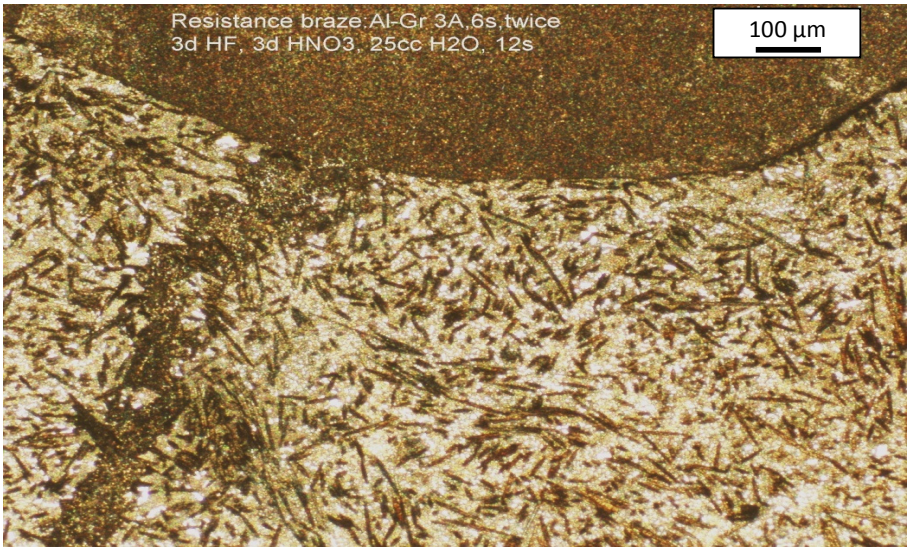

Figure 43 Filler material filling the crack in composite
(RSW- AlGr, Al822, 3A, 6sec, 2 cycles)

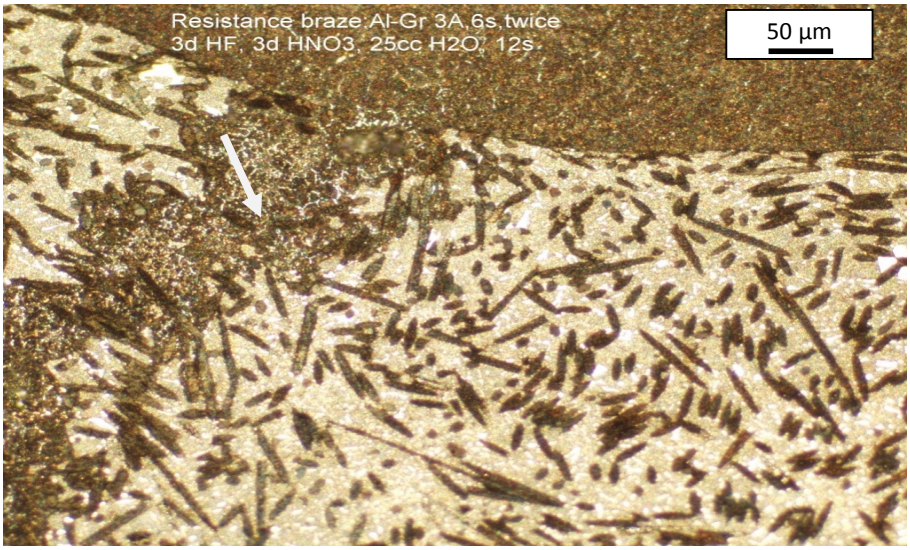

Figure 44 Closer view of the crack (at arrow) in composite
(RSW- AlGr, Al822, 3A, 6sec, 2 cycles)

This gives an extra advantage to resistance spot brazing when compared to providing heat with a laser source as the laser heat is more concentrated to a point rather than heating the entire sample in the same time. This can be observed in the Figure 44. Figure 45 shows the absence of aluminum carbide formation in resistance spot brazing. This proves that resistance spot brazing is advantageous as the joint

properties are not deteriorated by any aluminum carbide formation. This is because the melting temperature of the filler material is lower than the melting temperature of composite. Less amount of heat input is enough to melt the filler material and join the composite. Lower heat concentration prevents the melting of the matrix and the fiber, and thus avoids the formation of aluminum carbide.

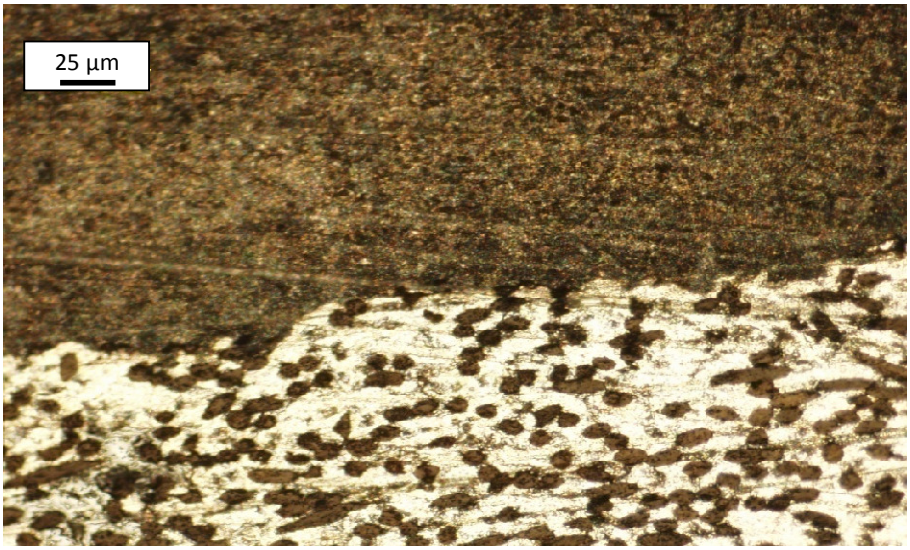

Figure 45 Resistance brazed composite microstructure
(RSW-AlGr, Al822, 3A-6sec, after etching)

For proper bonding, the filler must thoroughly "wet out" the surface to be bonded. "Wetting out" means the filler flows and covers the surface to maximize the contact area. This will increase the attractive forces between the filler and the bonding surface. For the filler to properly wet the base, its surface energy must be lower than the surface energy of the base, or the surface energy of the base should be raised. One method to increase the surface energy is to modify the surface of the composite by plating. Electroplating with a metal whose surface energy is higher than the filler will increase the adherence of the filler to the base surface. The surface energy of

aluminum is 1.143J/m^2, carbon is 0.119J/m^2, zinc is 0.993J/m^2 and tin is 0.709J/m^2 (Vitos, et.al; 1998). The filler and composite used in this study have different concentrations of these elements, their surface energies will be in the range of the values mentioned. Two different coatings are selected for this study.

Resistance spot brazing is also performed on the tin and zinc coated composites. Coated composites also had a good flowing of the filler material when the microstructure is observed.

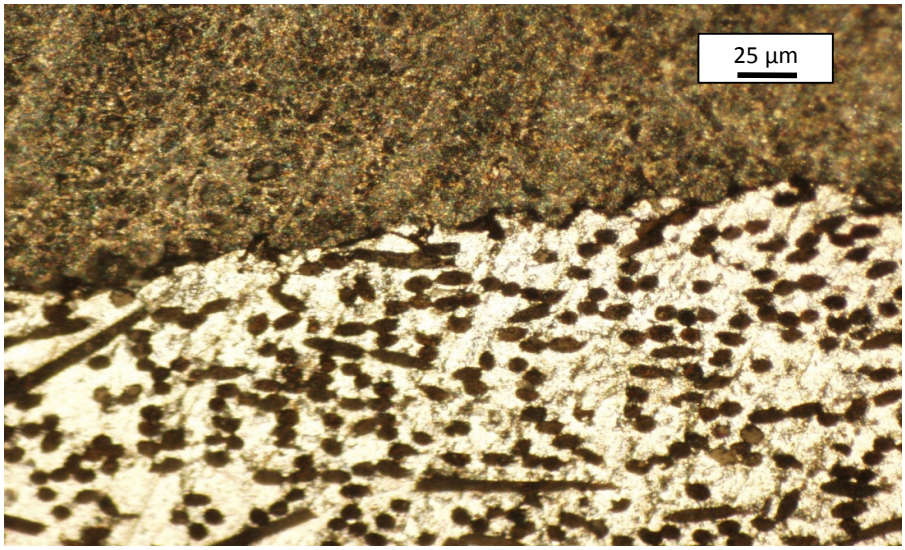

Figure 46 Microstructure of the resistance brazed tin coated composite (RSW-AlGr, Sn coating, Al822, 3A-6sec, after etching)

Shiny material is observed in the joint surface along with the filler material. This could be the tin and zinc coatings mixing with the filler material during brazing at the heated zone. Figure 46 shows the microstructure of the tin joint after brazing. There is no presence of carbide found in the microstructure. At some places, porosity is observed in the tin coated joints, as shown in Figure 47. Such defects may be cause by trapped air or uneven adhesion of tin plating on graphite fibers and aluminum matrix which degrade the mechanical properties of the joint.

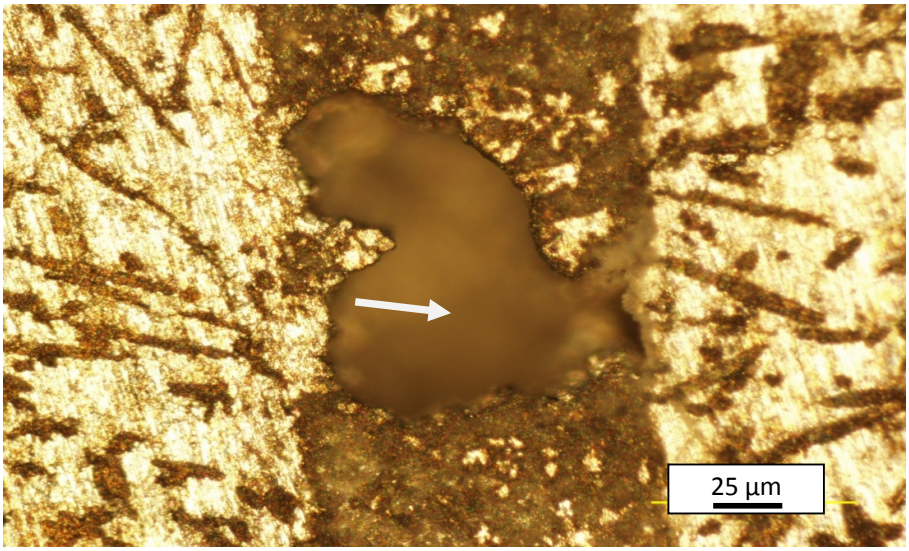

Figure 47 Porosity (at arrow) observed in tin coated composite joint (RSW-AlGr, Sn coat Al822, 3A, 12sec, 240kPa)

Figure 48 shows the microstructure of the composite brazed after coating it with zinc. The zinc coated composite also joined well, and the microstructure shows a proper flow of the filler material near the joint surface. There is no presence of carbides in the brazed zone when observed in the microscope. Further analysis using the scanning electron microscope has to be done to observe the coating and do the chemical analysis to know the composition of the joint.

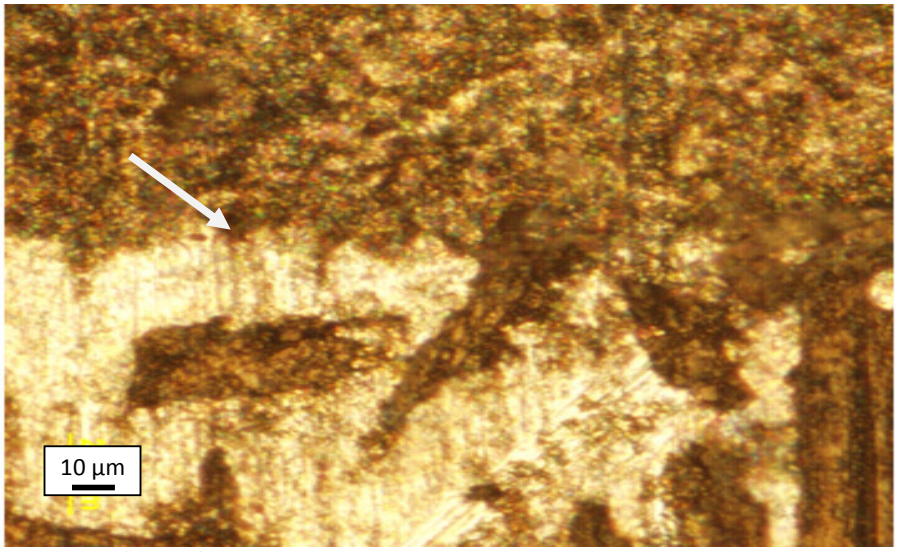

Figure 48 Microstructure of zinc (at arrow) coated composite
(RSW-AlGr, Zn coat, Al822, 3A, 12sec, 240 kPa)

Also similar to the tin coated joints, porosity and shiny material is found in the microstructure of the joints. This has to be analyzed to understand the effect of coating on the joints. Porosity is observed in this joint at some points on the surface. Figure 49 shows the pores formed in the zinc coated joint.

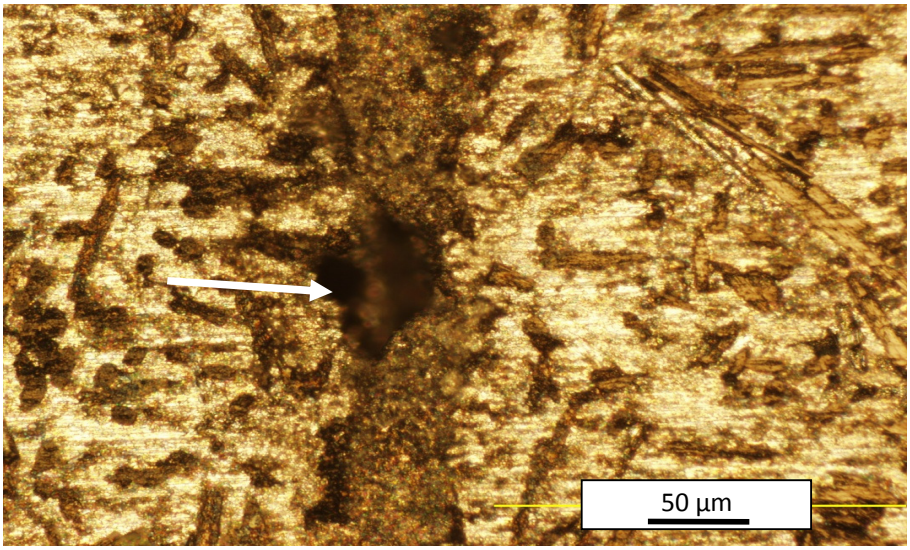

Figure 49 Pores (at arrow) formed in the zinc coated composite joint
(RSW- AlGr, Zn coat, Al822, 3A, 12sec, 240 kPa)

4.2.2 SHEAR TESTING RESULTS

Without any coating-

Parameters used: Current – 3A
Time- 7sec
Cycles- 4
Clamping pressure- 206kPa

Microstructure of the composite after mechanical testing is evaluated. Figures 50 and 51 show the presence of graphite fibers in the brazed area. This proves that the filler material flowed and mixed with the composite at the brazed zone.

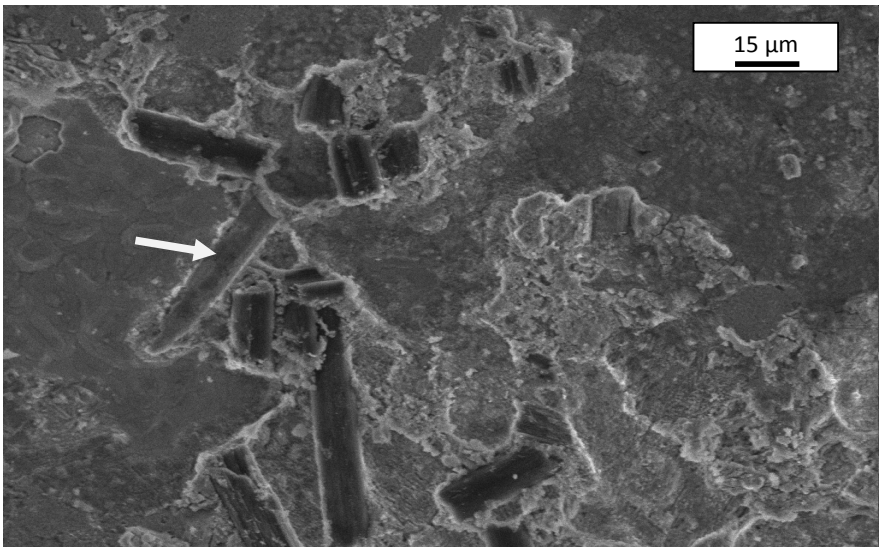

Figure 50 Graphite fibers (at arrow) in the brazed zone of spot brazed Al-Gr (RSW-AlGr, no coat, Al822, RSW, 3A, 7sec, 4 cycles, 200 kPa)

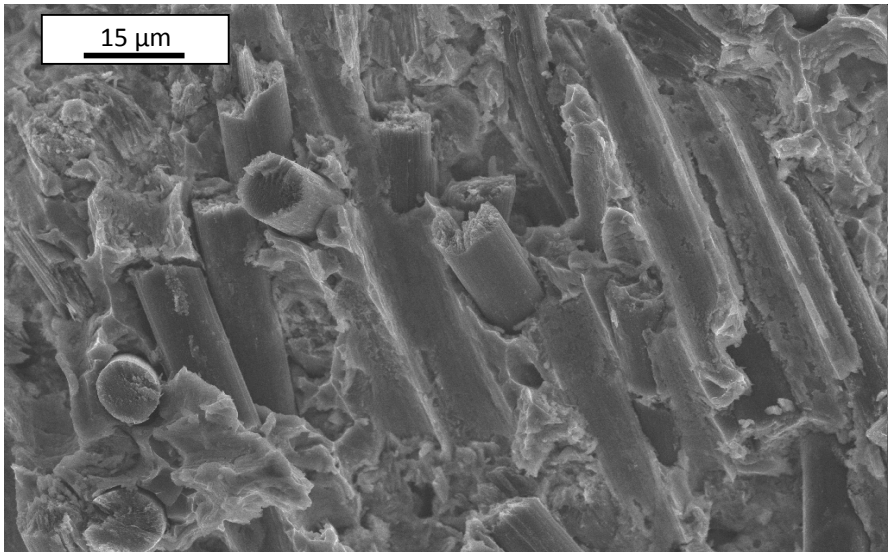

Figure 51 Presence of graphite fibers in the brazed zone for spot brazed Al-Gr (RSW-AlGr, Sn coat, Al822 , 3A, 7sec, 3 cycles, 200 kPa)

Figures 52 and 53 show the broken graphite fibers in the brazed area:

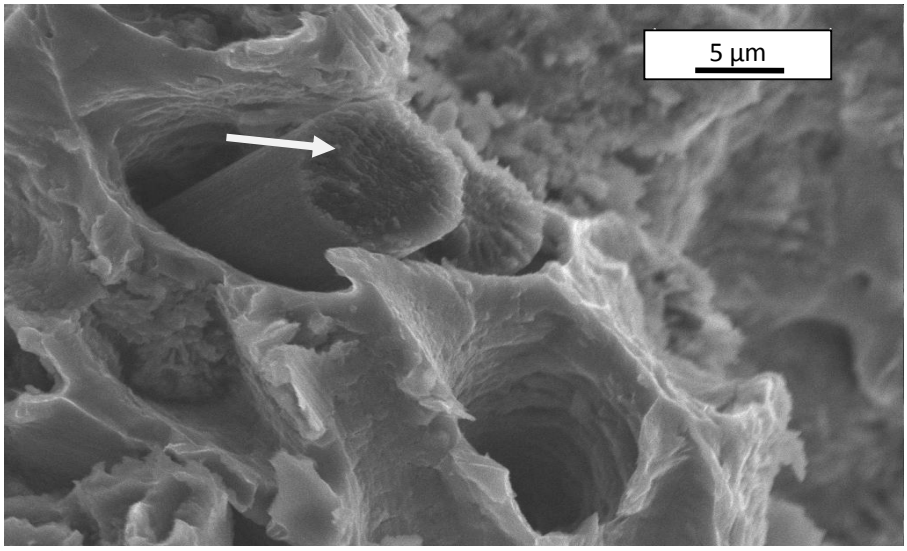

Figure 52 Broken Gr fibers (at arrow) and cavity in the brazed area for spot brazed Al-Gr (RSW-AlGr, no coat, Al822, 3A, 7sec, 4 cycles, 200 kPa)

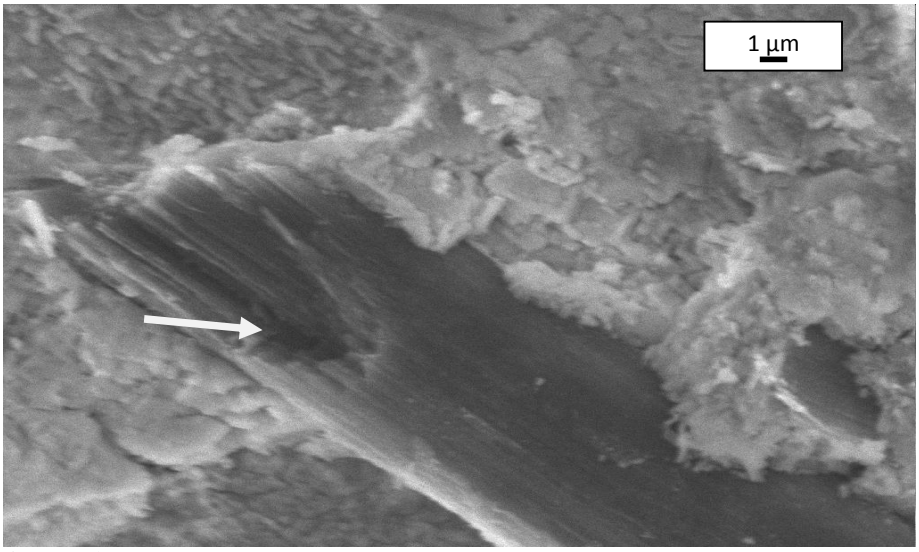

Figure 53 Broken graphite fibers (at arrow) in the brazed area for spot brazed Al-Gr (RSW-AlGr, no coat, Al822, 3A, 7sec, 4cycles, 200 kPa)

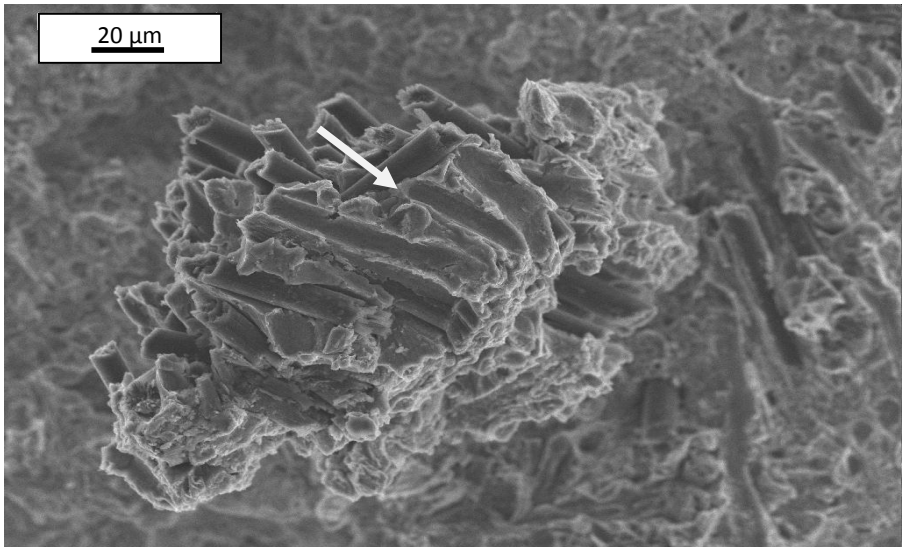

Figure 54 Cavities formed (at arrow) after shear testing for spot brazed Al-Gr (RSW-AlGr, no coat, Al822, 3A, 7sec, 4 cycles, 200 kPa)

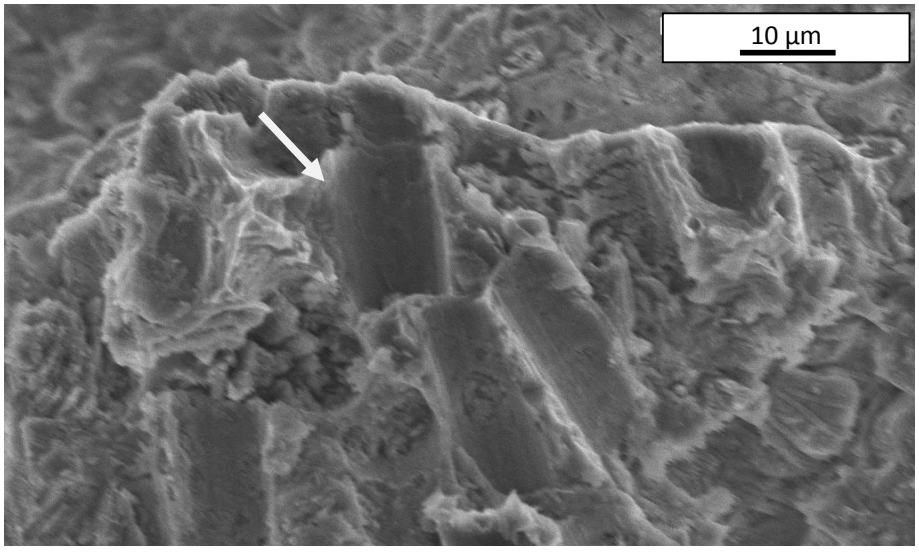

Figure 55 Closer look (at arrow) of the cavities after shear testing for spot brazed Al-Gr (RSW-AlGr, no coat, Al822, 3A, 7sec, 4 cycles, 200 kPa)

As the current flows through the composite samples and the filler, heat produced due to the resistance will melt the filler and composite resulting in a flow at the melted zone and forming a bond.

Figures 54 and 55 shows the cavities formed after pulling the fibers from the joint surface during mechanical testing. The opposite surface to the one filled with fibers has some cavities formed due to the pulling done during mechanical testing. This proves that the fibers accumulated in the melted zone after brazing. Also mechanical testing is done to the coated samples which are joined by spot brazing.

Tin Coating-

Parameters used: Current- 3A
Time- 7sec
Cycles-3
Clamping force- 206kPa

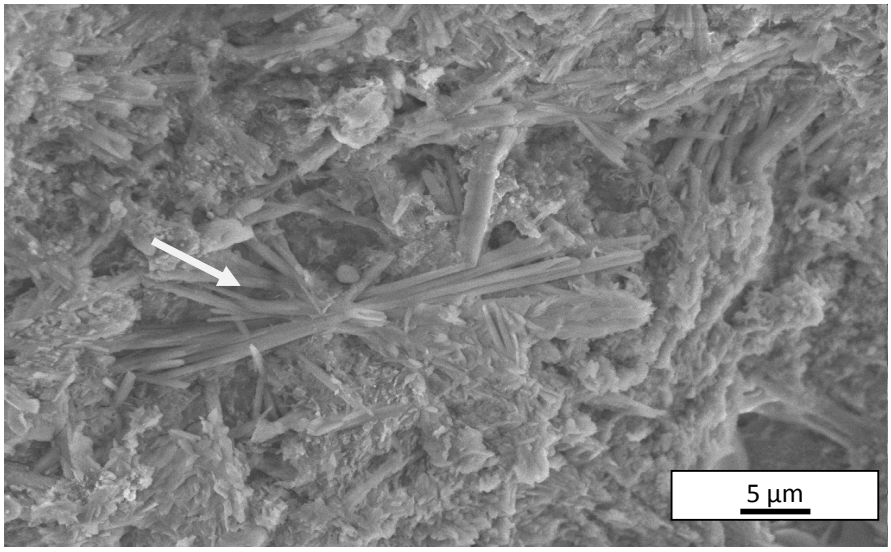

Figure 56 New material (at arrow) observed on tin coated composite joint (RSW-AlGr, Sn coat, Al822, 3A,7sec, 3 cycles, 200 kPa)

Figure 56 shows the microstructure of the tin coated samples which are joined by resistance spot brazing and tested to find the shear stress. It shows presence of some new material in the joints when the samples are coated with tin. Futher chemical analysis has to be done to know if the new material formed is composed of tin.

Zinc Coating-

Parameters used: Current- 3A
Time- 7sec
Cycles-2
Clamping pressure- 206kPa

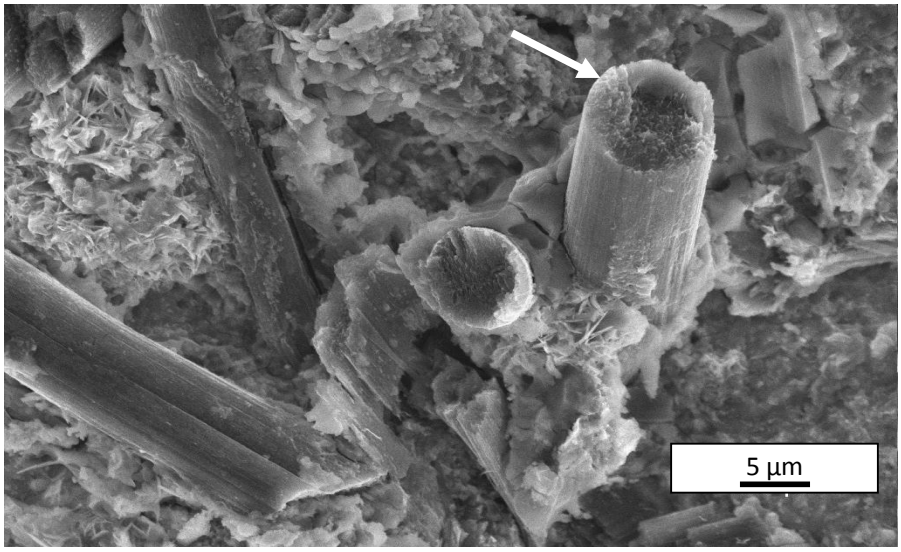

Figure 57 Broken graphite fibers in the resistance brazed area for zinc coated Al-Gr (RSW- AlGr, Zn coat, Al822, 3A, 7sec, 2 cycles, 200kPa)

Figure 57 shows the delaminated graphite fibers in the brazed area. This is due to the pulling force applied at the joint area.

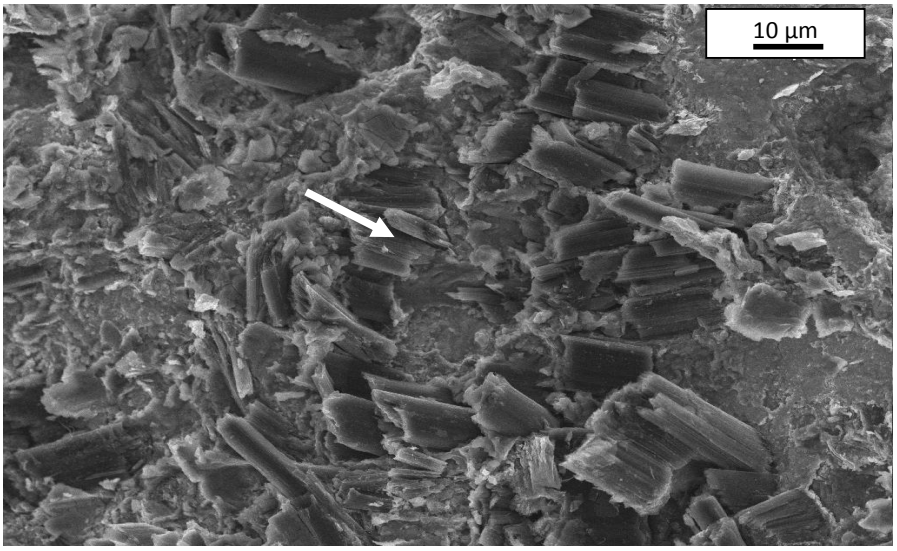

Figure 58 Concentration of graphite fibers (at arrow) in the weld area (RSW-AlGr, Zn coat, Al822, 3A, 7sec, 2 cycles, 200 kPa)

Figure 58 shows the concentration of graphite fibers in the weld area

To calculate the shear stress, force exterted on the joints as a function of position is found. Also the weld area is measured by drawing a grid of 0.4mm × 0.4mm on the picture of the sheared surface, countings the squares and measuring the brazed area. Then shear stress of each of the joints is calculated. This is explained in detail in the appendix D.

Shear stress for the samples brazed without any coating, tin coating and zinc coating are found and the values are compared to understand the joint quality and the strength of the brazed joints. For knowing the maximum force exerted, samples are held and a preload is tested and then once the system is ready, specimen is pulled on a tensile tester at 12.5 mm/min.

Table 22 tabulates the shear stress calculation for brazed lap joints.

Table 22 Shear stress of resistance brazed lap joints

Specimens	**Maximum force (N)**	**Shear area (mm^2)**	**Shear stress (MPa)**
A413-Gr composite	267	19.04	14.0
Sn-plated composite	356	16.56	21.5
Zn-plated composite	271	13.60	20.0

Referring to Table 1, the published tensile strengths of the composites are 93 MPa (in xy plane) and 38 MPa (along z-direction). Therefore, the estimated shear strengths are 46.5 MPa-in xy plane) and 19 MPa -along z direction (50% of tensile strengths). When shearing a brazed specimen with mixed fiber orientations, the failure would be at the weakest component corresponding to 19 MPa. Shear stresses on both Zn and Sn plated lap joints are 20-21 MPa and are comparable to the composite shear

strength. Variation of measured shear strength on different samples up to ± 5 MPa could possibly due to:

- Brazing defects. Isolated porosities and shrinkage cavities are seen along the interface of a joint. These defects act as stress raisers where crack would originate from.
- Material defects. Diffusion of brazing/plating atoms into the composite might affect the joint mechanical properties. Annealing of the A413 matrix at brazing temperature, however, could improve the composite strength.
- Test misalignment. Possible misalignment during clamping of a lap joint on the tensile tester would cause both bending and shearing stresses at the interface.

Despite all these variations, all resistance brazed samples exhibit successful joining characteristics since the fracture surfaces are mostly in the composites rather than in the brazing material or along the interface (Ellis, 1996). Shearing and pulling-out of graphite fibers indicate delamination of fiber and matrix interfaces. Significant plastic deformation of aluminum matrix indicates possible annealing and softening of the matrix near a joint interface during brazing. The smooth surfaces of some graphite fibers suggest insignificant Al_4C_3 is formed. This is in agreement with other studies that Al_4C_3 does not form at a low brazing temperature between 482-540°C (Gopinathan, et.al; 1993).

4.3 LASER BRAZING

Laser brazing is more applicable for microscale joining since its Ø50-100 µm beam can effectively penetrate a very shallow depth. As resistance brazing process successfully joined Al-Gr composite, heat required for laser brazing is calculated using the resistance brazing input parameters.

Heat Calculations- Heat generated in resistance spot brazing is expressed by the equation (Groover, 2004),

$$E = I^2 \times R \times t \quad (15)$$

where, E = heat energy (J)

I = current = 3A

R = electrical resistance = 0.7 Ω (measured as mentioned in 3.3.2.3)

t = time that the current is applied = 18sec

Substitute these values in equation (15) to get the heat generated,

$E = (3A)^2 \times (0.7\Omega) \times (18sec) = 113.4$ J

Unit energy for melting is expressed as (Groover, 2004),

$$U_m = KT_m^2 \quad (16)$$

where, T_m = melting temperature of Al-Gr composite (°K) = 858°K

K = constant = 3.33×10^{-6}

Substituting these values in equation (16) give,

$U_m = 3.33\times 10^{-6} \times 858^2 = 2.45$ J/mm^3

Power needed for welding is given by (Groover, 2004),

$$P_w = \frac{E_w}{t} = \frac{U_m(A_w \times d)}{t} = U_m \times A_w \times V_w \quad (17)$$

where, Pw = Power needed for welding (W)

E_w = Energy needed for welding (J)

t = time taken for the welding (sec)

V_w = welding feedrate = 4.2 mm/sec

A_w = Area of the weld = 191259×10^{-6} mm^2

U_m = Unit energy for melting = 2.45 J/mm^3

Area of the weld is measured by drawing a grid of 0.4mm × 0.4mm on the melted area and counting the grids (as mentioned in 3.3.2.3).

Subsituting these values in equation (17) will give the power needed for welding as,

$P_w = 2.45$ J/mm^3 × (191259×10^{-6} mm^2) × 4.2 mm/sec = 1.96 W

Now, efficiency of the laser machine is calculated using the following equation,

$$Efficiency = \frac{P_w}{P_s} \quad (18)$$

where, P_w = Power for weld = 1.96W

P_s = Power from the laser source = 60W = 30% of the power of laser source with 200W maximum power

Substituting the values in equation (18) will give us,

$$\text{Efficiency} = \frac{1.96W}{65W} = 3.2\% \quad (19)$$

Similarly, efficiencies for laser powers for different experiments (mentioned in Table 19) are also calculated as shown in Table 23.

Table 23 Efficiencies calculated for laser brazing

Experiment #	**Laser Power %**	**Laser Power (W)**	**Feedrate (mm/sec)**	**Efficiency**
1	30	60	0.42	2.28×10^{-3}
2	40	80	0.42	1.66×10^{-3}
3	50	100	0.42	5.8×10^{-3}
4	60	120	0.42	0.052
5	70	140	0.42	0.085
6	70	140	4.23	0.0942
7	60	120	4.23	0.0233
8	50	100	4.23	0.0188
9	40	80	4.23	0.0158
10	30	60	4.23	0.032

Average efficiency = 0.03

Jou (2003) calculated the energy required for heating the weld nugget is 27.3% of the total heat in resistance spot welding for steel. Assume this number is the same for this Al-Gr. In this study, we will find the energy required for heating nugget in Al-Gr.

Total heat generated in resistance brazing is calculated using equation (15) as 113.4 J

Therefore, nugget heating = $\frac{27.3}{100} \times 113.4 = 31$ J

Laser welding feedrate considered is 4.23 mm/sec

Therefore, time taken to weld 50 mm of the workpiece is,

$$\frac{50mm}{4.23mm/sec} = 12sec \quad (20)$$

which gives, laser power to beaze the 50mm length is = $\frac{31J}{12\ sec} = 2.58\ W$ (21)

Now substituting these values in equation (18) gives,

$$\frac{2.58\ W}{P_s} = 0.03 \quad (22)$$

Therefore, power required for laser brazing is, $P_s = \frac{2.58\ W}{0.03} = 86\ W$ or 43% of 200 W maximum power.

Based on these calculations, laser power of 40% and 45% are considered for laser brazing tests in the experiments. Once the samples are brazed, metallographic analysis is done using scanning electron microscope. Both secondary electron and back scattered electron modes are used to obtain high resolution images of a specimen. Figure 38 describes the zones formed during brazing. Figure 59 shows laser brazed Al-Gr joint. Weld zone, HAZ, filler and composite areas are marked in the figure. Aluminum carbide formation is not seen in the joint area.

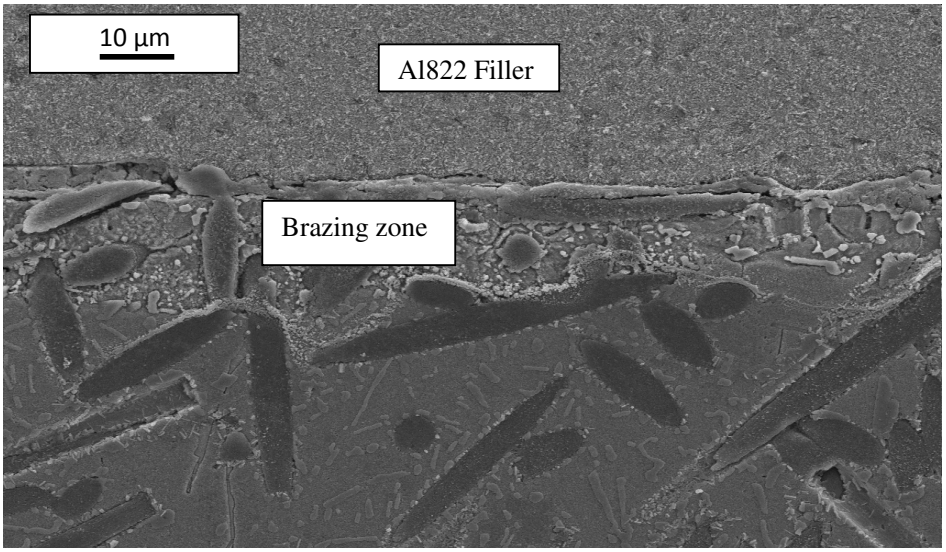

Figure 59 Laser brazed Al-Gr joint
(Laser- AlGr, Al822, 20kW/mm^2, 25 mm/min)

Figure 60 shows a closer view of the joint area. Flowing of filler material around the graphite fiber can be seen in Figure 60 and 61 and Al_4C_3 is not found.

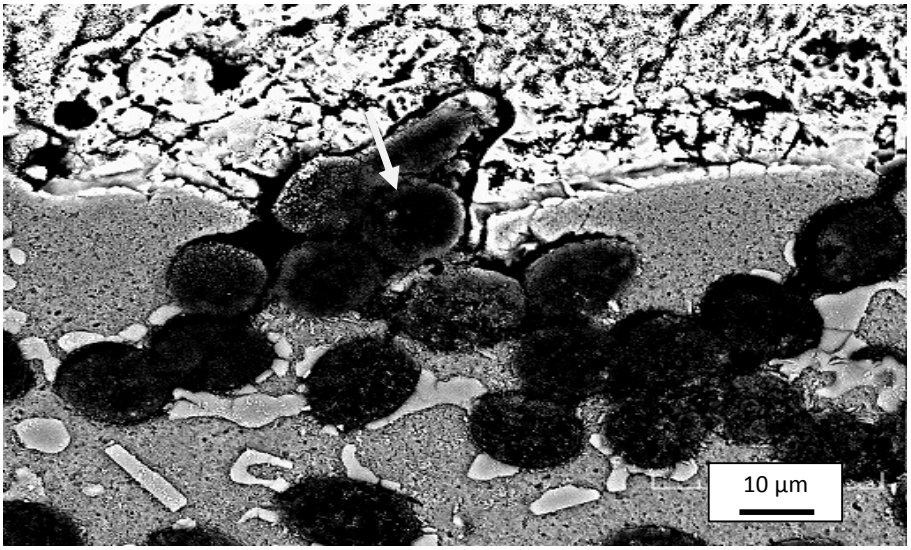

Figure 60 Flowing of Al822 filler (at arrow) around the graphite fiber
(Laser- AlGr, Al822, 16kW/mm^2, 25 mm/min, after etching)

Figure 61 shows the weld zone where the aluminum matrix reacts with the zinc filler to form a mixed zone in between.

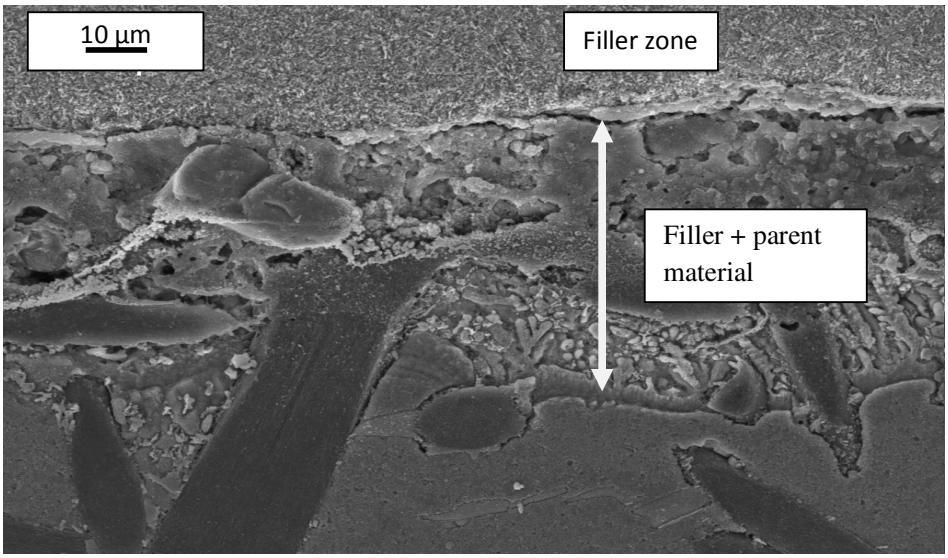

Figure 61 Reaction zone of filler and Al-Gr composite
(Laser- AlGr, Al822, 20kW/mm^2-25mm/min, after etching)

Reaction zone shown in Figure 61 has a flow of filler material into the composite matrix, reacting with aluminum matrix and forming a new material around the carbon fibers. Element spectrum of Figure 62 zone is analyzed to know the elements present in this region.

Figure 63 shows the element spectrum for Aluminum, silicon, carbon and zinc for the zone shown in the Figure 62. From this it is evident that Aluminum, Silicon and Zinc react at the brazed zone.

Also the EDX spectrum of this zone is shown in Figure 64. Presence of Aluminum (Al), Zinc (Zn), Gold (Au), Palladium (Pd) and Cesium (Cs) at high proportions is observed in this spectrum. Aluminum is found due to its presence in composite and filler material. Zinc is found due to the filler material composition. Palladium and gold are found due to the gold coating formed on the brazed zone for SEM analysis. Cesium is found due to its presence in the flux used for brazing process (as per conversation with Lucas Milhaupt)

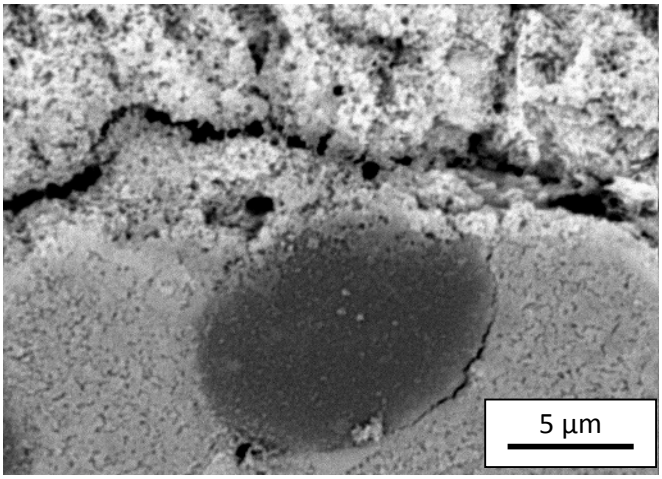

Figure 62 Joint zone at which element spectrum is found
(Laser- AlGr, Al822, 16 kW/mm^2, 25 mm/min, after etching)

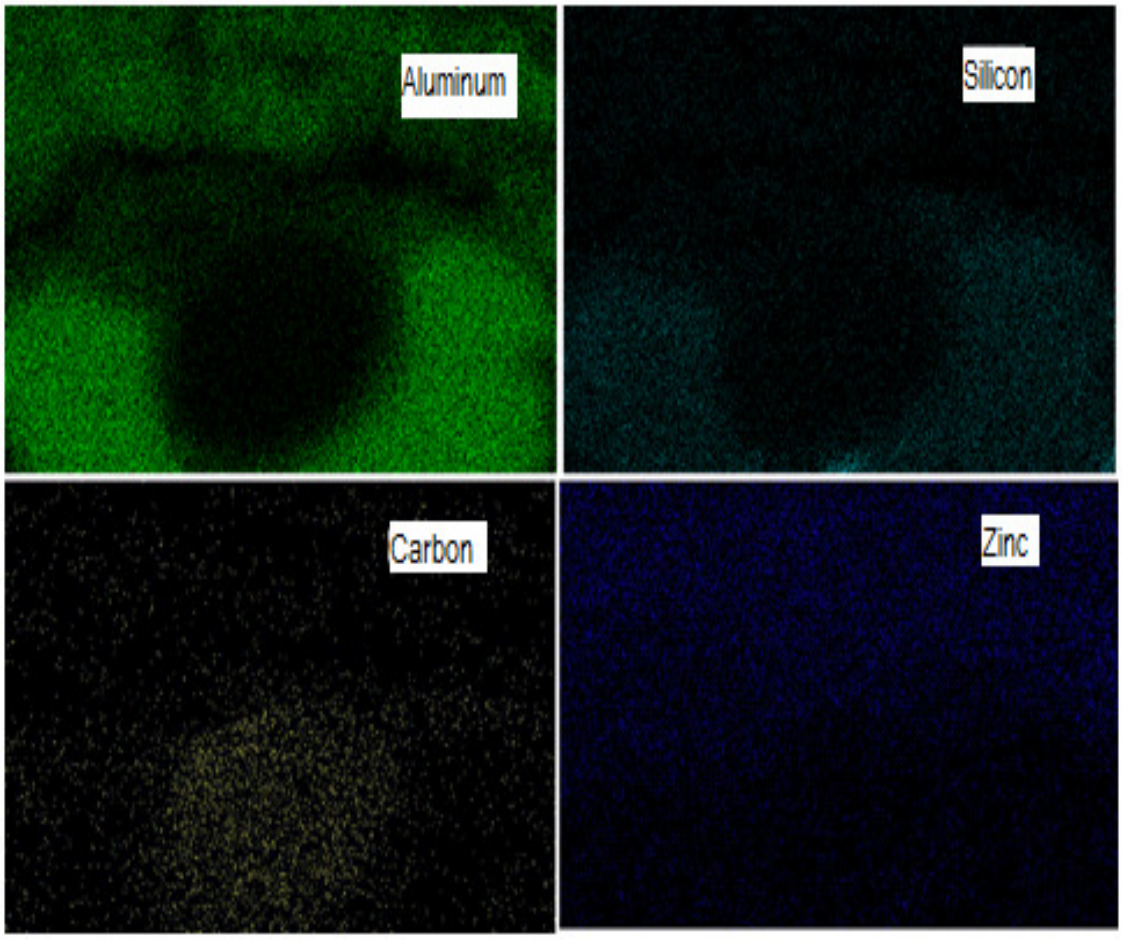

Figure 63 X ray mapping showing Al, Si, C, Zn at joint zone

EDX spectrum for the zone is shown in Figure 64.

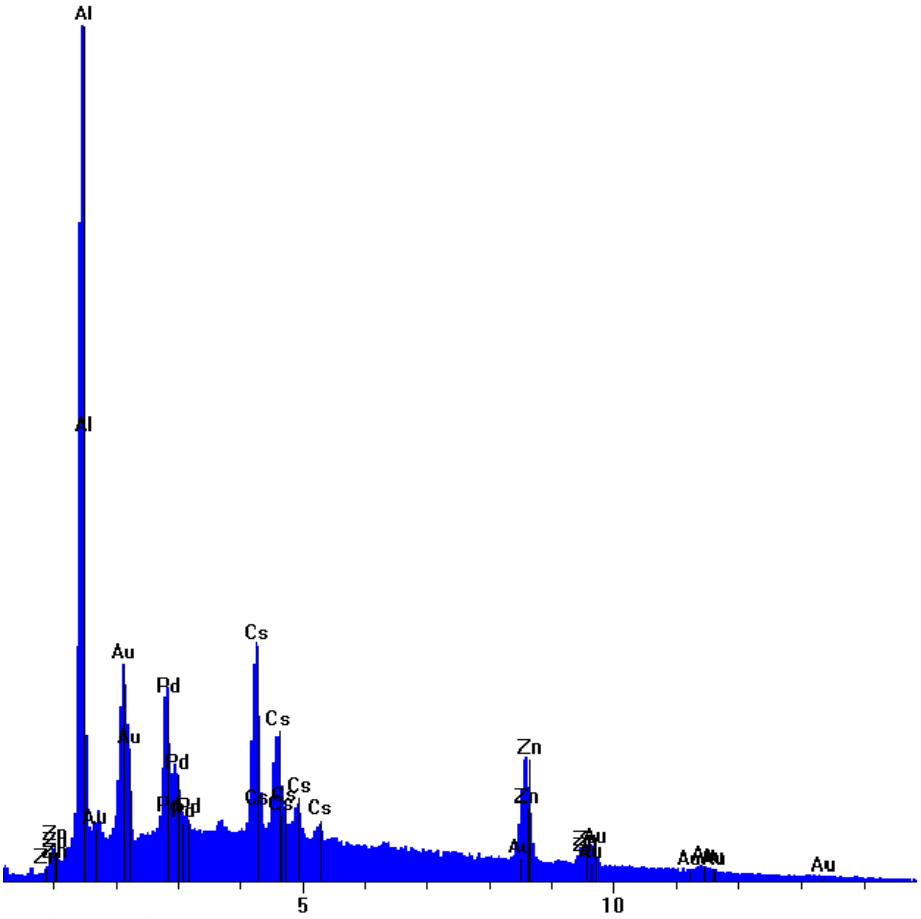

Figure 64 EDX Spectrum showing element compositions in the brazed zone

Mechanical test on laser microbrazed specimens is not performed due to the low resolution of available load cells that prevents accurate measurement of shearing force on very small laser brazed areas. But the joints made are pulled out to examine the weld cross section. Figure 65 (b) shows the laser brazed zones of the laser brazed specimen shown in Figure 65 (a).

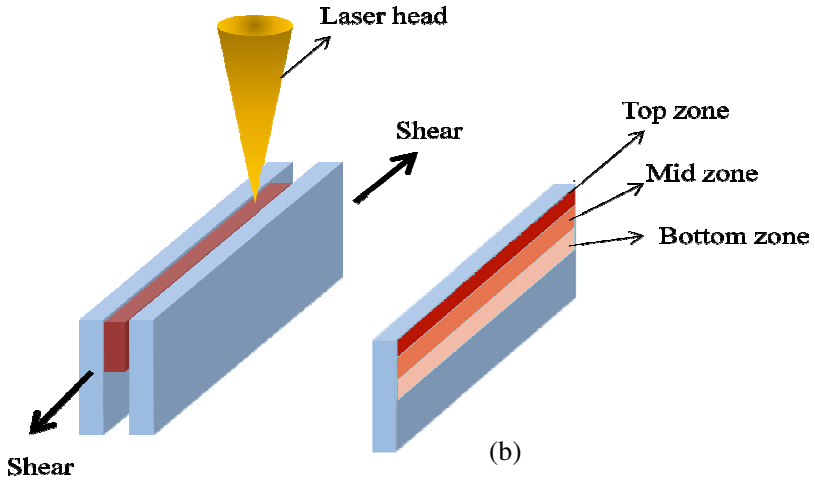

Figure 65 (a) Laser brazed specimen and (b) laser brazed zones of sheared specimen

Figure 66 shows the top zone at which the laser beam heat is concentrated.

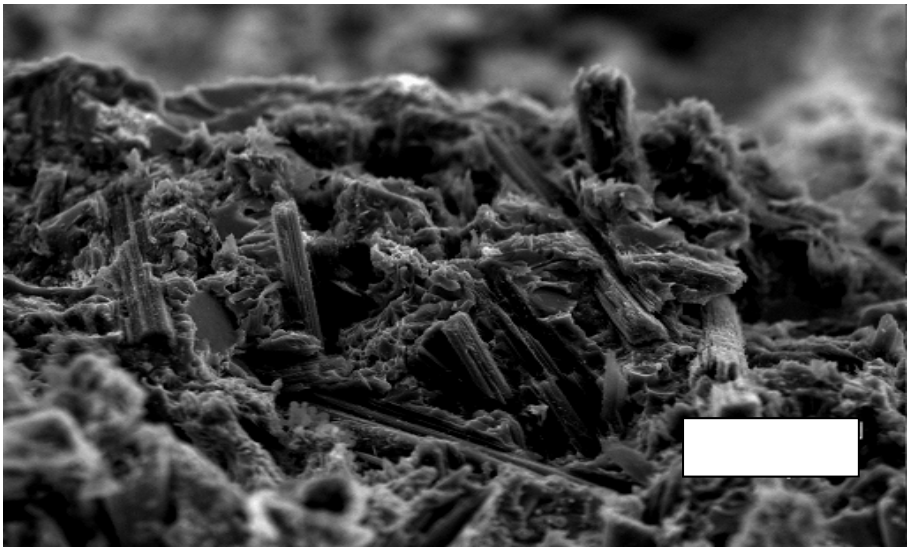

Figure 66 Broken graphite fibers of the laser brazed sample
(Laser- AlGr, Al822, 18 kW/mm^2, 38 mm/min)

Region below the top zone is shown in the Figure 67. Carbon fibers are visible in this zone which explains that the fracture is in the composites rather than in the brazed zone or filler material. The smooth surfaces of some graphite fibers in the Figures 67 and 68 suggest insignificant Al_4C_3 is formed. This is in agreement with other studies that Al_4C_3 does not form at a low brazing temperature between 482-

540°C. As mentioned, formation of Al_4C_3 requires a critical temperature of 827°C and critical cooling rate of 12,000 °K/sec (Gopinathan, et.al; 1993). As these temperatures and cooling rates are not reached in brazing, carbide formation is prevented. This shows the succesful joining through brazing. Figure 68 shows a cracked fiber in the top brazed zone.

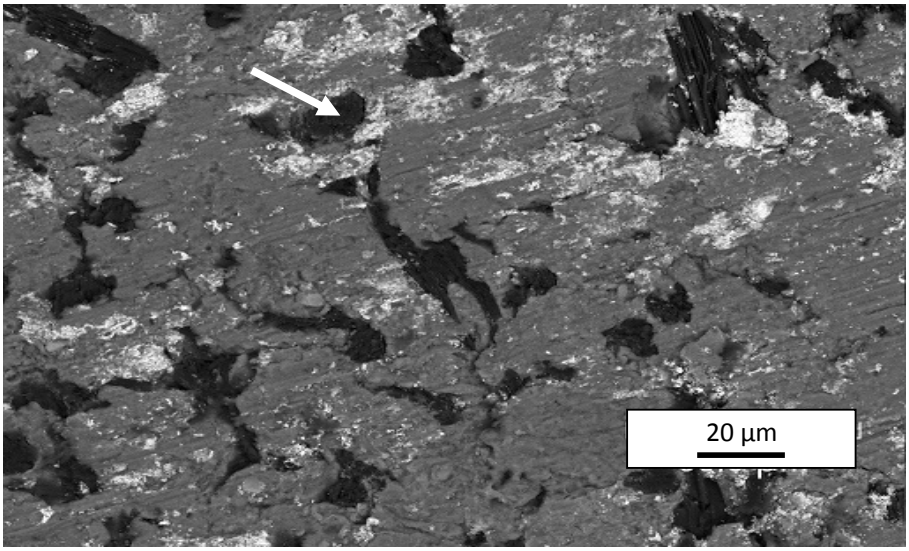

Figure 67 Brazed zone with visible graphite fibers (at arrow)
(Laser- AlGr, Al822, 18 kW/mm^2, 38mm/min)

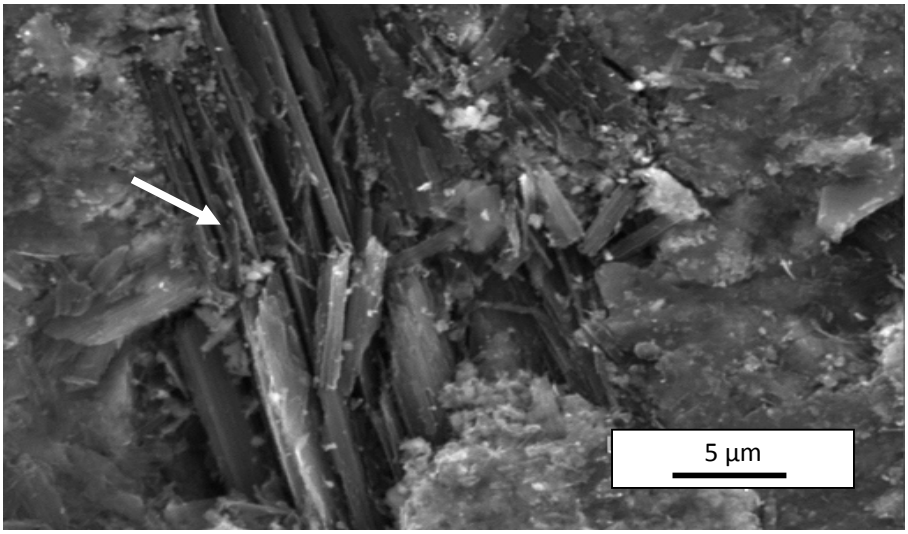

Figure 68 Broken carbon fiber (at arrow) in the brazed zone
(Laser- AlGr, Al822, 18 kW/mm^2, 38 mm/min)

5. CONCLUSIONS AND RECOMMENDATIONS

Joining of advanced aluminum graphite composite is investigated. The study shows:

1) Laser welding of A413-Gr does not provide a sound weld due to formation of Al_4C_3, shrinkage cavity, porosity, and unfavorable redistribution of the graphite fibers.
2) The Zn-Al alloy Al 822 can be successfully brazed to the composite. Its brazing temperature, below the melting temperature of A413, suppresses the formation of Al_4C_3. Fracture in the composite after a shear test suggests exceptional adhesion at the brazing interface.
3) Zinc or tin plating on the composite prior to brazing enhances the brazing adhesion and shear strength of the joint. Shear stress of a plated then brazed lap joint matches the shear strength of parent composite.
4) Laser brazing is suitable for micro-joining while resistance brazing is applicable for macro-joining of this composite.

In this study only few variables are considered significant and rest of them are kept constant for the factorial experiments. Though the significant variables are considered based on the literature data and pretesting, influence of constant variables has to be found to understand the process and the performance better. Variables like joint design, filler material, fiber orientation, shielding gas affect the weld quality. These variables have to be studied further by considering different values and

conducting design of experiments. This is not possible in the present study due to the limited availability of the composite material and time involved in the process. By taking more number of significant variables and performing more number of tests this phenomenon can be understood.

Also for laser brazing and laser welding the effect of laser pulse width and frequency are not studied due to the limited equipment. These two factors have a significant effect of the weld quality so it is recommended to study their effect on the weld. These factors have a strong influence on the bead width and void densities. Also a better coating strategy where the thickness of the coating can be controlled is recommended. This will help in understanding the surface energy and its effect on the weld performance and microstructure. Alternative fillers based on the melting point of the composite have to be found which have a better coalescence property with the composite surface. This will reduce the wettability problem and might result in a better weld joint.

Additionally a finite element analysis is recommended to understand the distribution of temperature during the welding. This will give us a better approximation on the amount of heat required to melt and form a bead at the weld zone. These will improve the process conditions and in turn improve the existing weld quality. Most of these couldn't be performed due to the expensive equipment set up, time involved and the limited availability of composite material.

REFERENCES

Aguilar, E.D. (2010) Influencia De Las Variables De Proceso Sobre Las Propiedades Microestructurales De Compuestos Avanzados De Aluminio/Grafito Soldados Por Láser Pulsado De Nd:YAG. M.S Thesis, COMIMSA, Mexico.

Caswell Inc, tin and zinc brush plating (Accessed Aug 2009), http://www.caswellplating.com/.

Chen, Y.L.; Shaban, A.; Wang, H.M. (1999) Laser beam welding of SiC particle reinforced aluminum metal matrix composite. *Proceedings of SPIE,* 3682: 443-447.

Chen, Y.L.; Yu, L.G.; Wang, H.M. (2000) Effect of "in-situ" weld-alloying on microstructure of laser beam welded SiCp/6061Al metal matrix composite. *Proceedings of SPIE,* 3888: 143-146.

Cornie, J.A.; Zhang, S; Desberg, R; Ryals, M (2003) Discontinuous Graphite Reinforced Aluminum, and Copper Alloys for High Thermal Conductivity-Thermal Expansion Matched Thermal Management Applications, http://www.mmccinc.com/.

Duley, W.W. (1998) Laser Welding, *1st Edition, John Wiley & Sons Inc*., New York

Ellis, M.B.D. (1996) Joining of aluminum based metal matrix composites. *International Materials Reviews,* 41(2): 41-58.

Etter, T.; Schulz, P.; Weber, M.; Metz, J.; Wimmler, M.; Loffler, J.; Uggowitzer, P.J. (2007) Aluminum carbide formation in interpenetrating graphite/aluminum composites. *Material Science and Engineering A,* 448: 1-6.

Fukumoto, S.; Zhou, Y. (2004) Mechanism of resistance microwelding of crossed fine nickel wires. *Metallurgical and Materials Transactions,* 35A: 3165-3176.

Gopinathan, S.; McCay, H.; and McCay, T. *(1993)* Continous wave CO_2 laser welding on SiC/A356 Al metal matrix composites: an analytical estimate for formation of aluminum carbide. *Processing of Advanced Materials,* 3: 213-224.

Groover, P; (2004) Fundamentals of Modern Manufacturing: Materials, Processes and Systems, *2nd Edition, John Wiley & Sons Inc*., Hoboken, New Jersey

He, P.; Liu, Y.Z.; Liu, D. (2006) Interfacial microstructure and forming mechanism brazing C_f/Al composite with Al-Si filler. *Material Science and Engineering A,*422: 333-338.

Hung, N.P.; Jana, S.; Yang, L.J.; Heng, C.H. (1995) Laser drilling of cast metal matrix composites, *Proceedings, The Symposium on Machining of Advanced Materials*, *ASME* 208: 87-92, Los Angeles, USA

Jou, M. (2003) Real time monitoring weld quality of resistance spot welding for the fabrication of sheet metal assemblies. *Journal of Materials Processing Technology,* 132: 102-113.

Kainer, K. (2006) Metal Matrix Composites, Wiley-Vch Verlag GmbH & Co. KGaA, Weinheim, Germany.

Knorovsky, G.A; MacCallum, D.O; Roach, R.A; Semak, V.V (2005) The effect of surface tension on microjoining, *ASM International, Joining of Advanced and Specialty Materials VII ,62-66.*

Lienert, T.J.; Baeslack, W.A.; Ringnalda, J.; and Fraser, H.L.; (1998) Inertia-friction welding of SiC-reinforced 8009 aluminum, *Journal of Material Science,* 31: 2149-2157.

Liu, L.; Zhu, M.; Xu, D.; Wang, T (2002) Study of the interfacial reaction of SiC-Al in 6061Al reinforced with SiC whisker at laser beam. *Composite Interfaces,* 9: 135-142.

Lippold, J. C. (2005) Recent developments in weldability testing for advanced materials. *ASM International, Joining of Advanced and Specialty Materials VII (#05116G).*

LucasMilhaput Inc, Al822 filler (Accessed Dec 2009), http://www.lucasmilhaupt.com/.

Mercier, S.; Ehrburger, P.; Lahaye, J. (1993) Interfacial reactivity in aluminum/carbon fibre composites. *Journal de Physique,* 3: 1723-1726.

Metal Matrix Cast Composites Inc., MMCC, (Accessed Feb 2009), http://www.mmccinc.com/.

Mitul, A.K. (2005) Welding of cast A359/Sic/10p metal matrix composites, M.S Thesis, Texas A&M University.

Powers, M.T. (2004) Room temperature lead-free soldering of microelectronic components using a local heat source, *ASM International, Joining of Advanced and Specialty Materials VII*, 75-79.

Qiu, C.; Metselaar, R. (1994) Solubility of carbon in liquid Al and stability of Al_4C_3. *Journal of Alloys and Compounds,* 216: 55-60.

Rocher, J.P.; Quenisset, J.M.; Naslain, R. (1989) Wetting improvement of carbon or silicon carbide by aluminum alloys based on K_2ZrF_6 surface treatment: application to composite material casting. *Journal of Material Science,* 24: 2697-2703.

Saida, K.; Song, W.; and Nishimoto, K. (2006) Laser brazing of alloy 600 with precious filler metals. *Science and Technology of Welding and Joining,* 11: 694-700.

Schwartz, M.; (2003), Brazing, *2nd Edition, ASM International,* Materials Park, OH

Urena, A.; Gomez De Salazar, J.M.; Escalera, M.D.; and Fernandez, M.I. (1997), Study of the brazeability of aluminum matrix composites. *Welding Journal,* 76:92-102.

Vitos, L.; Ruban, A.V.; Skriver, H.L.; Kollar, J. (1998) The surface energy of metals. *Surface Science,* 411: 186-202.

Yue, T.M.; Du, J.H.; Man, H.C. (1998) High power Nd-YAG laser welding of SiC particle reinforced aluminum alloy 2124. *Institute of Materials,* 14: 906-911.

Zhang, X.P.; Quan, G.F.; Wei, W. (1999) Preliminary investigation on joining performance of SiCp-reinforced aluminum metal matrix composite (Al/SiCp – MMC) by vacuum brazing. *Composites: Part A,* 30: 823-827.

APPENDIX A

DRAWINGS

Drawing 1 - Laser welding fixture

Drawing 2 – Resistance brazing fixture

Drawing 3 - Laser brazing fixture

Drawing 4 - Laser welding sample drawing

Drawing 5 - Resistance brazing sample drawing

Drawing 6 - Laser brazing sample drawing

Drawing 1 - Laser welding fixture:

Material : Aluminum

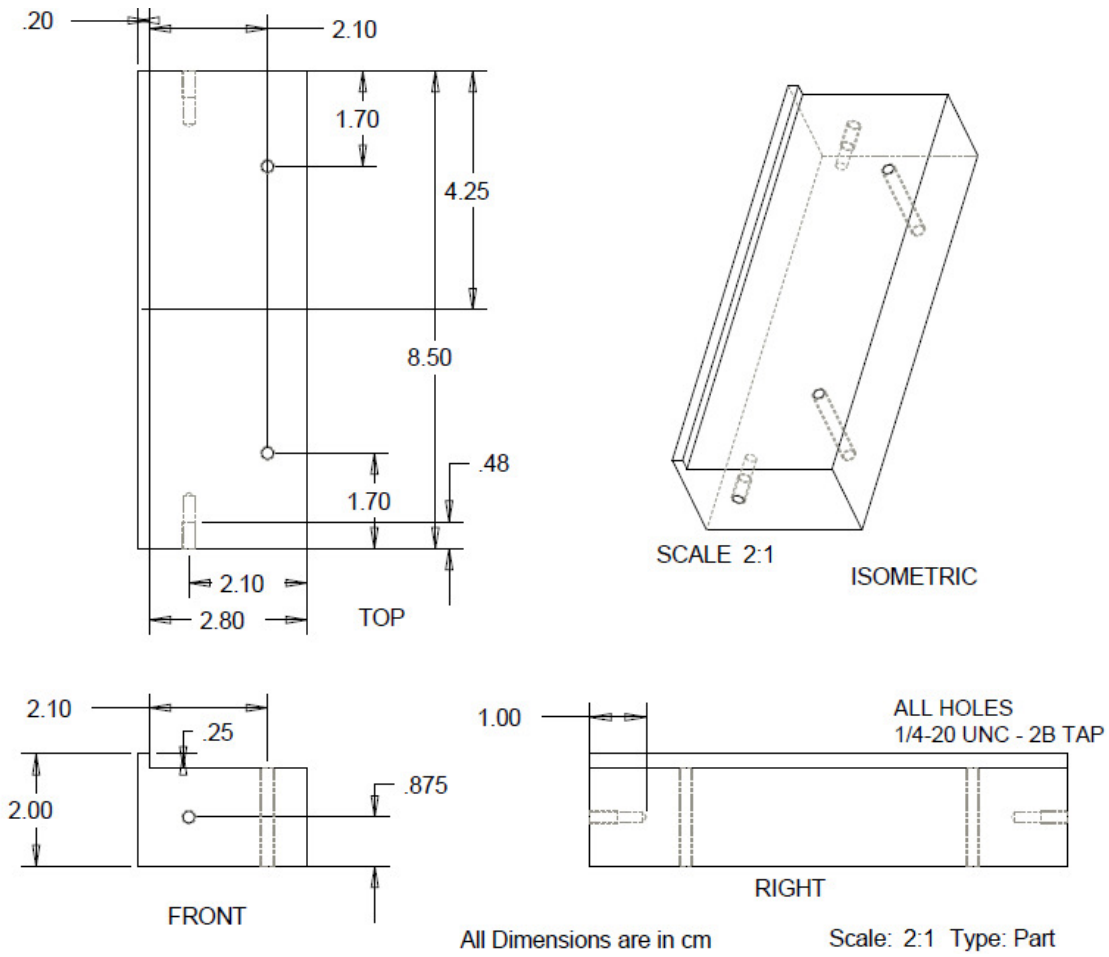

Drawing 2 - Resistance brazing fixture

Material- Aluminum

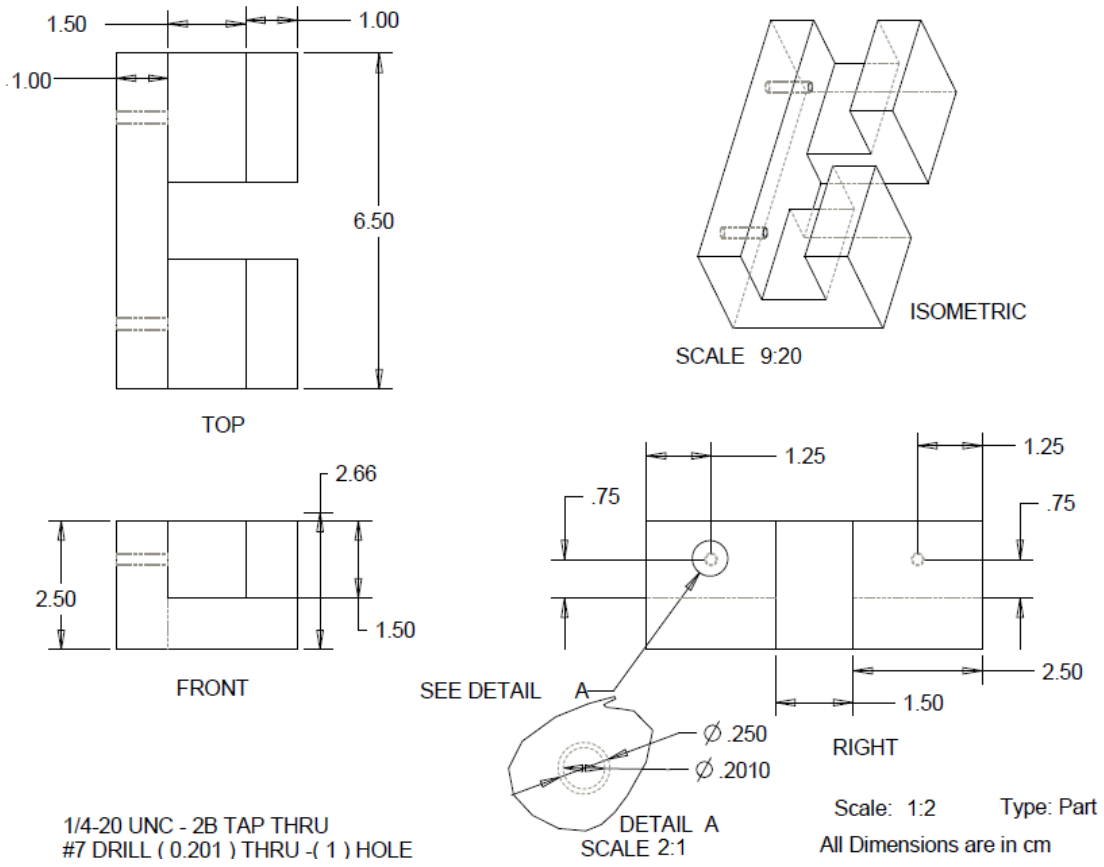

Drawing 3 - Laser brazing fixture

Material- Aluminum

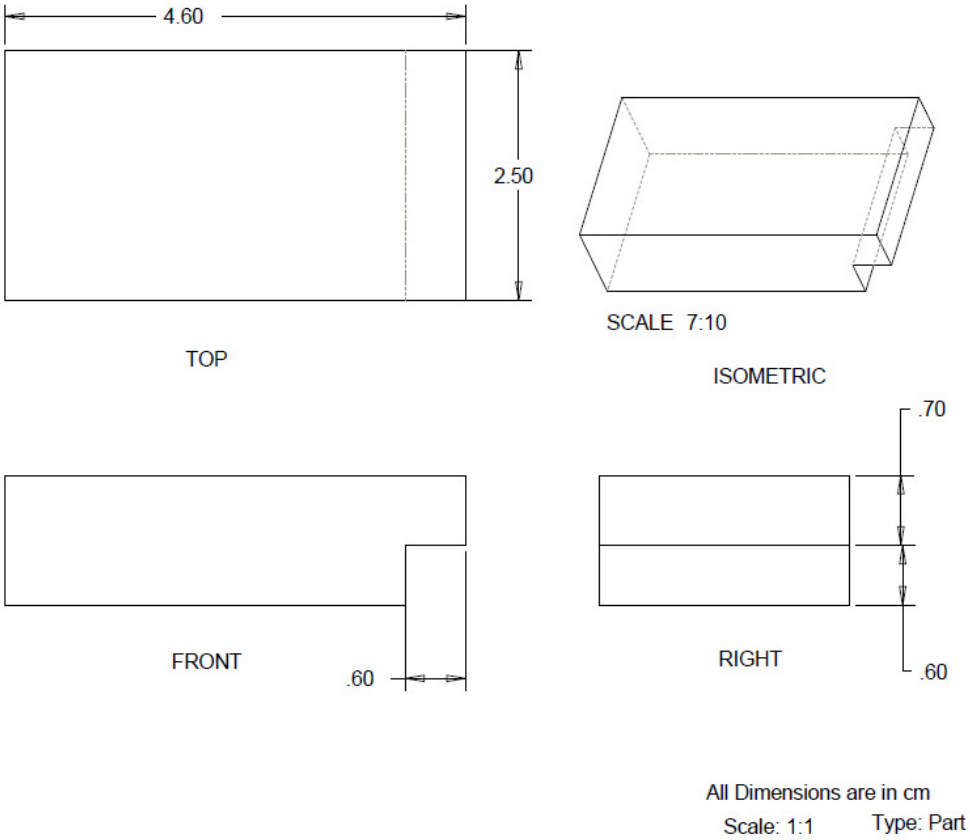

Drawing 4 - Laser welding sample drawing

Material- Al-Gr composite

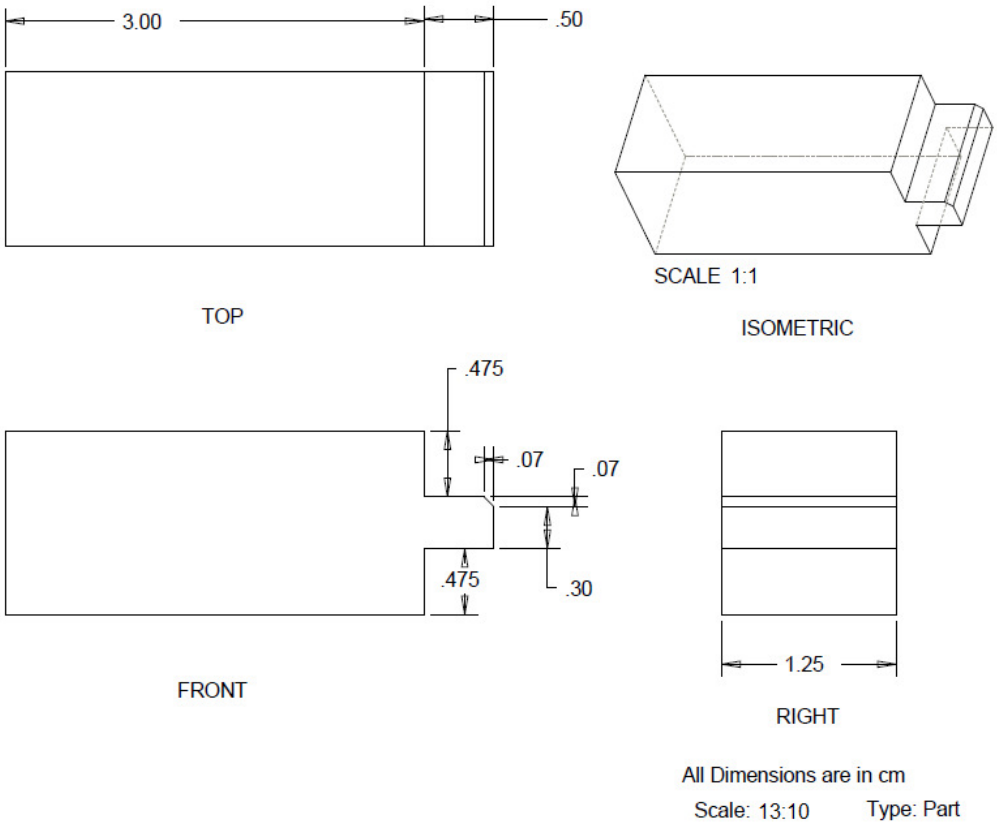

Drawing 5 - Resistance brazing Sample drawing

Material- Al-Gr composite

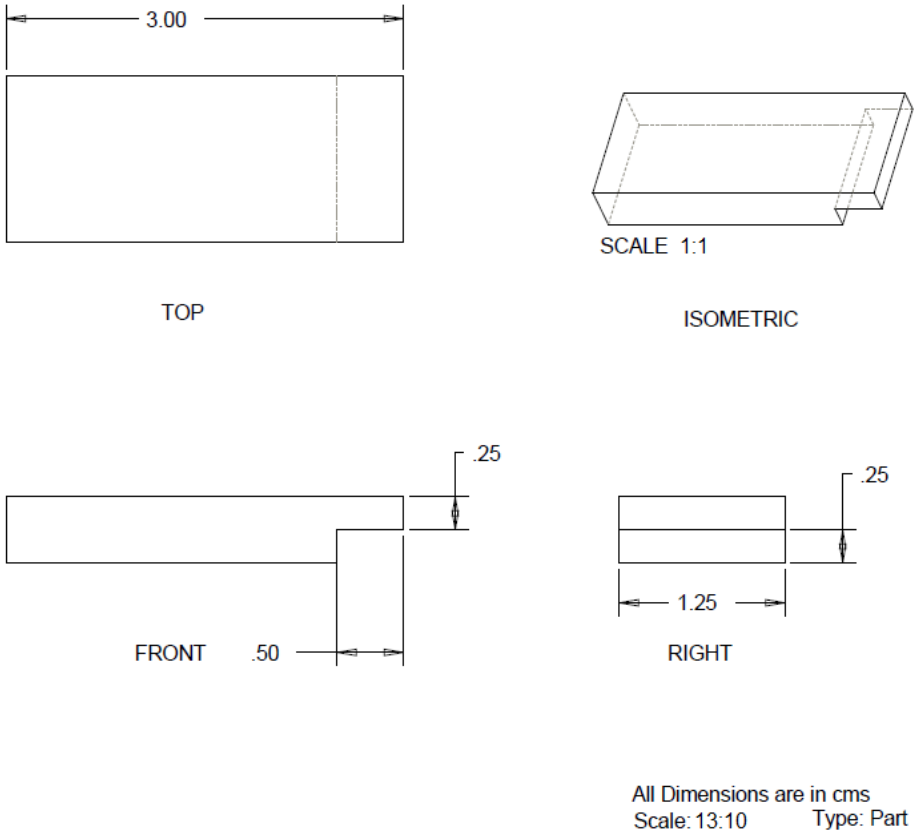

Drawing 6 - Laser brazing Sample drawing

Material- Al-Gr composite

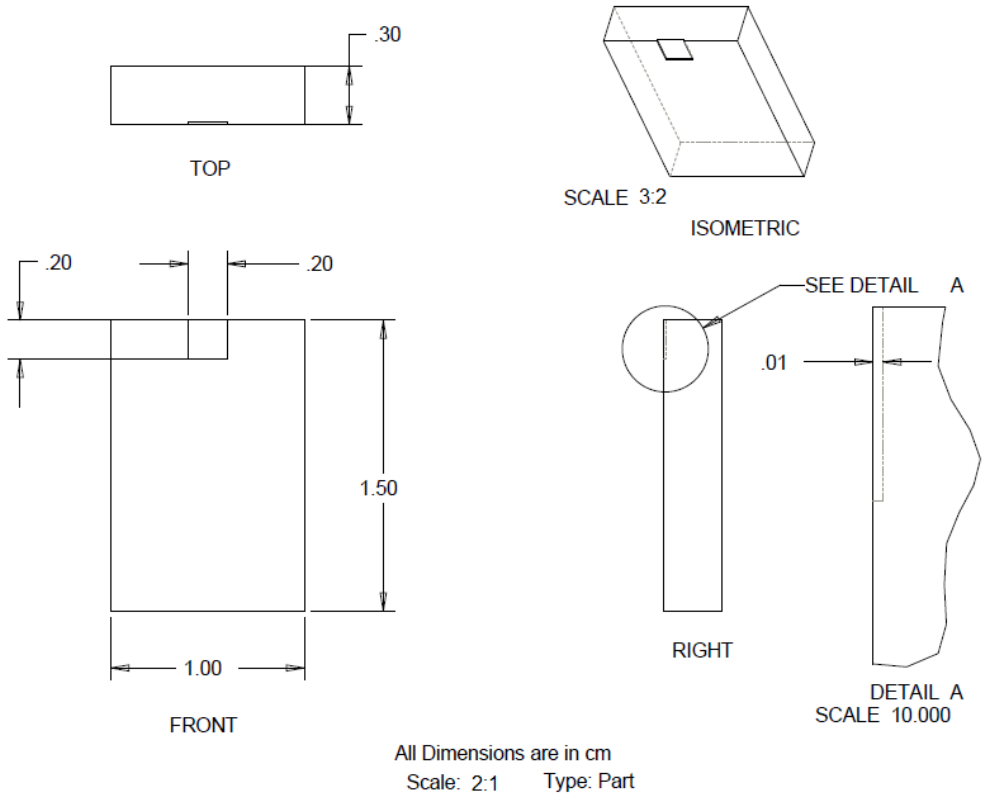

APPENDIX B

EQUIPMENT (B.1 and B.2)

Figure B.1 – Laser integrated Haas VF1 milling machine

Figure B.2 – Resistance spot welder

IPG laser source (200W max, 1.075µm wavelength) integrated to Haas VF1 milling machine:

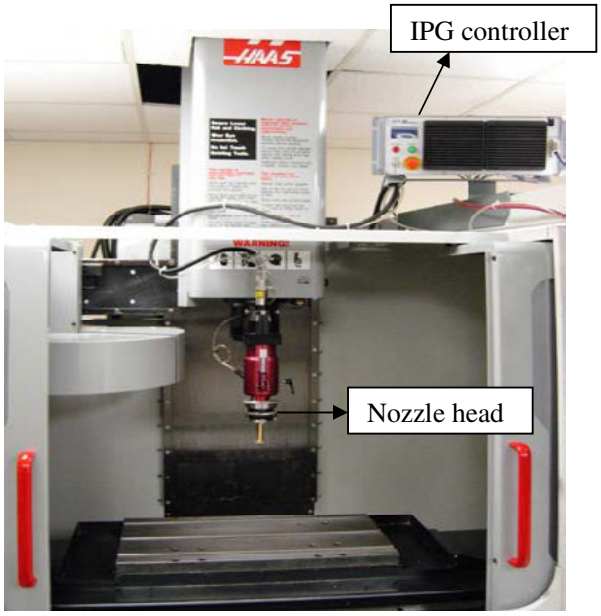

Figure B.1 Laser integrated Haas VF1 milling machine

Miller Resistance spot welder 20 KVA model:

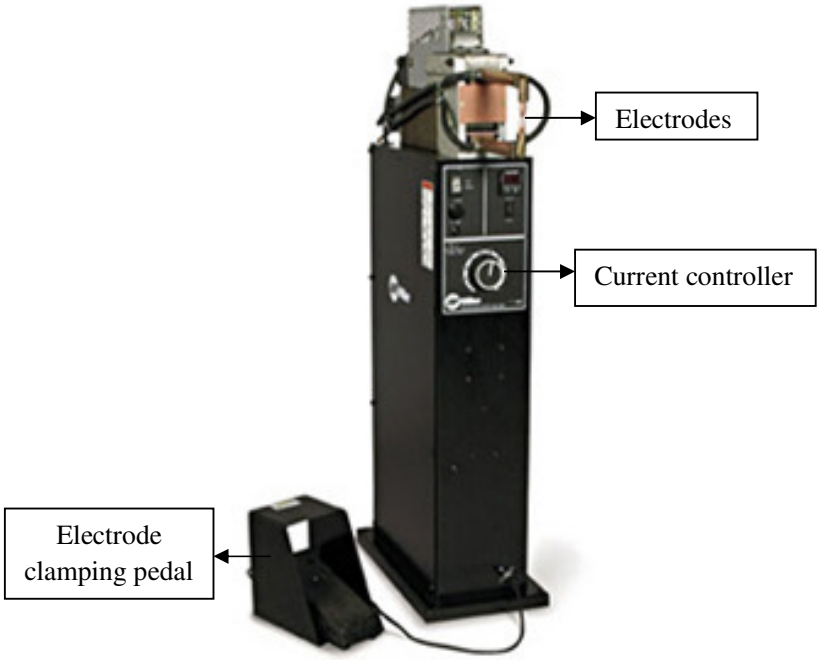

Figure B.2 Resistance spot welder

APPENDIX C

PROGRAM LISTING

Program C.1 - Program to move in a square and dwell

Program C.2 - Program to move back and forth in Y direction

Program C.1 - Program to move in a square and dwell

```
( POSTED FOR HAAS VF SERIES MILLS )
( BY FEATURECAM ON 08-12-2009 USING )
( Haas VF Series.CNC POSTPROCESSOR V9/99 )
N35 G00 G17 G40 G90
( TOOL: T1 = 0.01 dia. laser )
N45 T1
N50 G54 X0. Y0.
N55 G43 H01 Z0.1
N60 Z0.
N65 M51
N70 G04 P15.0
N75 G01 F0.5
N80 X0.027 Y0.027
N85 G04 P1.0
N90 G01 F0.5
N95 X0 Y0.054
N100 G04 P1.0
N105 G01 F0.5
N110 X-0.027 Y0.027
N115 G04 P1.0
N120 G01 F0.5
N125 Z-0.02
N130 X0 Y0
N135 G04 P1.0
N140 G01 F0.5
N145 X0.027 Y0.027
N150 G04 P1.0
N155 G01 F0.5
N160 X0 Y0.054
N165 G04 P1.0
N170 G01 F0.5
N175 X-0.027 Y0.027
N180 G04 P1.0
N185 G01 F0.5
N190 Z-0.04
N195 X0 Y0
N200 G04 P1.0
N205 G01 F0.5
N210 X0.027 Y0.027
N215 G04 P1.0
N220 G01 F0.5
N222 X0 Y0.054
N225 G04 P1.0
N230 G01 F0.5
N235 X-0.027 Y0.027
N240 G04 P1.0
N245 G01 F0.5
N250 Z-0.06
N255 X0 Y0
N260 G04 P1.0
N265 G01 F0.5
N270 X0.027 Y0.027
N275 G04 P1.0
N280 G01 F0.5
N285 X0 Y0.054
N290 G04 P1.0
N295 G01 F0.5
N300 X-0.027 Y0.027
N305 G04 P1.0
N310 G01 F0.5
N315 X0 Y0
N320 G04 P1.0
N325 M61
N330 G01 Z1. F15.0
( END OF PROGRAM )
N400 G28 G49 G91 Z0.
N425 G53 G90 X-20. Y0.
N430 M30
%
```

Program C.2 - Program to move back and forth in Y direction

```
( POSTED FOR HAAS VF SERIES MILLS )
( BY FEATURECAM ON 11-12-2010 USING )
( Haas VF Series.CNC POSTPROCESSOR V9/99 )
N35 G00 G17 G40 G90
( TOOL: T1 = 0.01 dia. laser )
N45 T1  N50 G54 X0. Y0.
N55 G43 H01 Z0.1
N60 Z0.
N65 M51
N70 G01 F1.5
N75 Y-0.12
N80 X0.002
N85 Y0.
N90 X0.004
N95 Y-0.12
N100 X 0.006
N105 Y0.
N110 X 0.008
N115 Y -0.12
N120 X0.01
N125 Y0.
N130 X0.012
N135 Y-0.12
N140 X0.014
N145 Y0.
N150 X0.016
N155 Y-0.12
N160 X0.018
N165 Y0.
N170 X0.02
N175 Y-0.12
N180 X0.022
N185 Y0.
N190 M61
N200 G01 Z1. F10.0
( END OF PROGRAM )
N400 G28 G49 G91 Z0.
N425 G53 G90 X-20. Y0.
N430 M30
%
```

APPENDIX D

SHEAR TESTING

A graph is generated for the change in position of the weld area with the force exerted. When the joint is about to break, maximum force exerted is marked in the graph which is used in the equation above to calculate the shear stress.

Graph in the Figure D1 shows the force versus position for the resistance spot brazed joint with no coating:

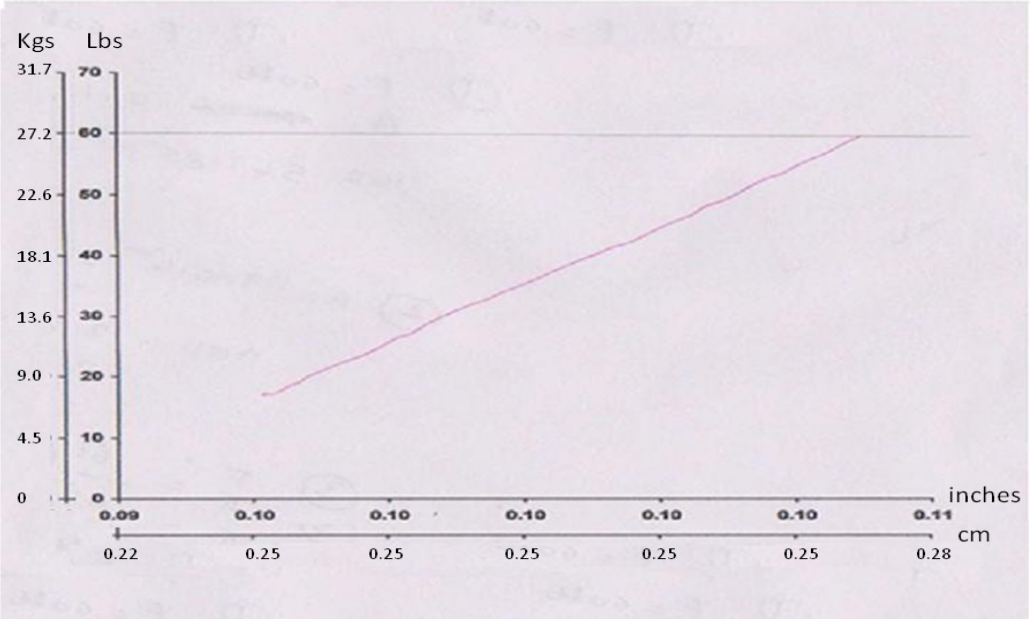

Figure D.1 Force vs Position for composite with no coating
(RSW-AlGr, no coat, Al822, 3A, 7sec, 4 cycles, 200 kPa)

Figure D.2 Nocoat- Grid drawn on the composite surface to measure the marked area

From this, the maximum force exerted on the joint to break the bond can be seen. An actual shear area is estimated by superimposing sqaure grits of known dimensions onto digital pictures of sheared surface as shown in the Figure D2 and the area of the weld is calculated. Surface is observed in the microscope and the weld area is seen and measured as follows:

<u>For No coating:</u>

Force = 267N

Weld Area= number of grids * grid area = 119 * 0.4^2 = 19.04 mm^2 = $19.04*10^{-6}m^2$

Shear Stress = Force/Area = 14.02MPa

Similarly for tin coating and Zinc coating the calculations are done to measure the shear stress of the brazed joints. For Tin coating, graph for force versus position is shown below in the Figure D.3.

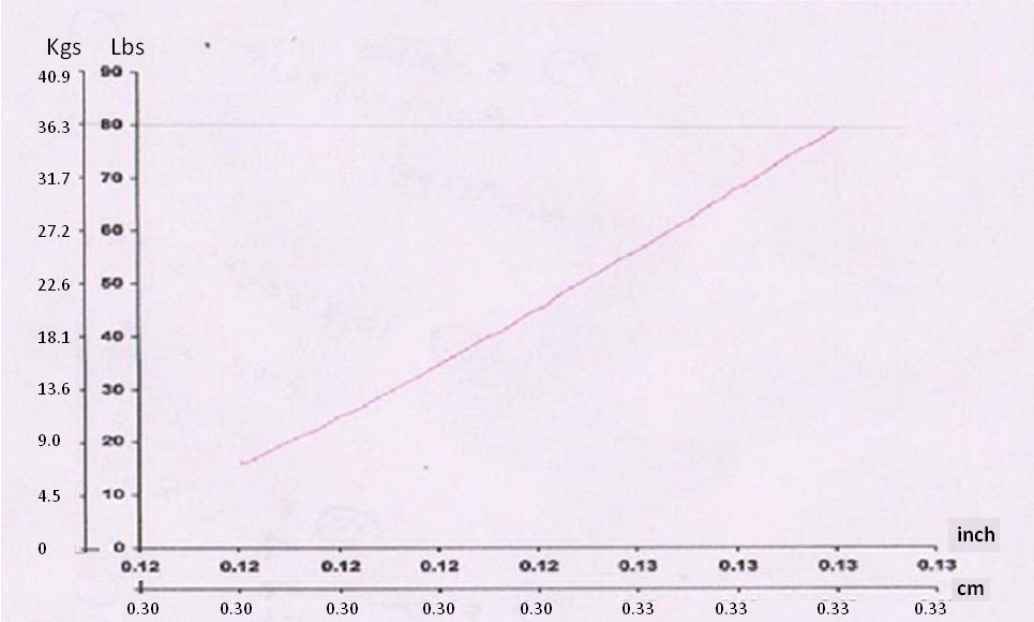

Figure D.3 Force vs Position for composite with tin coating
(RSW-AlGr, tin coat, Al822, 3A, 7sec, 3 cycles, 200 kPa)

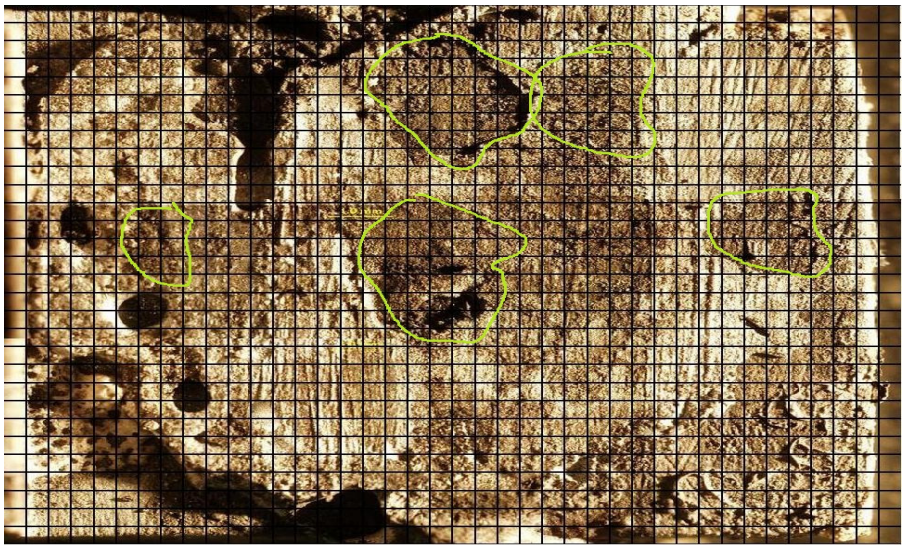

Figure D.4 Tin coat- Grid drawn on the composite surface to measure the marked area

<u>For Tin coating:</u>

Force = 356N

Weld Area = number of grids * grid area = 121 * 0.37^2 = 16.56 mm^2= 16.56*$10^{-6}m^2$

Shear Stress = Force/Area = 21.5MPa

For Zinc coated samples, force vs position graph is shown below in the Figure D.5.

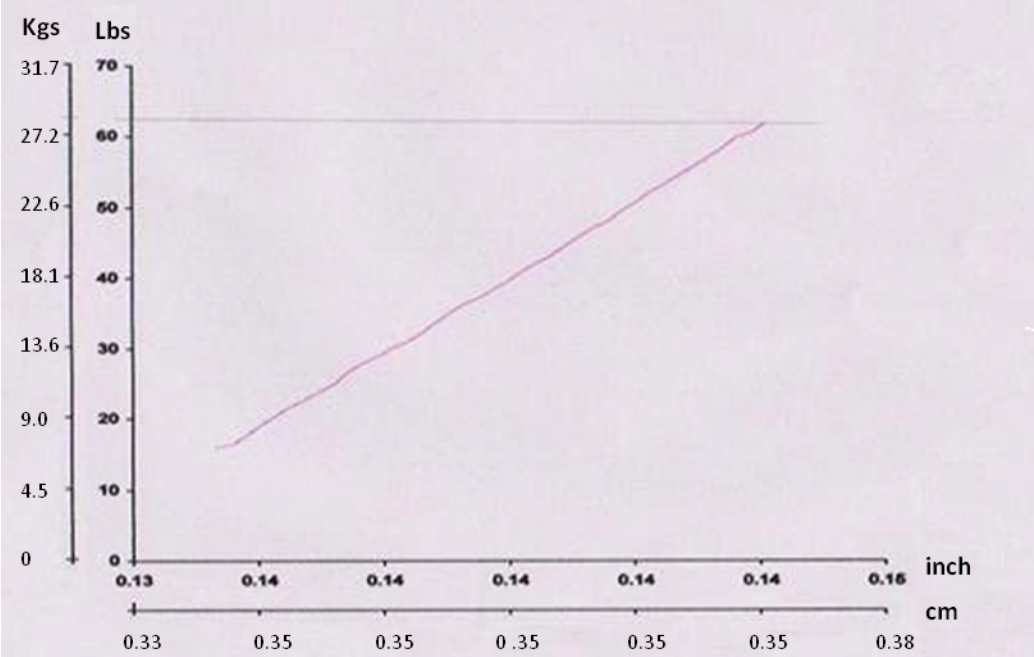

Figure D.5 Force vs Position for composite with zinc coating
(RSW-AlGr, Zn coat, Al822, 3A, 7sec, 2 cycles, 200 kPa)

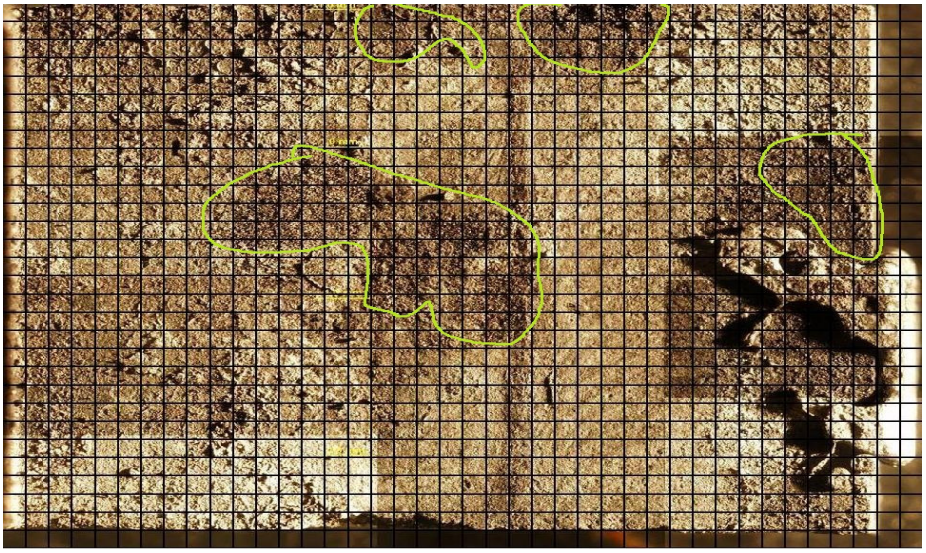

Figure D.6 Zinc coat- Grid drawn on the composite surface to measure the marked area

For Zinc coating:

Force = 271.45N

Weld Area = number of grids * grid area = 85 * 0.4^2 = 13.6 mm^2= $13.6*10^{-6}m^2$

Shear Stress = Force/Area = 20.0MPa

VITA

Manasa Velamati

Texas A&M University,
Department of Mechanical Engineering
3123 TAMU, College Station, TX – 77843-3123

EDUCATION

M.S., Texas A&M University, College Station, Mechanical Engineering, May 2011.

B.E.(*Hons.*), Birla Institute of Technology and Science, Pilani, India, mechanical engineering, May 2006.

PROFESSIONAL EXPERIENCE

Graduate Teaching Assistant, Department of Engineering Technology, Texas A&M University (January 2004 – May 2005); Assisted students with various manufacturing processes including welding and casting, and grading assignments.

Program Analyst, Cognizant Technology Solutions, Chennai, India (July 2006 – April 2008); Provide software services to clients

Engineering Intern, GE Healthcare, Bangalore, India (July 2005- December 2005); Manufacturing and testing of parts of an X-ray generator